UNIVERSITY OF SOUTHAMPTON

# Observations of the Velocity Structure of the Agulhas Current

Lisa M Beal

Submitted for the degree of Doctor of Philosophy

Department of Oceanography

August 1997

UNIVERSITY OF SOUTHAMPTON

ABSTRACT

FACULTY OF SCIENCE
OCEANOGRAPHY

Doctor of Philosophy

# OBSERVATIONS OF THE VELOCITY STRUCTURE OF THE AGULHAS CURRENT

by Lisa M Beal

The Agulhas Current is the Western Boundary Current (WBC) of the Southwest Indian Ocean and is the second largest WBC in the world's oceans. The full depth velocity field of the Agulhas Current has been directly measured for the first time using a lowered acoustic Doppler current profiler (LADCP), a technique not used before by British scientists. The technique involves a 150kHz ADCP in a 6000m pressure casing which is lowered through the water column to obtain an absolute velocity profile. Fifteen combined CTDO2/LADCP stations were occupied across the Agulhas Current at 32°S in February-March 1995. Careful comparisons with shipboard ADCP, bottom tracking data and geostrophic estimates suggest that LADCP profiles are accurate to within about $6cms^{-1}$.

From LADCP velocities the deep dynamics of the Agulhas Current were found to be very different than previously estimated using geostrophic estimates. In particular, traditional geostrophic calculations generally use near-horizontal levels of no motion from which to obtain absolute velocities, but LADCP velocities show that there is a V-shaped pattern for the level of no motion in the WBC. As a result the LADCP data reveals an Agulhas Undercurrent flowing equatorward below 800m depth directly underneath the core of the Agulhas Current. This Undercurrent is estimated to carry 6Sv of primarily North Atlantic Deep Water into the Indian Ocean.

The volume transport of the Agulhas Current is estimated to be 71Sv using a combination of LADCP velocities and geostrophic estimates. This is 14Sv less than the most recent estimate in the literature and the difference is principally due to the Undercurrent. Using the LADCP section in combination with a transindian hydrographic section across 32°S from November 1987, and taking a climatological Ekman flux of 0.5Sv and an Indonesian Throughflow of 6.4Sv, the heat flux divergence over the Indian Ocean north of 32°S is calculated to be 1PW. The interior transport across 32°S, below 2000db is estimated to be 17Sv equatorward, requiring a basin-averaged upwelling rate of $4\times10^{-7}$ $ms^{-1}$, close to half the most recent estimate.

I was like a child playing on the sea-shore, and diverting myself now and then finding a smoother pebble or a prettier shell than ordinary, whilst the great ocean of truth lay all undiscovered before me.

Isaac Newton

# ACKNOWLEDGEMENTS

I would like to thank my supervisor and mentor, Harry Bryden, who not only instilled me with enthusiasm for this thesis, but for all things oceanographic. His love of oceanography and his shear enjoyment in its pursuit has inspired me to want to follow in his footsteps and dedicate my life to investigating the oceans.

From Discovery cruise 214, I would most like to thank Nick Crisp for his friendly help and advice with everything LADCP. Also Stuart Cunningham and Mike Griffiths who collected and cleaned the CTD and GPS data that I used, and to the rest of the scientists and crew who put up with a first-time student.

From the Algoa cruise I am grateful to Brian King for encouraging me and involving me in the cruise planning and to Nick Crisp, Stuart Cunningham, Keith Goy, Ian Waddington and Mark Hartman who all worked very hard in difficult conditions.

Many people have had a significant role in encouraging my work and helping me have fun during my thesis. In particular I would like to thank Henry Charnock who picked me up and dusted me off when I was feeling low with my research, my office mates Helene Banks and Mark Bean for much stimulating scientific discussion, Peter Saunders who encouraged me always to question, Julian Castaneda and Raul Aguirre-Gomez who offered help in those early months and Jason Holt for his close friendship and support.

I am very grateful to Eric Firing who provided all his LADCP processing software and made himself freely available for help and advice via email. Also Steve Alderson for his pstar expertise and Paul Robbins for matlab advice. This thesis research was supported by a WOCE Special Topic grant.

# CONTENTS

# CHAPTER ONE

# *AN INTRODUCTION TO THE AGULHAS CURRENT*

## 1.1 Motivation

The Agulhas Current has long been of interest to mariners due to its position on one of the world's busiest trade routes. At the end of the fifteenth century Portuguese mariners seeking a sea route to India were the first to document the Agulhas Current and within a century of its discovery its strength and general path were sufficiently known that ships could avoid it on their outward passage to the east (Pearce, 1980). The first charts of the Agulhas Current were prepared by Rennell (1778), who was well aware of its great temporal variability. In the eighteenth and nineteenth centuries mariners were primarily concerned with the surface manifestations of the Agulhas Current so that they could gain safe and quick passage around the Cape and along the south east coast of Southern Africa. More recently the Agulhas Current has become an important topic of research to oceanographers. The first modern scientific surveys were designed to map the complicated system of surface currents in the Southwest Indian Ocean (e.g. Dietrich, 1935). Subsequently oceanographers have come to recognise that knowledge of the Agulhas Current, its associated dynamics and water masses has importance not just on local currents and surface waves but also on weather systems, mesoscale eddy patterns, the intensity of the Southwest Indian Ocean gyre, basin overturning and even global thermohaline circulation.

The theory of western intensification lies at the heart of ocean physics (Stommel, 1948) and predicts that the interior Sverdrup transport due to wind stress curl (Sverdrup, 1947) should be balanced by Western Boundary Current (WBC) transport. The southern Indian Ocean is forced by an average wind stress which is predominantly eastward south of 32°S and westward farther north (Hellerman & Rosenstein, 1983). The resultant wind stress curl drives a strong subtropical circulation with an equatorward interior flow and a poleward WBC, the Agulhas Current (Munk, 1950). The Agulhas Current has one of the largest transports of any current in the world's oceans and is thought to be second only to Gulf Stream transport. Accurate observations and measurements of the Agulhas

Current, and other WBCs, are an important way in which our understanding of modern ocean dynamics can be tested by the comparison of such measurements with analytical and predictive models.

The Agulhas Current flows along the African continental slope carrying warm waters poleward and although its core is only about 100km wide a large portion of the ocean, to the east and south of the African continent, is influenced by its recirculation and retroflection regions. The spatial extent of these warm water zones is highly dependent on the dynamics of the Agulhas Current further upstream. Walker (1990) found that altered surface heat flux distributions in the oceans around Southern Africa enhanced low-level instability within the atmosphere, thus optimising conditions for summer rainfall. He found that two major Agulhas Current "warm events" , where sea surface temperatures were 1°C to 3°C warmer than usual, were closely related with above normal rainfall over much of the subcontinent, implying that the variability of the Agulhas Current can have a profound effect on local climate.

Recent understanding of the rate of overturning in the Indian Ocean describes the basin-wide upwelling velocity required to balance the estimated heat divergence north of 32°S as 4 to 5 times faster than upwelling in the Pacific (Toole & Warren, 1993). Toole & Warren suggest that the heat divergence over the Indian Ocean north of 32°S is dominated by a vertical cell consisting of northward flow of cold, deep waters and southward flow of warm, thermocline waters in the Agulhas Current, thus requiring vigorous overturning. The estimated volume transport of the Agulhas Current has a significant influence on the strength of this overturning: if the southward transport of warm waters is reduced, the resultant heat divergence does not necessitate such large vertical velocities but can be largely satisfied by the horizontal eddy fluxes of the ocean gyre. Thus an accurate estimate of the temperature flux of the Agulhas Current can modify and clarify our understanding of the anomalously fast replacement rate of abyssal waters in the Indian Ocean.

The Agulhas Current also plays an important role in the global thermohaline circulation. The Indian Ocean is closed to the north (excepting the warm Indonesian Throughflow entering from the Pacific) and there is a net gain of heat (a divergence) and buoyancy in the basin where there is no local deep water formation (Wyrtki, 1973). In the conveyor belt concept of global thermohaline circulation (Broecker, 1991) the Indian and Pacific oceans are the oceans in which cold water driven to depth in the Atlantic and Southern oceans upwells and is warmed. The paths for the return flow of these

thermocline waters to the Atlantic are via the Agulhas Current from the Indian Ocean and via the Southern Ocean through the Drake Passage from the Pacific Ocean. However, there is uncertainty about the relative contributions to the thermohaline circulation of the flows south of Africa and south of America. Gordon (1986) considers the flow of warm waters through the Drake Passage to be negligible and that the Agulhas Current is the major pathway. Broecker *et al* (1990) estimate that the Agulhas Current accounts for only one quarter of the return flow. From inverse methods Rintoul (1991) discounts a large flow of warm waters into the South Atlantic from the Indian Ocean. However there is strong evidence, from tracer chemistry (Gordon et al, 1992), altimetry (Gordon & Haxby, 1990), thermal imagery (Lutjeharms & van Ballegooyen, 1988a) and hydrography (Duncombe Rae, 1991) of considerable inter-basin exchange of thermocline and intermediate waters around Cape Agulhas.

Clearly there is a need for a careful assessment of the size and variability of the Agulhas Current in order to quantify the supply of thermocline waters to the South Atlantic and hence the significance of the Agulhas Current to the global thermohaline exchange.

## 1.2 An introduction to the physical oceanography of the Southwest Indian Ocean and its western boundary current

In this section a brief introduction to the circulation of the southern subtropical gyre of the Indian Ocean, the Agulhas Current at its western boundary and the Agulhas Retroflection region to the south of the African subcontinent, provides a general background to the dynamics and water masses of the area. Leading on from this is a more particular review of the features of the Agulhas Current as it flows swift and narrow along the east coast of South Africa.

### 1.2.1 Hydrography of the Southwest Indian Ocean

The circulation of the warm thermocline waters in the Southwest Indian Ocean is dominated by a wind driven anticyclonic gyre. Figure 1.1 is a bathymetric map of the Southwest Indian Ocean, highlighting the steep continental slopes off southern Africa and Madagascar and the north-south ridges crossing the basin. Figure 1.2 is a cartoon, taken from Duncombe Rae (1991), showing the main features of the gyre in the high

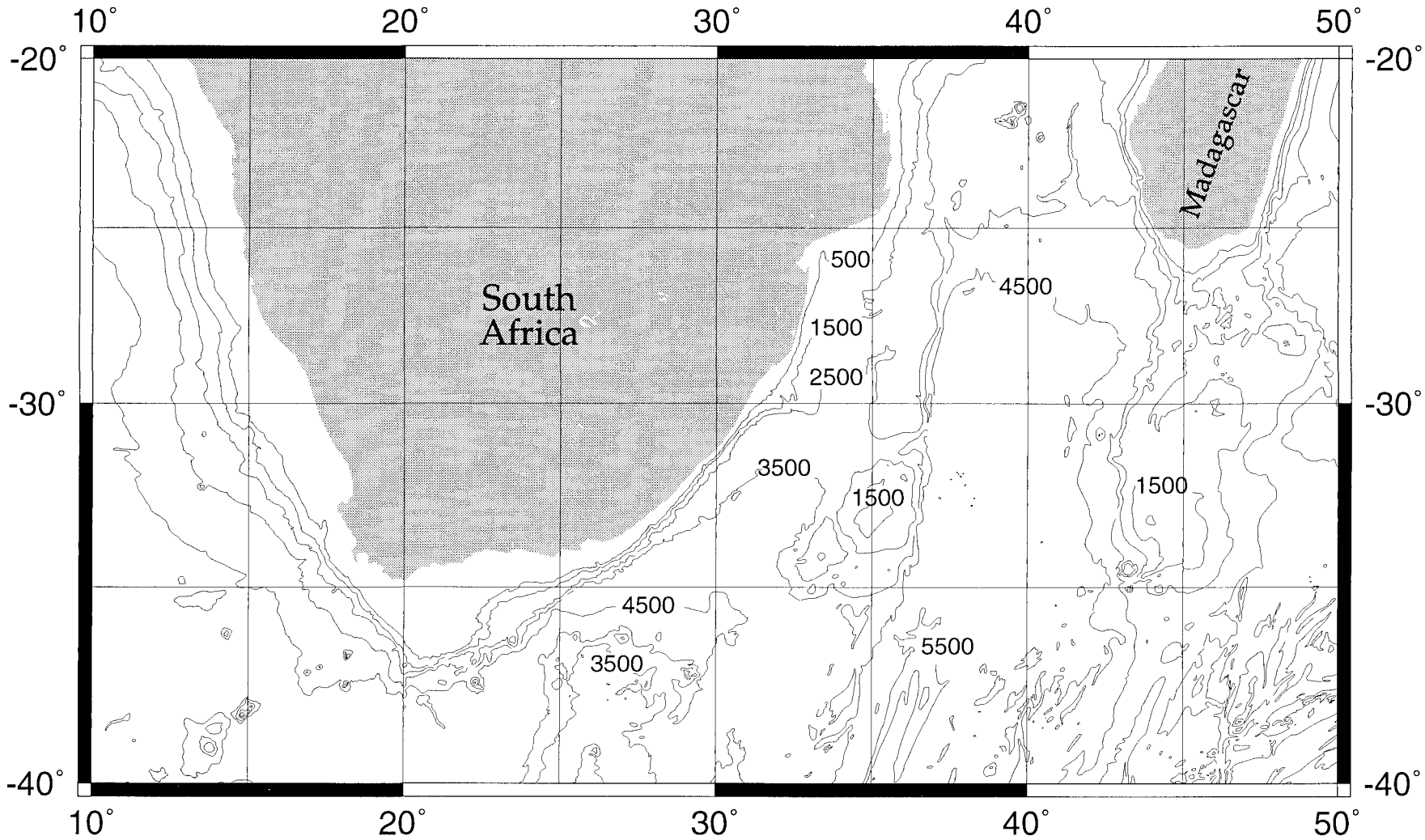


Figure 1.1 Bathymetry of the Southwest Indian Ocean. The Mozambique Ridge runs north-south at about 35°E, the Madagascar Ridge is at 44°E and the Agulhas Plateau is to the south of the African continent at about 27°E.

energy region of the western boundary, where the circulation is heavily influenced by constrained currents and steep topography.

In the north, the South Equatorial Current (SEC) flows westward at about 20°S until it reaches the west coast of Madagascar where the flow splits. During the south-west monsoon the northern arm of the SEC feeds into the northward flowing Somali Current just south of the equator, but during the north-east monsoon the Somali Current has a weak southward flow and the northern branch of the SEC circles back to the east along the equator as the Equatorial Current. About one third of the SEC water is deflected southward at Madagascar (during both monsoons) and accelerates along the steep continental slope into a fast and narrow WBC known as the East Madagascar Current.

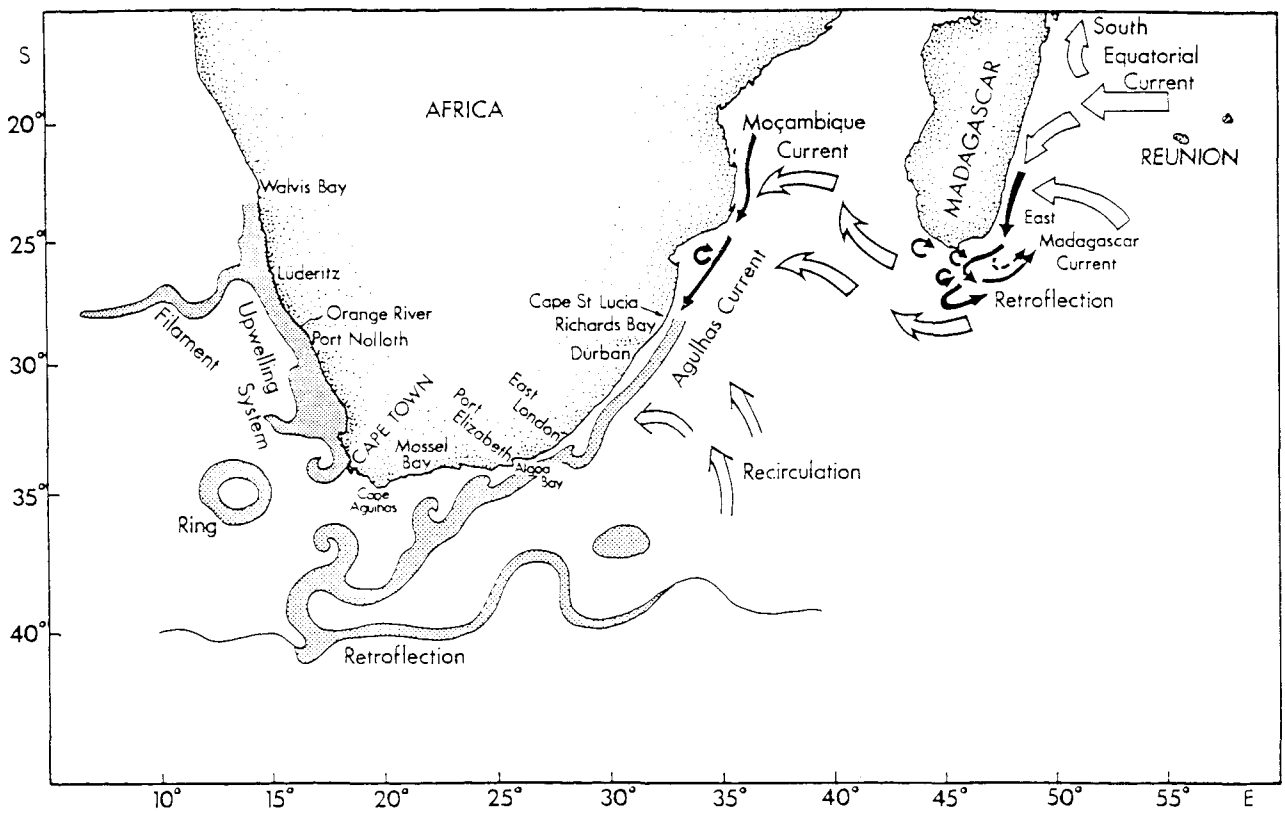


Figure 1.2 The circulation in the western boundary region of the Southwest Indian Ocean gyre, featuring the Agulhas Current and the East Madagascar Current. Characteristics of the Agulhas Current are shown - meandering jet off eastern Africa, inshore eddies and filaments over the Agulhas Bank, rings shed from the retroflection into the South Atlantic, meanders in the current over the Agulhas Plateau and cold core rings in the Indian Ocean. (from Duncombe Rae, 1991)

Beyond the southern tip of Madagascar the WBC retroflects and flows to the east, back into the interior (Lutjeharms *et al*, 1981). Water from the East Madagascar Current only reaches the Agulhas Current system in the form of spun-off rings or warm filaments that have drifted across the mouth of the Mozambique Channel (Lutjeharms, 1988). The circulation of the upper 1000m of the Mozambique Channel is dominated by two anticyclonic gyres and a number of smaller cyclonic eddies (Saetre & Jorge da Silva, 1984). In the vicinity of the Mozambique Ridge at 35°E (figure 1.1) is an energetic eddy field (Grundlingh, 1985a; Grundlingh *et al*, 1991) which may act as a feed back loop for the Agulhas Current to the west (Cheney & Richardson, 1976).

The Agulhas Current flows south-west along the shelf edge of the southern African continent from about 27°S to 37°S. At 34°S the continental shelf edge separates from the coast of South Africa and continues south-westward down to the Agulhas Bank where the Agulhas Current finally separates from the topography and retroflects between 15°E and 20°E (Harris & van Foreest, 1978). About 10% of the warm WBC waters are leaked into the Atlantic (van Ballegooyen *et al*, 1994) by Agulhas Rings shed to the west at the retroflection. Seven to nine rings are spawned per year. The main current flows eastward from the retroflection region, back into the southern Indian Ocean as the Agulhas Return Current. The Return Current generally follows the subtropical convergence at about 40°S (Lutjeharms, 1985), enhancing the intensity of this front. The path of the Agulhas Return Current responds to the topographic features of the Agulhas Plateau and the Mozambique Ridge with large meanders northward (Gordon *et al*, 1987).

The retroflection region is characterised by very high mesoscale variability, as revealed by sea surface temperature patterns from satellite images(Lutjeharms & van Ballegooyen, 1988a & b), and drifters (Grundlingh, 1978). Sea surface height anomaly from satellite altimetry shows the area to be one of the most energetic regions of the world's oceans . The Agulhas Current, Retroflection and Return Currents enclose a pool of warm water which supports a large exchange of heat to the atmosphere (Bunker, 1988).

As regards the water masses, the surface layer, down to about 200m is dominated by subtropical surface water (STSW) of salinities higher than 35.5 (Duncan, 1970). This water mass originates east of 58°E and between latitudes 15° and 35°S (Wyrtki, 1971) where evaporation exceeds precipitation. STSW reaches the Southwest Indian Ocean via the East Madagascar current and advects west into the Agulhas Current in warm eddies

shed from the retroflection at the tip of Madagascar. STSW has a strong presence in the upper waters of the Agulhas Current despite there being no direct flow from the southern tip of Madagascar. Tropical Surface Water (TSW), formed near the equator by warming and precipitation excess, propagates southward through the Mozambique Channel and at its mouth caps STSW, resulting in a subsurface salinity maximum here and southward into the Agulhas Current.

Below the STSW, making up most of the thermocline waters, is South Indian Central Water (SICW) or Subtropical Convergence Zone Water (Mamayev, 1975), which is formed at the subtropical front by the sinking of mixed subtropical and subantarctic surface water masses. At about 1000m depth a salinity minimum (S<34.6) signifies Antarctic Intermediate Water (AAIW) which is subducted at the subpolar front and moves northward into the South Indian Ocean. AAIW recirculates anticyclonically and is carried south again in the Agulhas Current. Also at intermediate depths Red Sea Water (RSW) is transported through the Mozambique Channel (Saetre & Jorge da Silva, 1984; referred to as North Indian Intermediate Water), identifiable as a salinity maximum and oxygen minimum. When it meets AAIW of comparable density, south of the channel, a variety of stirring, mixing and interleaving processes form filaments and lenses of RSW (somewhat diluted and sometimes referred to as Modified AAIW) (Grundlingh, 1985b). Valentine *et al* (1993) have identified traces of RSW as far south as the Agulhas retroflection region.

At depths below 2000m North Atlantic Deep Water (NADW) enters the Indian Ocean immediately south of Africa (Mantyla & Reid, 1995) and flows northward, its progress to the west restricted by the Crozet Plateau and Madagascar Ridge.

### 1.2.2 The structure of the Agulhas Current

Generally the surface features of the Agulhas Current are similar to the other great WBCs, the Gulf Stream and Kuroshio (Pearce, 1977). An intense cyclonic shear region only a few kilometres wide, separates the current from cooler water on the continental shelf. In the core of the WBC speeds exceed $1ms^{-1}$ and surface waters are warm. Offshore of the current core a diffuse region of anticyclonic shear dominates. Instabilities such as plumes, eddies and meanders grow in both shear regions either side of the jet-like current core (Lutjeharms *et al*, 1989).

Between Durban at 30°S and Port Edward situated 200km downstream along the South African coast, the continental shelf narrows and at the same time the maximum

depth of the basin increases, as shown on the bathymetric map in figure 1.3 (Schumann, 1981). This topographic variation causes the Agulhas Current to become concentrated close to the coast and its speed to increase (due to a gain in relative vorticity), until offshore of Port Edward the Agulhas Current generally behaves like a narrow jet (Gill & Schumann, 1979), flowing swiftly and deeply along the steep continental slope. Hence the current is closest to the coast here and deviates the least in width or position (Grundlingh, 1983), making it an ideal location for measuring its volume transport.

Due to the short term variability in the position and speed of the Current near 32°S, its general structure and seasonal variability are not well known. Pearce (1977) measured peak speeds in the core of the current of 2.5ms$^{-1}$ at the surface and found the core to be positioned 50km offshore on average. He estimated the width of the current to be between 90 and 100km taken between the 0.5ms$^{-1}$ isotachs. Grundlingh (1983) estimated that the core is generally positioned 30km offshore. Toole & Warren (1993) found the warmest sea surface temperatures indicative of the inshore edge of the current 13.5 km offshore and using an Acoustic Doppler Current Profiler (ADCP) measured peak speeds of 1ms$^{-1}$.

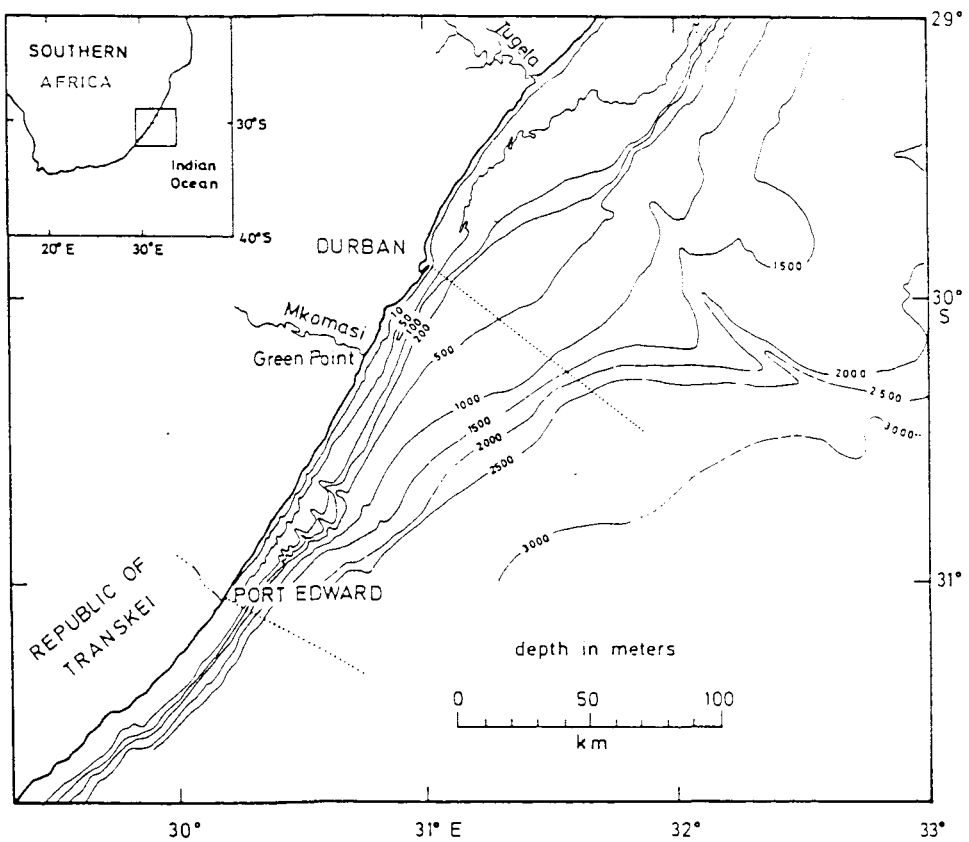


Figure 1.3 Bottom topography between Durban and Port Edward (from Gill & Schumann, 1979).

They used the position of the maximum in transport streamfunction to suggest that the current extends 350km from the African coast. However this maximum may include the influence of an anticyclonic eddy on the offshore side of the current, a feature often observed in the past (Pearce, 1977).

Mesoscale variability in the path of the current has been reported by a number of investigators. Pearce (1977) and Grundlingh (1979) and more recently Lutjeharms & Roberts (1988) have noted that the Agulhas Current, during isolated events, meanders up to 200 km offshore. The origin for these transient events is suggested by Lutjeharms & Roberts (1988) who studied infra-red satellite images and combined their observations with hydrographic data. They proposed that the propagation downstream of a coastally trapped cyclonic eddy formed in the Natal Bight pushes the Agulhas Current wide of its normal course and have termed these events as Natal Pulses. They make no suggestion as to how the formerly trapped eddy escapes downstream however. Grundlingh (1983) noted that the current was to be found far offshore 23% of the time, from repeated hydrographic surveys. With better spatial coverage from the use of satellite images, Lutjeharms & Roberts (1988) estimated that a Natal Pulse was present off Durban about 17% of the time.

Reports on the seasonal variability of the Agulhas Current have come up with conflicting results. Rennell (1778) considered the current to be strongest during winter from observations of ship drift. Africa Pilot (1915) found no evidence for seasonal variation. Barlow (1931) made an extensive study of available ship drift reports and concluded that the current was most intense in January, March and April and weakest from May to July. Darbyshire (1964) calculated geostrophic velocities to be greatest in April and least in October. Tripp (1967) went back to ship drift to estimate that velocities are a maximum in Spring and Autumn and a minimum in Summer and Winter, thus implying a semi-annual oscillation. Duncan (1970) found that geostrophic currents were greater in Autumn and Winter than in Spring and Summer. Thus a seasonal minimum has been suggested to occur in all the seasons of the year. Pearce & Grundlingh (1982) re-examined the quality of all this conflicting evidence and used additional ship drift and direct current measurements. They suggested that much of the confusion was due to the inadequate definition of the Agulhas Current proper. Inshore of the current, counter currents and eddies may be found (Pearce *et al*, 1978), whilst offshore the flow is associated with a semi-permanent anticyclonic eddy (Duncan, 1970). In order to separate

the current from these marginal, weak and variable flows Pearce & Grundlingh (1982) chose to define the Agulhas Current as that area where surface speeds exceed 1 $ms^{-1}$. They concluded that "there is no major seasonal variation in the flow", but comment in the discussion that "seasonal changes in the subsurface structure (and hence transport) of the Current" are not ruled out.

To summarise, the Agulhas Current is a typical WBC with a swift, narrow core flanked by regions of high shear with associated meanders, plumes and eddies. Off Port Edward the Current is closer inshore than anywhere else along its length and its path is most stable, providing a good location from which to measure its transport. The warm current core has south-westward velocities exceeding $2ms^{-1}$ at the surface and is generally positioned about 20km offshore. The main current is between 100 and 250km wide. The position and intensity of the its core is subject to both short term variability and meandering events known as Natal Pulses which can divert the Current up to 200km offshore.

## 1.3 A review of volume transport estimates for the Agulhas Current

Grundlingh (1980) reviewed some estimates of the transport of the Agulhas Current close to 32°S beginning with the work of Dietrich (1935). The estimates have varied by an order of magnitude, from 9 to 91Sv. Dietrich (1935) calculated a geostrophic transport of 19Sv, using hydrographic data with station depths limited to 1000m. Also restricted to shallow stations, Duncan (1970) estimated, by extrapolation of the velocity distribution, that 80% of the flux in the Agulhas Current takes place in the top 1000m. Using this estimate he found geostrophic transports relative to 2500m of 67Sv in summer and 91Sv in winter, giving an average volume transport of 79Sv. Lutjeharms (1972) re-analysed historical hydrodynamical data and estimated a mean transport of 56Sv. Darbyshire (1972) estimated the transport to be between 9 and 63Sv. In his theoretical model based on Sverdrup dynamics and wind stress curl Veronis (1973) estimated a transport of 72Sv. Harris (1972) calculated velocity profiles using 27.8 as the sigma-t reference surface (about 2500m) and from those estimated a transport of 67Sv. Jacobs & Georgi (1977) completed a section from Durban to eastern Enderby Land, Antarctica and found the transport of the Agulhas Current, relative to 1300m, was 37Sv. Harris & van Foreest (1978), limited to sampling depths of 1000m, referenced their transports to the 27.2 sigma-t level (about 1100m) and estimated the transport off Port Edward to be 30Sv.

Using Duncan's (1970) method of extrapolation they argued that the total transport, relative to 2500m, would be 78Sv.

Grundlingh (1980) was the first to use direct observations to reference geostrophy. By matching current measurements from a drifting ship with geostrophic calculations over the top 1000m of ocean he found a transport of 62Sv, extrapolating to 75Sv over the whole water column, using Duncan's flux approximation. Toole & Raymer (1985) extracted over 1000 profiles of archive current measurements within 100km of the coast near Durban and sorted them by distance from the coast into nine groups before averaging them. Matching surface currents from Grundlingh (1980) to their mean geostrophic shears they obtained a transport of only 44Sv, compared with Grundlingh's 62Sv for the upper 1000m. This low estimate is probably due to the effect of the meandering of the Agulhas Current off Durban, as mentioned above, which implies that the current would not have been sampled within 100km of the coast for one fifth of the time. Most recently using full depth hydrographic measurements and a reference level inferred from water mass features Toole & Warren (1993) estimated an Agulhas Current transport of 85Sv.

| Reference | Volume transport $1Sv = 1 \times 10^6 m^3 s^{-1}$ | Comments |
|---|---|---|
| Dietrich (1935) | 19 | ↓1000, ref.1000 |
| Duncan (1970) | 67 ; 91 | ↓1000, ⇓extra, ref.2500, sum ; win |
| Lutjeharms (1972) | 56 | ref.2300 |
| Darbyshire (1972) | 9 to 63 | |
| Veronis (1973) | 72 | from Sverdrup dynamics |
| Harris (1972) | 67 | ref.2500 |
| Jacobs & Georgi (1977) | 37 | ↓1300, ref.1300 |
| Harris & Van Foreest (1978) | 30 ; 78 | ↓1000, ref.1100 ; ⇓extra, ref.2500 |
| Grundlingh (1980) | 62 ; 75 | ↓1000, ref.currentmeter ; ⇓extra |
| Toole & Raymer (1985) | 44 | ↓1000, ref.currentmeter |
| Toole & Warren (1993) | 85 | ref.~2300 (from water masses) |

Table 1.1 Geostrophic volume transport estimates, taken from the literature, for the Agulhas Current near 32°S (off Durban and Port Edward). The abbreviated comments are as follows: casts limited to 1000m depth (↓1000), transport referenced to 1000m (ref.1000), transport extrapolated to the bottom (⇓extra), summer (sum), winter (win).

The wide spread of transport estimates (table 1.1) must be due in part to the limitations of measurement techniques. With the invention of the CTD, and later the ADCP, and even more recently the GPS-3DF attitude sensor and differential GPS navigation (see Chapter 2), the accuracy of ship-board hydrographic and current measurements have been revolutionised. Before the mid eighties, casts were rarely deeper than 1000m and velocity measurements in the Agulhas Current were made from a drifting ship tracked with radio navigation systems of limited accuracy. Grundlingh (1980) suggests that the large variation of Agulhas Current transports could be attributed to two factors: indiscriminate station spacing and more especially, an incorrect assumption of a "level of no motion". He states that, "the former is evident from historic cruises where the first inshore station is estimated to have been almost midway across the current and the latter is an ever-present problem where geostrophics are concerned."

From table 1.1 it is clear that before 1980 most reference levels were chosen at or close to 1000m, in most cases because of the limited depth of the hydrographic casts. Grundlingh (1980) used current meter measurements taken close to the surface in order to eradicate the reference level problem but, as you will read later in section 1.4.2, this technique is not without its own problems. More recently, since full depth stations have become common place in most hydrographic sections, many studies have used a reference level which is generally deep and horizontal (or following topography), based on the understanding that velocities close to the sea floor are small. The next section introduces the geostrophic method formally and discusses other techniques that have been used to estimate a geostrophic reference velocity. Most are examples from the Gulf Stream, which as a WBC is dynamically comparable to the Agulhas Current. The section concludes with a brief investigation of the sensitivity of transport estimates to changes in the level of no motion.

## 1.4 Geostrophic velocity and the level of no motion

### 1.4.1 The geostrophic approximation

The full vector equation of motion for a fluid parcel is,

$$\frac{\partial U}{\partial t} + (U \cdot \nabla)U = -2\Omega \times U - \frac{1}{\rho}\nabla p + g + \nu \nabla^2 U \qquad 1.1$$

where the symbols are standard for flow on the rotating earth (e.g. Pedlosky, 1986). To estimate a flow from hydrographic data the geostrophic approximation of the equation of motion is used, whereby the steady circulation is a balance of the horizontal pressure gradient and the local horizontal component of Coriolis force (Pedlosky, 1986). This approximation holds providing the motion is dominated by rotation and that non-linear and dissipative effects are small. This means that the equation of motion can be greatly simplified when applied to large scale, slowly varying currents in the ocean. In local Cartesian co-ordinates the geostrophic balance is given by these three equations,

$$fv = \frac{1}{\rho_s}\frac{\partial p}{\partial x} \qquad 1.2$$

$$fu = -\frac{1}{\rho_s}\frac{\partial p}{\partial y} \qquad 1.3$$

$$\rho g = -\frac{\partial p}{\partial z} \qquad 1.4$$

where $f = 2\Omega \sin\phi$ is the local normal component to the earth's rotation called the Coriolis Parameter, $u$ and $v$ are the horizontal velocity components in direction $x$ and $y$ respectively, $\rho_s$ is the static density and $p$ is pressure.

Absolute pressure gradients cannot be measured in the ocean, however the density distribution can be calculated from profiles of salinity and temperature and by using the equation of state for sea water (Gill, 1982). The geostrophic approximation above can be written in terms of the horizontal density distribution (by first differentiating equations 1.2 and 1.3 with respect to depth z and then eliminating pressure using the hydrostatic approximation in equation 1.4) to derive the thermal wind relations,

$$f\frac{\partial v}{\partial z} = -\frac{g}{\rho_s}\frac{\partial \rho}{\partial x} \qquad 1.5$$

$$f\frac{\partial u}{\partial z} = \frac{g}{\rho_s}\frac{\partial \rho}{\partial y} \qquad 1.6$$

so the geostrophic **shears** $\frac{\partial v}{\partial z}, \frac{\partial u}{\partial z}$ can be found from the horizontal density gradient. In order to calculate the absolute geostrophic velocity from the integral of these shears the velocity at one level must be known, or equivalently the depth-averaged (barotropic) velocity must be estimated. By choosing a horizontal or isopycnic surface where the velocity of the water is assumed to be zero, the absolute velocities can be inferred by

adjusting the integrated shear profile to this reference condition, but the task of objectively determining such a reference level has always been problematic.

### 1.4.2 Techniques for referencing geostrophic velocities

One of the earliest methods for estimating the position of a reference level was introduced by Defant (1941) who suggested that the level at which the vertical shear of velocity vanished coincided with the level of no motion. This is now thought to be inappropriate in many cases because zero shear often implies a maximum or minimum in velocity, for example in deep western boundary currents (DWBC). Another technique used for choosing a level of no motion is to assume that the juxtaposition of water masses can be a guide. For example, Toole and Warren (1993) chose a zero velocity surface (ZVS) for their Agulhas Current data which lies between AAIW and NADW. Often isopycnic surfaces have been chosen as reference levels, either subjectively or based on more rigorous mathematical testing of the data (Bower *et al*, 1985). Wunsch & Grant (1982) developed an inverse method, where the flow is quantitatively constrained by conservation laws and thus absolute fluxes may be estimated. However, inverse methods are complex and field measurements must form a closed box, making the method impractical for many cases, such as a single section across a boundary current.

Probably the most straightforward way to find a reference velocity is to directly measure the flow, but the presence of ageostrophic currents, such as Ekman flux, tides and inertial oscillations can make the interpretation of such measurements difficult. Numerous techniques for measuring velocity have been implemented in the Gulf Stream in particular, where the problem of making accurate transport estimates is a long standing one. Both Lagrangian and Eulerian measurements have been employed by using a wide range of instruments including floats, moorings and acoustic currentmeters. Warren & Volkmann (1968) used Swallow's neutrally buoyant floats at 2500m depth to measure absolute currents in the deep Gulf Stream. They claimed uncertainties in their estimate of Gulf Stream transport of 20-30% but remarked, "Given the greater uncertainty in the arbitrary assumptions of level isobaric surfaces . . . such an error as this seems tolerable at present." More recent float technology has seen the use of POGO for referencing geostrophic shear (Liu & Rossby, 1993). POGO is an acoustically tracked drifter which is launched off the stern of a ship and sinks at a constant rate to a certain depth where it releases a weight and rises to the surface again to be recovered

(Rossby et al, 1991). The displacement between launch and recovery and the known depth of penetration gives a vertically integrated current over that depth.

Since the late 1980s acoustic Doppler current profilers (ADCPs) have enabled velocity profiles of the top 300m of the water column to be measured continuously on-station and whilst the ship is underway. However until recently ADCPs had not made as much impact on the improvement of hydrographic data as was expected, for two reasons. Firstly, inertial and tidal currents have a maximum amplitude in the upper waters so that ADCP current measurements can differ significantly from geostrophic currents. Secondly, gyrocompass heading errors caused unreliability in ADCP velocities, until the recent GPS-3DF technology enabled accurate observations of ship attitude to be made and thus improved the measurements by an order of magnitude (King & Cooper, 1993; Saunders & King, 1995a).

Current meter moorings are particularly useful for measuring time mean velocities which are perhaps more appropriate for referencing geostrophic velocities than one time observations. The difficulty is to determine what time interval to average over for comparisons with a synoptic hydrographic section. In addition moorings are limited to spot measurements and cannot, for instance, follow the meanderings of a WBC. However, Hall & Bryden (1985) ingeniously employed one mooring to make a transport estimate for the Gulf Stream by using the strong cross-stream temperature change to interpret the movement of the Gulf Stream across the mooring. Hence they were able to estimate the width and transport of the Current without resorting to geostrophy.

Pickart & Lindstrom (1993) made comparisons of four techniques for referencing geostrophic velocities: isotherm referencing (based on water mass distribution), POGO, ADCP and moored current meter measurements. They used these techniques in the DWBC of the North Atlantic and their results (figure 1.4) illustrate the considerable differences in the geostrophic velocities obtained from the different methods. The POGO and ADCP results are qualitatively similar but still quantitatively quite different. Through considerations of the known existence of topographic Rossby waves, Pickart & Lindstrom decided that the isotherm and mooring methods were the least successful. They found that the shipboard ADCP data was less appropriate than the POGO due to strong ageostrophic effects near the surface and the limited depth penetration of the

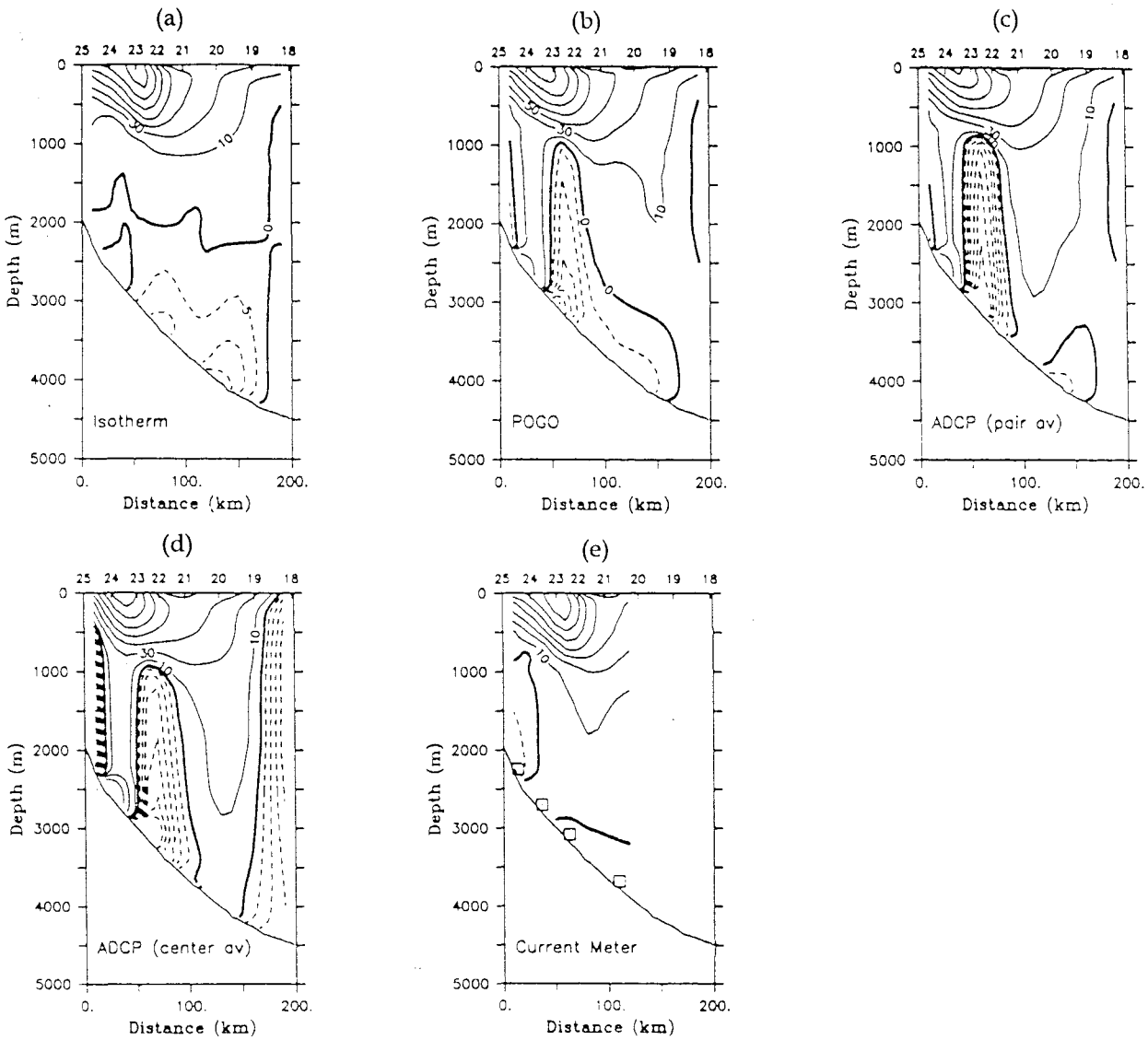


Figure 1.4 Sections of absolute geostrophic velocity in the North Atlantic deep western boundary current, referenced using five different techniques. Contour intervals are 10 to 150cms$^{-1}$ in 20cms$^{-1}$ increments and -30 to 0cms$^{-1}$ in 5cms$^{-1}$ increments. The five techniques are: (a) isotherm zero velocity surface at 3.5°C, (b) POGO floats, (c) ADCP pair-averaged, (d) ADCP centre-averaged, (e) bottom current meters. From Pickart & Lindstrom (1993).

measurement. Overall the POGO float was concluded to be the best method for referencing geostrophic velocities in deep water.

In summary, many techniques have been used to estimate geostrophic reference velocity, each resulting in somewhat different absolute geostrophic velocity fields. Pickart & Lindstrom's comparisons suggest that vertically integrated measurements of velocity down to great depth may be the most successful referencing method. Lowered Acoustic Doppler Current Profiler (LADCP) measurements offer such full depth integrated velocities and furthermore are more easily made in conjunction with hydrographic stations (see Chapter 2). Hence there is clearly an opportunity to improve geostrophic estimates using LADCP velocities.

### 1.4.3 The sensitivity of transport estimates to changes in the level of no motion

In November-December 1987 *RRS Charles Darwin* occupied a transindian hydrographic section nominally along latitude 32°S. At the beginning of the section eleven full depth stations were occupied in the Agulhas Current, between 2km and 250km off the coast of South Africa. The station line was oriented perpendicular to the continental slope so that the flow of the Agulhas Current should be normal to the section. Figure 1.5 shows the positions of the eleven stations across the Agulhas Current in relation to Africa and the local bathymetry. Toole & Warren (1993) give a detailed report of the results from the entire transindian section. The *Darwin* data has been used to investigate the variation of geostrophic volume transport with changes in the assumed level of no motion.

Geostrophic velocities were calculated at each station pair, for various horizontal reference levels from 1000db to 3500db in steps of 500db (figure 1.6). The velocities were then integrated across the section from the position of the first station pair to the pair farthest offshore in order to estimate geostrophic volume transport. No attempt has been made to fill bottom triangles between the data and the topography, even though the steep continental slope causes some data gaps. More than the entire range of volume transport estimates found in the literature and tabulated previously was obtained from just this one data set (table 1.2). In fact, using 1000db as a reference level, which was a common approximation in many of the early oceanographic studies of the Agulhas Current, yields a northward transport of more than 30Sv! This is due to the high vertical shears in the current core between 600 and 1200db (figure 1.6a) causing a shallow level of no motion to force a large northward transport at depth. However, most of the studies

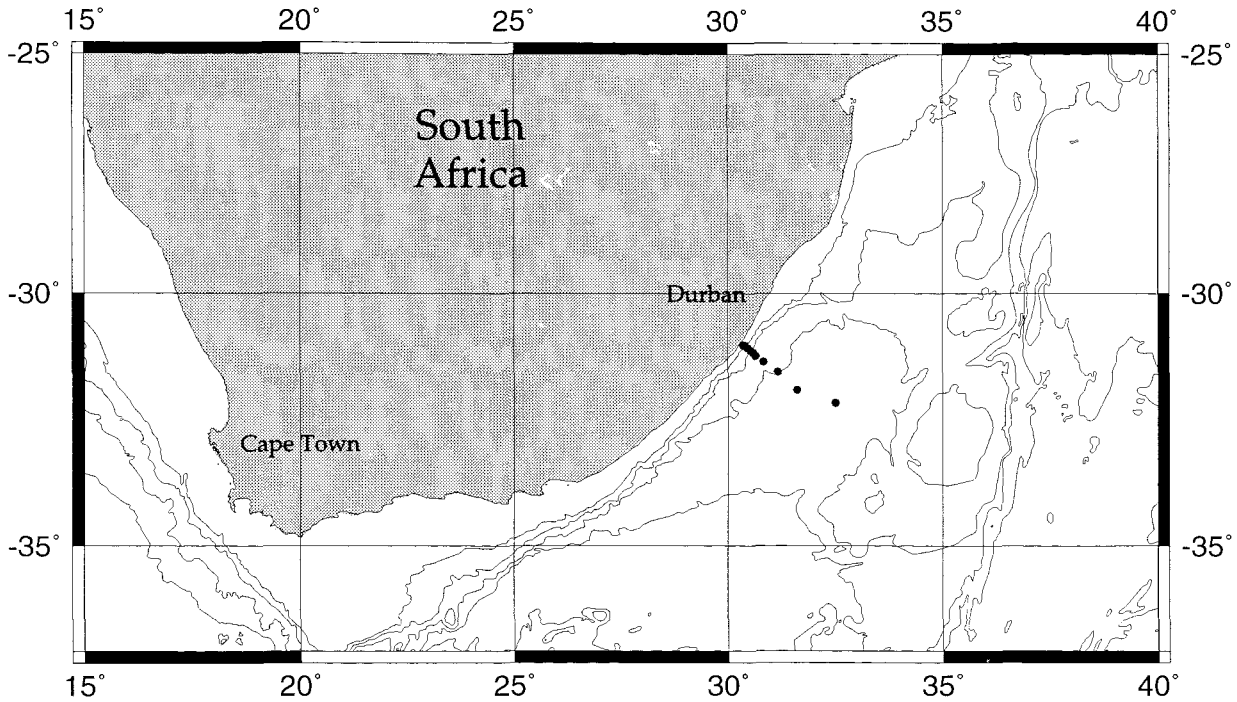


Figure 1.5 Bathymetric chart showing the positions of eleven stations across the Agulhas Current taken during November 1987 aboard RRS Charles Darwin as part of a transindian section along 32°S. Contours are at depth intervals of 1000m.

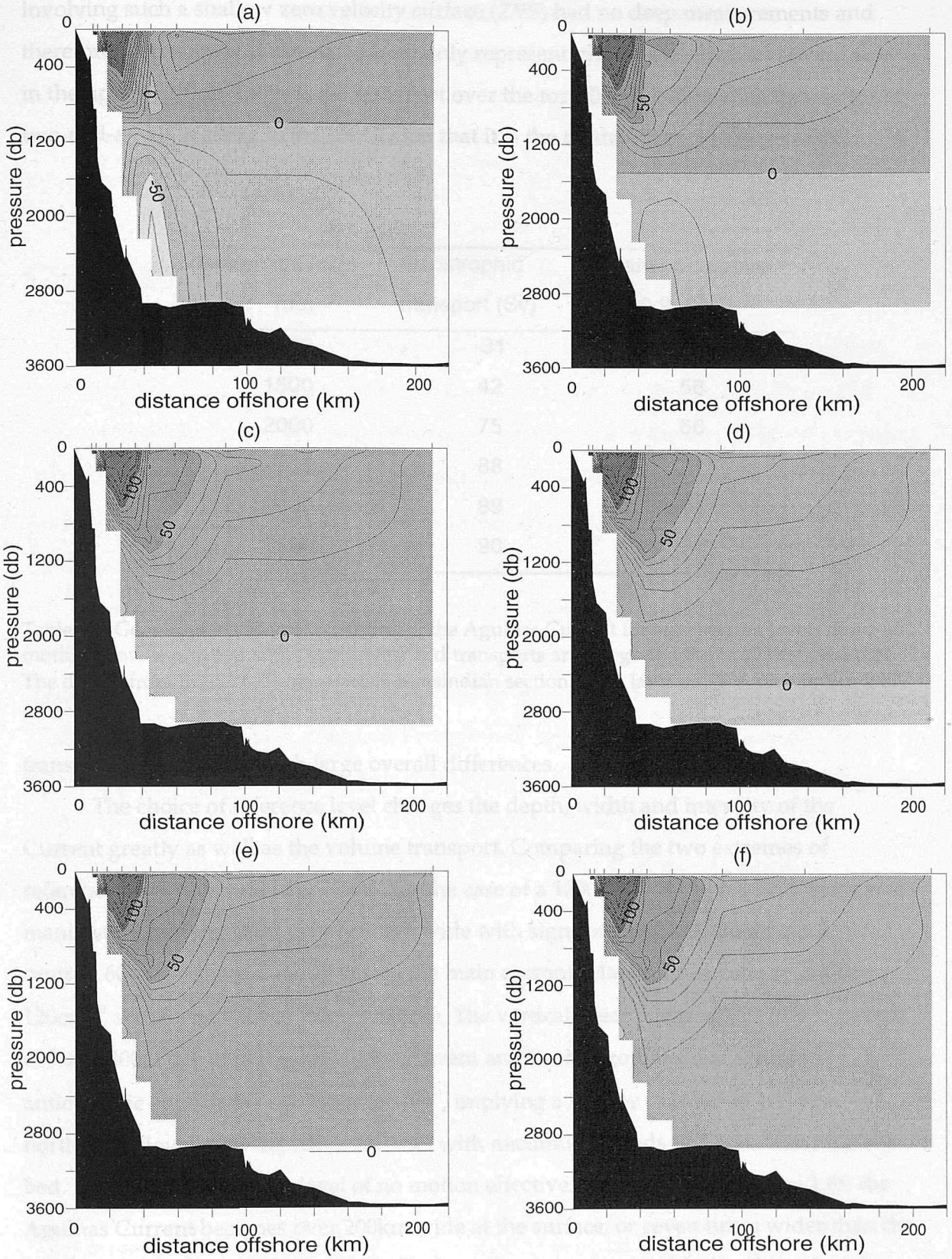


Figure 1.6 Geostrophic velocity of the Agulhas Current at 32°S in November 1987. Isotach intervals are every 10cms$^{-1}$ and the grey scale changes every 50cms$^{-1}$, the lightest shade represents speeds of more than 50cms$^{-1}$ north-eastward and the darkest represents speeds greater than 100cms$^{-1}$ to the south-west. The position of each station pair is marked along the top axis. Absolute geostrophic velocities are referenced to a zero velocity surface at (a) 1000db, (b) 1500db, (c) 2000db, (d) 2500db, (e) 3000db, and (f) 3500db.

involving such a shallow zero velocity surface (ZVS) had no deep measurements and therefore their transport estimates were only representative of the south-westward flow in the upper 1000db. Indeed, the transport over the top 1000db only varies by a factor of two-and-a-half, leading to the conclusion that it is the treatment of the deep water

| Reference level (db) | Geostrophic transport (Sv) | Transport above 1000db (Sv) |
|---|---|---|
| 1000 | -31 | 30 |
| 1500 | 42 | 56 |
| 2000 | 75 | 66 |
| 2500 | 88 | 71 |
| 3000 | 89 | 74 |
| 3500 | 90 | 74 |

Table 1.2 Geostrophic volume transports of the Agulhas Current for six different levels of no motion. Flow is positive to the south-west and transports are integrated out to 220km offshore. The data is from the *RRS Charles Darwin* transindian section along latitude 32°S, November 1987.

transport which causes such large overall differences.

The choice of reference level changes the depth, width and intensity of the Current greatly as well as the volume transport. Comparing the two extremes of reference level illustrates this point. For the case of a 1000db ZVS (figure 1.6a) the surface manifestation of the WBC is only 30km wide with signs of a weaker, shallower jet centred 60km offshore flowing beside the main current. Maximum speeds of just over 120cms$^{-1}$ are reached about 28km offshore. The vertical shear peaks at $2.5\times10^{-3}s^{-1}$ between 600 and 800m depth in the core of the current and the horizontal shear across the anticyclonic edge of the current is $8\times10^{-5}s^{-1}$, implying a Rossby number of 1.1. The northward flow below 1000db is intense, with maximum speeds of 70cms$^{-1}$ near the sea bed. In comparison, with a level of no motion effectively at the sea bed (figure 1.6f) the Agulhas Current becomes over 200km wide at the surface, or seven times wider than the WBC referenced to a ZVS at 1000db. The horizontal shears associated with the inshore edge of the current remain much the same, since the sea bed is shallower than 1000db within 20km of the coast, but the anticyclonic edge of the current is far broader and thus horizontal shears are reduced to $6\times10^{-6}s^{-1}$, implying a Rossby number of only 0.08, or over

ten times smaller than in the shallow ZVS case. Moreover, in contrast to the strong northward flow at depth that occurs when the ZVS is shallow, in the case of the deepest reference level there is no such flow at all. In conclusion the choice of reference level is critical, not only to obtain realistic transport estimates but also in order to study the dynamics and structure of the current.

## 1.5 Heat budget and overturning of the Indian Ocean north of 32°S

Both Toole & Raymer (1985) and Toole & Warren (1993) (hereafter TR and TW) have made direct (from oceanographic data) estimates of the net meridional heat flux across 32°S. Both studies use the method employed by Hall & Bryden (1982) in the North Atlantic. TR took the volume transport of the Agulhas Current to be 44Sv and estimated a net heat gain north of 32°S of 0.6PW. They found that 5Sv of the flux occurs below the 2.5°C surface and since the Indian Ocean is closed to the north at depths below 1000m this flux must upwell across isotherms. From this they estimated that the average basin-wide overturning rate is $1.3\times10^{-5}$cms$^{-1}$. TW estimated the net heat flux divergence of the Indian Ocean north of 32°S to be 0.98PW, taking an Agulhas Current volume transport of 85Sv and assuming an Indonesian throughflow of 6.7Sv. Their deep flow of 27Sv below 2000m depth corresponds to an upwelling rate of $6.9\times10^{-5}$cms$^{-1}$, or five times larger than TR's estimate. For comparison the overturning rate for the Pacific Ocean is estimated to be between 1.3 and $1.8\times10^{-5}$cms$^{-1}$ (TW). From air-sea exchange data Hastenrath & Lamb (1979) estimate the heat gained north of 30°S as 0.5PW and from Bunker data TR estimate 0.4PW. Warren (1981) found, from the 18°S transindian section, an average upwelling velocity of $4\times10^{-5}$cms$^{-1}$.

These figures all vary a great deal (and each involve large uncertainties), but most seem to support the more modest upwelling rate of TR. So why is the most recent estimate so high? It implies that the overturning rate in the Indian Ocean is 4 to 5 times that in the Pacific and no physical mechanism for its relative intensity has been suggested. It could be argued that TR do not consider the several Deep Western Boundary Currents that flank the three Ridge systems of the Indian Ocean, however Warren (1981) was aware of the high fluxes they may represent and his estimate for the overturning rate is only 60% of the TW value. Since the Agulhas Current transports used by TR and TW vary by a factor of two, it seems likely that this value is an important

component to the problem of determining the heat budget and the overturning of the Indian Ocean.

## 1.6 The aims of this study

The Agulhas Current is an integral part of the oceanography of the Indian Ocean and its intensity affects important heat and fresh water exchange. This is motivation enough to measure the Agulhas Current transport, but there have already been many estimates, so why is another needed? Although the Agulhas Current has been studied many times over two centuries, whilst its spatial characteristics have become comparatively well understood its deep vertical structure remains virtually unknown. Accurate measurements of its volume transport have been hampered by the lack of direct observations at depth. All previous transport estimates have relied on the geostrophic approximation in order that ocean currents be known for all depths and in most cases this has introduced large errors due to the difficulty in estimating an appropriate reference level. Grundlingh (1980) (Toole & Raymer, 1985 used Grundlingh's data) is the only one to have used direct surface current measurements to alleviate the reference level problem, but such measurements are not wholly appropriate due to the ageostrophic nature of the dynamics in the upper mixed layer. Now new technology is available, in the form of the LADCP, that can measure full depth velocity profiles which will improve and expand on previous measurements in the Agulhas Current.

The aim of this research is to improve on previous estimates of the volume transport of the Agulhas Current by using the first full depth section of direct velocity measurements to be made across it. The Lowered ADCP measurements were made during a one time hydrographic survey on board *RRS Discovery* in 1995. In addition this research aims to describe the water mass distribution in the Agulhas Current and estimate its heat and fresh water fluxes. The observations will be combined with the *RRS Charles Darwin* transindian section of 1987 to make new estimates of the heat flux divergence and the rate of thermohaline overturning in the Indian Ocean north of 32°S.

The field experiment on board *RRS Discovery* is described in the next chapter, as well as the new technique for taking deep velocity measurements, Lowered ADCP. Chapter 3 presents the hydrographic results and a traditional estimate of the geostrophic transport, to be compared to previous work by Toole & Warren (1993). In chapter 4 the

results from the direct velocity measurements are discussed and carefully compared with geostrophic estimates. Finally the heat and fresh water fluxes in the Agulhas Current and their effect on Indian Ocean overturning are estimated in chapter 5.

# CHAPTER TWO

# *DATA*

## 2.1 RRS *Discovery* cruise 214

### 2.1.1 Objectives

During 1995 the Indian Ocean was studied intensely as part of the World Ocean Circulation Experiment (WOCE). One UK contribution to this international program of cruises was to study the Agulhas Current, the most intense thermocline current of the Indian Ocean (Bryden *et al*, 1995). Although the Agulhas Current is probably second only to the Gulf Stream in transport, direct measurements of its overall size and temporal variability have not been made before. Additionally, geostrophic transport estimates have varied enormously, primarily due to the problem of objectively choosing a reference level (see previous chapter).

The primary objective for RRS *Discovery* cruise 214, the Agulhas Current Experiment (ACE), was to deploy an array of moored current meters across the Agulhas Current to collect data on its transport and temporal variability over the period of a year. The second objective was to make a closely spaced, full depth, section of hydrographic stations across the Agulhas Current in order to make a high quality synoptic transport estimate. It is this second objective with which this thesis is concerned, although the time series data is used to corroborate some of the results.

### 2.1.2 Data and instrumentation

The Agulhas Current Experiment took place between 26th February and 9th March 1995. The hydrographic section across the Agulhas Current starts on the South African continental shelf offshore of Port Edward at 31°S, about 120km down the coast from Durban. The section was oriented at 130°T to cross the steep bottom topography of the South African continental slope perpendicularly, so that the south-westward flow of the Agulhas Current should be normal to the cruise track (figure 2.1). This section was chosen, in the first instance, as the latitude at which the Agulhas Current is most narrow,

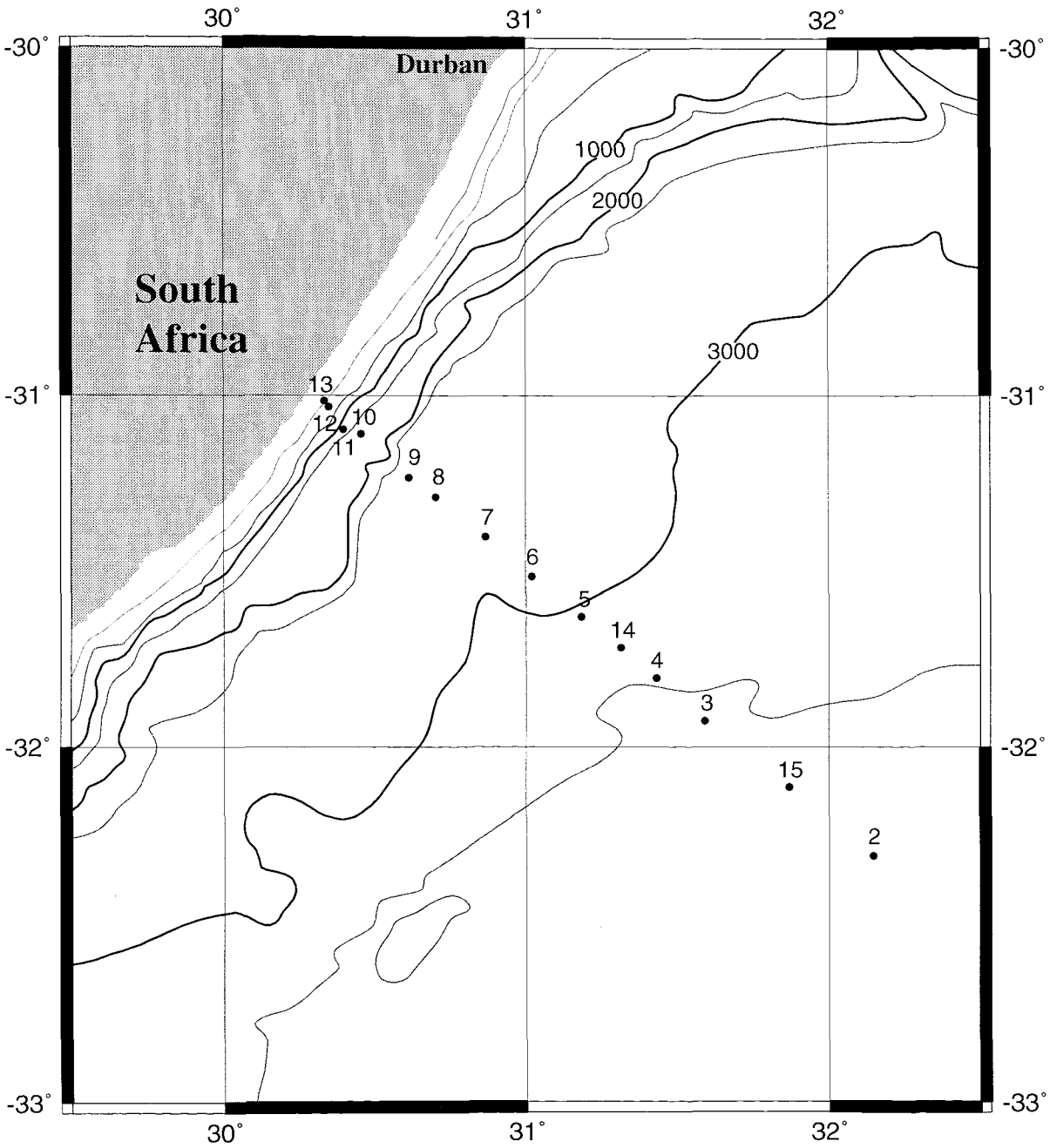


Figure 2.1 Hydrographic station positions from RRS *Discovery* cruise 214, the Agulhas Current Experiment (ACE). Bathymetric contours are shown for 100m, 200m, 500m and 1000m and thereafter in 500m intervals.

has a relatively stable path and flows closest to the shore and secondly as a repeat section of the RRS *Charles Darwin* stations taken in November 1987 (Toole & Warren, 1993).

An initial survey was conducted along the ACE section in order to define the near-surface structure of the Agulhas Current before deploying the moorings. A steady course was maintained along 130°T at a moderate speed of 5 knots to ensure good quality underway acoustic Doppler current profiler (ADCP) measurements. The survey also allowed for the collection of bathymetry data via a Precision Echo Sounding fish transducer and for the testing of the developmental ACCP (see below).

Subsequent to the initial survey, six moorings each comprising four current meters were deployed along the section. Hydrographic stations were taken either side of each mooring position with additional stations made onshore and offshore of the mooring array making fourteen hydrographic stations in all. The average station spacing is 19km and over the continental shelf and slope the station spacing averages only 10km. The station closest inshore is just over 6km from the coast in waters 50m deep. The station furthest offshore is 230km from the coast in waters of 3570m depth. At each station pressure, temperature, conductivity and oxygen were measured to full depth with a Neil Brown Mk III WOCE CTD and water bottle samples were collected for calibration from a 24×10 litre GO rosette (Bryden *et al*, 1995). Also at each station a Lowered ADCP measured instantaneous ocean currents to full depth. Near-surface ocean currents were measured continuously by a hull-mounted ADCP and a prototype Acoustic Correlation Current Profiler (ACCP) profiled currents to a depth of 1000m. The following section describes all of the acoustic techniques in more detail.

## 2.2 Acoustic techniques

To improve the estimate of absolute geostrophic velocities in the Agulhas Current, new and developing acoustic current profiling techniques were implemented during the cruise. Although a ship-mounted ADCP is now standard instrumentation for profiling ocean currents over the upper 350m of the ocean, during ACE two techniques were used to improve the accuracy of ADCP measurements by an order of magnitude in derived currents. Heading information from GPS-3DF was used to improve gyro-compass data (King & Cooper, 1993) and differential GPS (DGPS) navigation was used to improve positioning. These techniques are described in more detail in section 2.2.1.

An RD Instruments pre-production instrument called an Acoustic Correlation Current Profiler (ACCP) was on trial during ACE and is briefly described in section 2.2.2. The ACCP utilises a different physical principle for data collection to the ADCP and has the potential to profile ocean currents down to 1200m depth. The third acoustic technique is called Lowered ADCP (LADCP) in which an ADCP is mounted on the CTD frame and lowered through the water column at each station to give a full depth profile of the ocean currents (section 2.2.3).

### 2.2.1 Acoustic Doppler Current Profiler (ADCP)

The ADCP mounted in the hull of RRS *Discovery* is a 150kHz, broadband unit which profiles routinely to depths between 300 and 350m. Absolute ocean currents are derived from the vector difference between the ship's velocity over the ground, determined by GPS navigation, and the ship's velocity through the water, as measured by the ADCP and ship's gyrocompass. Both these components have been subject to large errors in the past, due to GPS signal dithering (as a result of deliberate military strategy) and inherent gyrocompass errors.

King & Cooper (1993) describe the use of GPS-3DF instrumentation to measure more accurate heading information than was possible with a gyrocompass, and their technique was used during ACE. They showed that when compared with headings from the ship's gyrocompass, GPS-3DF data is much steadier, particularly on station and up to an hour after leaving station when gyrocompass errors can be as large as 3° (Saunders & King, 1995a). The GPS-3DF (Ashtech) instrumentation on board *Discovery* consists of an array of four GPS receivers arranged at bridge level to measure the ship's roll, pitch and yaw. The ADCP cannot be interfaced directly with GPS-3DF heading data because the Ashtech data-stream is not continuous. Therefore a heading correction, taken as the difference between gyrocompass heading and GPS-3DF (or true) heading, was applied to the raw ADCP data after it had been combined with gyrocompass heading and logged in the usual way.

The dither in GPS positioning information is O(100m), which when used in underway ADCP ten-minute averaged velocities causes an error of O(10cms$^{-1}$). King *et al* (1996) first described the use of differential GPS (DGPS) navigation to improve positioning accuracy and therefore improve ADCP derived velocities. DGPS involves the use of stationary, land-based transducers of known position that enable the dithering of the GPS signal to be measured and removed and they estimated that it improved the

accuracy of underway measurements from O($10cms^{-1}$) to O($1cms^{-1}$). DGPS positioning data was collected during ACE and used to improve the standard GPS navigation data during post-processing. Subsequently the initial, continuous underway ADCP survey of the Agulhas Current described in the previous section was reprocessed. However the on-station ADCP data was not DGPS corrected.

### 2.2.2 Acoustic Correlation Current Profiler (ACCP)

The principle of operation of a correlation profiler is far more complex than a Doppler profiler (Griffiths *et al*, 1995): "...the objective in the correlation system, is to transmit two identical signals separated by a known time interval and then to search for a separation vector and a time delay for which the correlation (of the received signal) is a maximum." (Dickey & Edward, 1978). A prototype ACCP was fitted into the hull of RRS *Discovery* just prior to the cruise and two engineers from RD Instruments joined the cruise to operate it. The specifications for the instrument indicated that it would profile underway to a depth of 1200m. The trial was quite successful. The ACCP was functional and collected data throughout the cruise, although initial analysis by Griffiths *et al* (1995) revealed that the top 130 m of data and data below 1000 m suffered from low signal to noise ratios and was often discarded. No further use of the ACCP data is made in this thesis, since the instrument is very much developmental. Suffice to say that an initial comparison of the three acoustic techniques; ADCP, LADCP and ACCP is favourable and can be seen in the cruise report (Bryden *et al*, 1995) and in Griffiths *et al* (1995).

### 2.2.3 Lowered Acoustic Doppler Current Profiler (LADCP)

ACE was the first British experiment to utilise a Lowered ADCP and since it is a new technique to British oceanographers there is as yet no standard instrument setup, data path or processing procedure. Therefore more details on these aspects of the data collection are given in this section than was thought necessary for the ADCP section. Advice on the initial instrument settings and the data processing software for the LADCP were all provided by Dr. Eric Firing of the University of Hawaii.

The LADCP used during ACE was a 150kHz, self-contained, broadband ADCP with 20° beam angles. These wider beam angles reduce wake interference which can degrade the data during an upcast. The instrument and its battery packs are enclosed in a 1.2m long, 6000db pressure case in order to withstand the pressure cycling during a cast. The pressure case was mounted in the centre of a specially lengthened CTD frame,

0.2m below the rosette firing mechanism to allow for the turning radius of the end cable. The photographs in figure 2.2 show how the LADCP was mounted, with the transducer heads looking downward, in the extended frame.

The LADCP produced good quality data on all the hydrographic casts, except for the two inshore stations, 12 and 13, over the continental shelf which were each less than 100m deep. Poor data was due to the combination of a long blank after transmit (no data is collected within 30m of the transducer heads) and a 30m-thick bottom interference layer, both these effects could have been reduced by using a shorter bin length. For these stations the ship-mounted ADCP provides full depth velocity profiles. The LADCP was programmed to collect bottom tracking (BT) data on four stations out of the fourteen. The first pair of BT stations, 10 and 11, are in the core of the current, over the continental slope and the last two, stations 14 and 15, are in deep, relatively slow moving water towards the end of the section. More details about BT and the advantages and draw-backs of the technique are given in the section 2.2.3.4.

2.2.3.1 Deployment and Recovery

The LADCP parameters, such as ping rate, ensemble length, water tracking mode and bottom tracking are set up for each cast before deployment using standard PC based RD Instruments ADCP software. The set up is communicated from PC to the instrument via cable. Most of the instrument parameters used, such as bin length and time per ensemble were those recommended by Firing through his early experience with LADCP. Some parameters were set specifically with the high velocity environment of the Agulhas Current in mind, for example water tracking mode and ambiguity velocity. Some settings were experimental, for instance the use of BT. For details of instrument set up see appendix 1.

The communication cable is then disconnected from the instrument and replaced with a blank to seal out the sea water during deployment. No communication with the LADCP is possible for the duration of the cast. At the end of the cast the data is recovered to PC and written into a database. The details of instrument deployment and recovery are given in appendix 2.

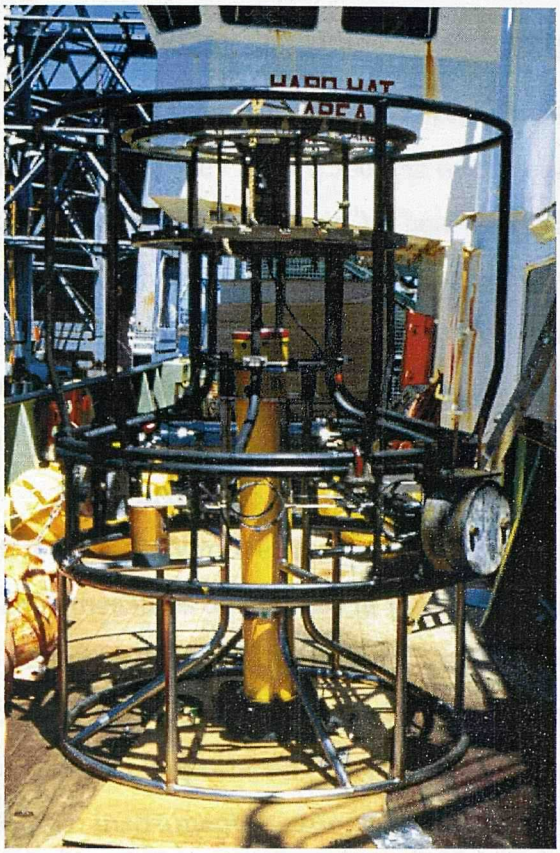

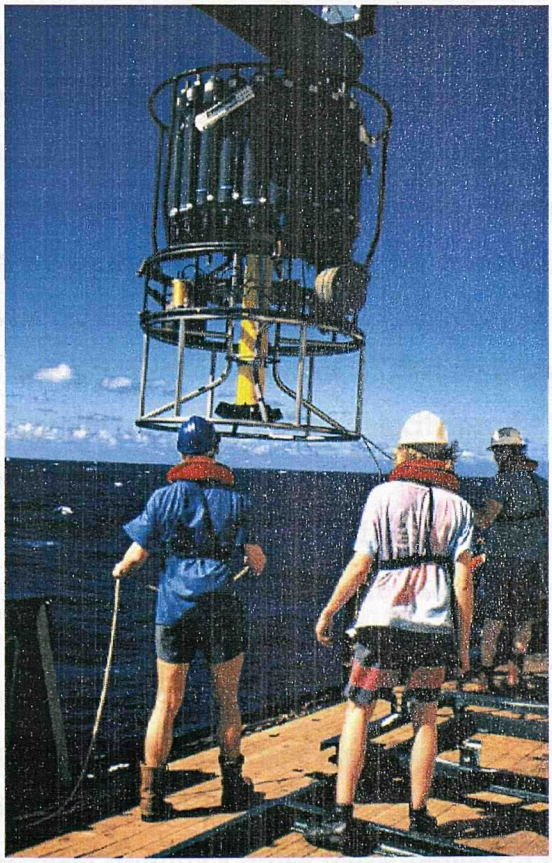

Figure 2.2 Photographs of the LADCP in the extended frame.

Top left shows the LADCP mounted in the special frame before the sample bottles are added

Top right is a close up of the transducer heads of the LADCP.

Bottom left shows a deployment of the package from the starboard deck of RRS *Discovery*. The deck railings were removed during deployment due to the unusually tall frame.

2.3.3.2 Data handling - obtaining absolute velocities from a moving instrument

The first scientists to use an ADCP for deep velocity profiling were Firing & Gordon (1990). They used a 300kHz narrow band instrument to obtain relative velocities with working errors O(10cms$^{-1}$). Their method has since been extended by Fischer & Visbeck (1993) to give absolute velocities. Subsequently Firing has reduced errors further by the use of a broadband ADCP and by the incorporation of CTD data into the processing method. During ACE all the LADCP data processing was achieved using Firing's software.

As an LADCP is lowered through the water column during each hydrographic cast, it essentially moves independently of the ship below about 200m depth. The LADCP measures its attitude in the water using heading and tilt sensors and therefore the vector property of the measured velocity is known (local magnetic deviation is used to correct the velocities to true compass direction). However, the instrument cannot measure the component of the measured velocity that is due to its own motion. This unknown instrument motion causes a unique problem to LADCP users, since it must be removed from measured velocities in order to obtain the real ocean currents.

Thus the raw velocity measurements are a combination of the motion of the instrument and the ocean currents, but while the ocean currents may change over the depth range of a single ping velocity profile (or ensemble, typically 200-250m), the instrument velocity contribution will be the same throughout the profile; in other words it has no vertical shear in an individual ensemble. The diagram in figure 2.3 illustrates this. By vertically differentiating the horizontal velocities over each ensemble the unwanted instrument velocity can be removed, but calculating the shears also eliminates the mean current component, so that on integrating all the shears over the full depth of the cast the resulting relative velocity profile has an unknown mean or barotropic component.

There are a number of different ways to estimate the barotropic component of the ocean current and thus obtain absolute velocities from LADCP measurements. Shipboard ADCP measurements can be used to adjust the LADCP relative velocities close to the surface, but this method does not provide a depth integrated mean component, only a surface approximation. Alternatively the LADCP can be set up to collect bottom tracking data (see appendix 1) during the cast. Bottom tracked velocities effectively provide a direct measurement of the movement of the LADCP relative to the

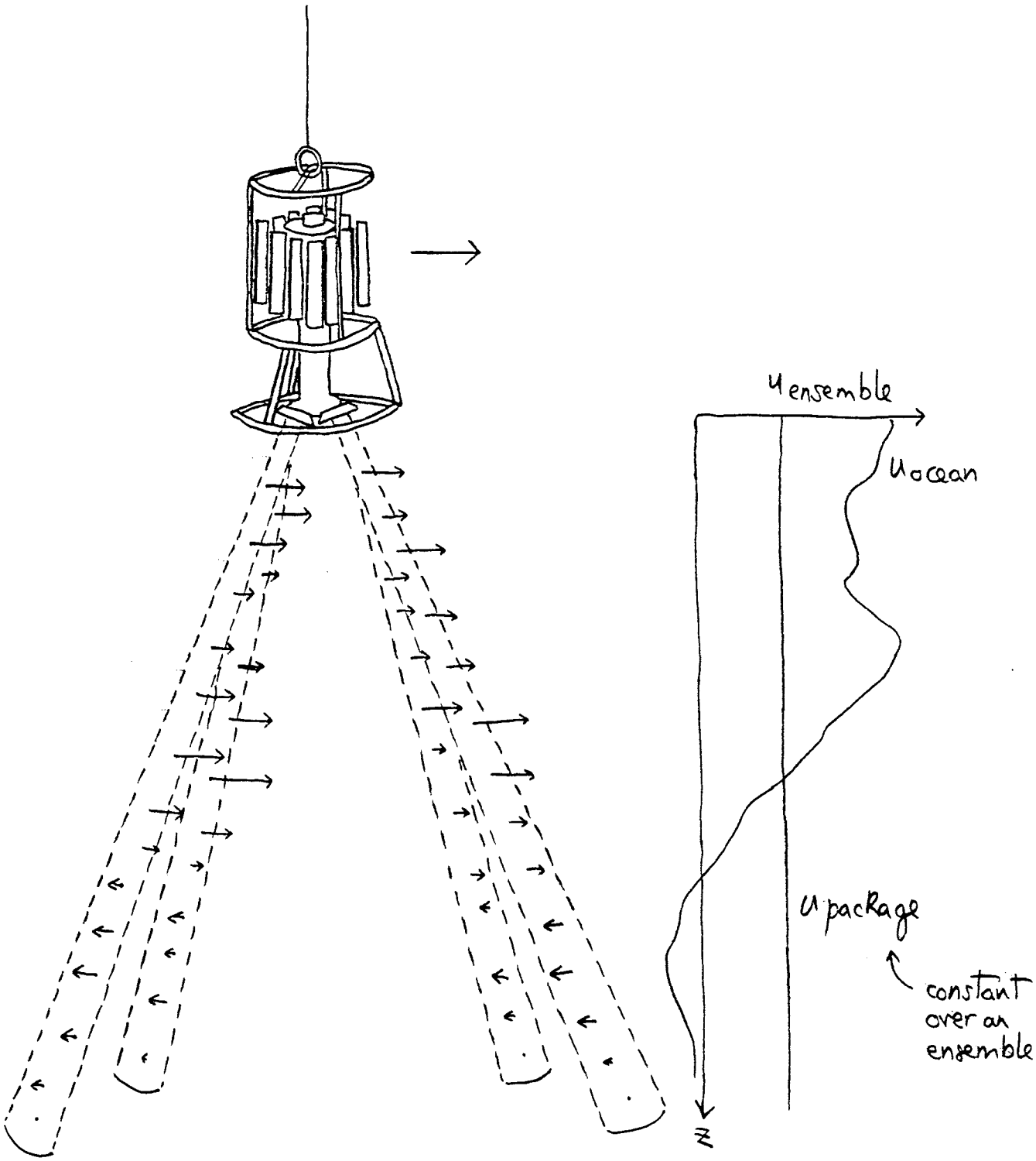


Figure 2.3 A cartoon showing what the LADCP is measuring on each ping. The instrument profiles about 300m of the water column on each ping; this is an ensemble. The velocities are collected in bins of length 16m and each velocity contains a component from the ocean current plus a component from the motion of the instrument itself. The component of velocity due to the motion of the instrument must be the same in each bin of an ensemble, therefore by differentiating the measured velocities over an ensemble the motion of the instrument is removed. The ensemble shears are then strung together, demeaned and integrated up over the complete depth of the cast to give relative velocities.

sea bed so that by vector addition with the observed horizontal velocities, the absolute ocean current can be calculated. Unfortunately there is one major draw-back to operating the LADCP with BT pings.

In practice, due to signal attenuation, the sea bed can only be tracked from about 400m altitude at best, however bottom tracking must be switched on (or off) for the whole of a cast since the LADCP is self-contained and cannot be reprogrammed during a deployment. Each bottom tracking (BT) ping has a duration of about 1s (in order that sufficient energy is transmitted into the water), whereas a water tracking (WT) ping has a duration of only half a second. Therefore, in order to accommodate one BT ping and one WT ping per ensemble, the ensemble time must be more than twice as long as it is to accommodate WT pings alone. This leads to a decrease in the number of independent water velocity measurements collected which in turn leads to an increase in the standard deviation (SD) of these measurements by a factor of about $\sqrt{2}$ throughout the water column. Despite the disadvantage four stations during ACE used BT data as an attempt to estimate the accuracy of absolute LADCP velocities, since it is a relatively new technique. The results are described in section 2.2.3.4 together with results from a comparison of near-surface currents as measured by LADCP and shipboard ADCP.

The method for obtaining absolute currents as proposed by Fischer & Visbeck (1993), is the single method that effectively gives a depth integrated barotropic velocity. It is also the primary method used for processing all the LADCP data during ACE. Basically, when the measured velocity is integrated over the period of the cast the high frequency instrument motion vanishes and the barotropic current can be determined. This idea is explained in detail below:

The velocity measured by the LADCP can be written as three components; the baroclinic component (from velocity shear) and the unknown barotropic component of the ocean current, plus an unknown component from the motion of the LADCP through the water:

$$U_{measured}(t) = U_{barotropic} + U_{baroclinic}[z(t)] - U_{LADCP}(t) \qquad 2.1$$

The motion of the LADCP can also be broken down into components: the movement of the ship relative to the ground plus the motion of the instrument relative to the ship.

$$U_{LADCP} = U_{ship} + U_{instrument} \qquad 2.2$$

The first component of equation 2.2 is determined from GPS positioning data, leaving the second component still unknown. However, by integrating equation 2.1 in time over the period of the whole cast $T$, $\int_0^T U_{instrument}\, dt$ vanishes because the instrument must begin and end the cast at the ship. Hence $U_{barotropic}$ can be determined,

$$U_{barotropic} = \frac{1}{T}\left\{\int_0^T U_{measured}(t)\, dt - \int_0^T U_{baroclinic}[z(t)]\, dt + \int_0^T U_{ship}\, dt\right\} \qquad 2.3$$

and finally the absolute ocean current is given by,

$$U_{ocean}(t) = U_{baroclinic}[z(t)] + U_{barotropic}. \qquad 2.4$$

The barotropic component is calculated in this way as an integral part of the processing of LADCP data in Firing's software. When absolute currents from LADCP are given in the following chapters they have been determined using this method. For a discussion on the accuracy of this method see section 2.2.3.4, where absolute velocities from the LADCP are compared to shipboard ADCP and BT determined absolute velocities.

The LADCP data processing is typically done in two passes. The first pass is a quick, preliminary calculation of the relative velocities using only the measurements made by the LADCP itself. The second pass adds information from the CTD and GPS data streams to refine the data and calculate the barotropic component as above. For the first pass the depth of the LADCP is calculated by a time integration of the vertical velocity where the integration for down and up casts is constrained to add up to zero and the speed of sound in sea water is assumed constant ($1500 ms^{-1}$). An example of the standard output from the first pass is shown in figure 2.4. The down, up and mean profiles of the u and v components of relative (de-meaned) velocity are plotted, together with profiles of the number of samples taken and the standard deviation (SD) of the shear. The shear SD is a function of the quality of the signal return only, so that one can expect the SD to increase in regions of high interference (such as 750m above the bottom for 1s ensembles, due to bottom reflection of the previous ping) and in regions where scatterers are scarce; it is not a function of the number of samples.

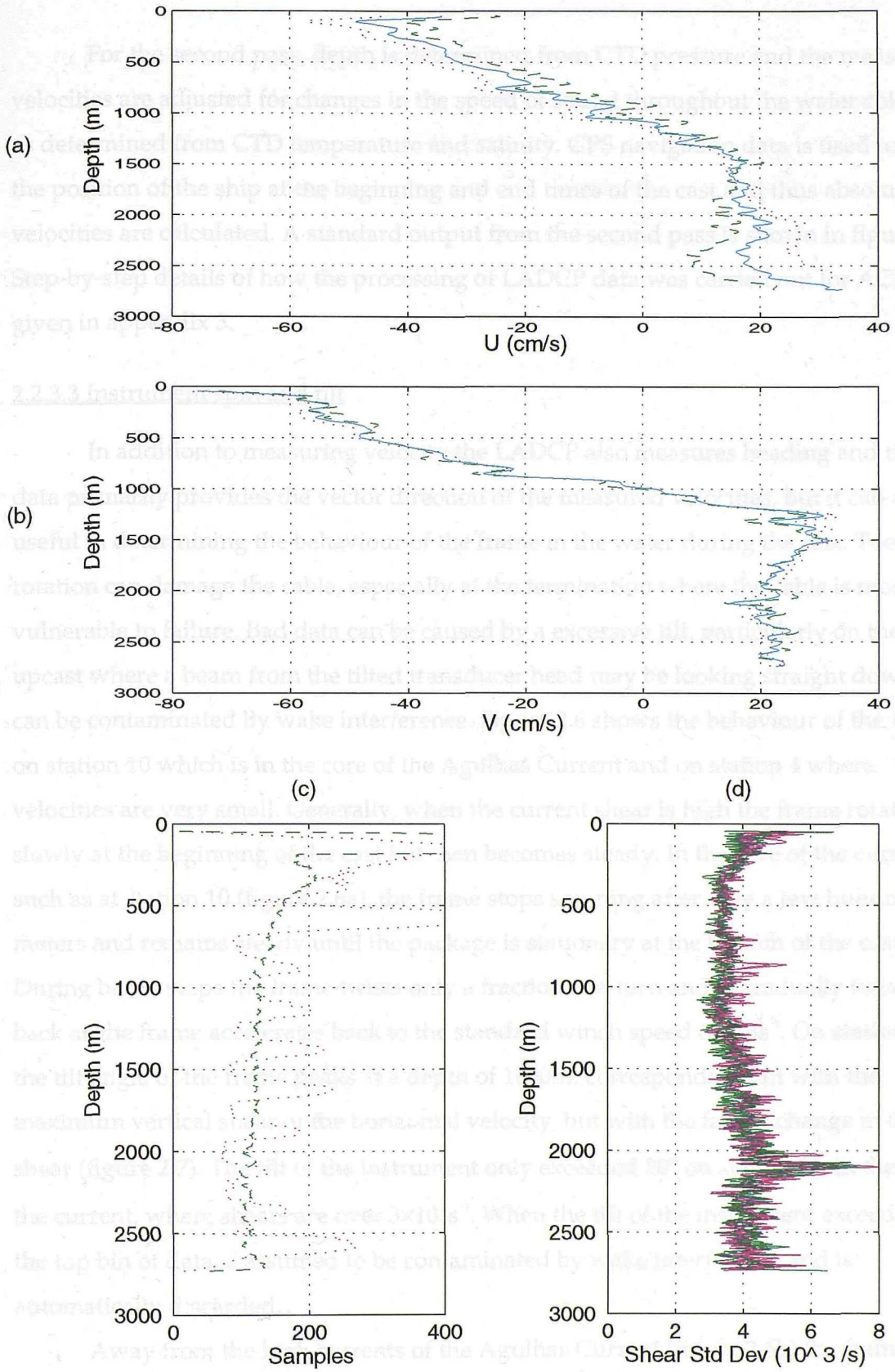


Figure 2.4 First pass LADCP data from station 9. Green is downcast data, pink is upcast data and blue is the mean of the up and downcast velocities. (a) Relative eastward velocities, (b) relative northward velocities, (c) number of samples taken per 5m bin, (d) standard deviation of the shears (note the large standard deviations about 750m off the bottom of the cast - this is due to bottom interference from the previous ping). Station 9 was set up with 1s ensembles and no bottom tracking pings. (see appendix 1 for more details of instrument configuration).

For the second pass, depth is determined from CTD pressure and the measured velocities are adjusted for changes in the speed of sound throughout the water column, as determined from CTD temperature and salinity. GPS navigation data is used to give the position of the ship at the beginning and end times of the cast and thus absolute velocities are calculated. A standard output from the second pass is shown in figure 2.5. Step-by-step details of how the processing of LADCP data was carried out for ACE is given in appendix 3.

2.2.3.3 Instrument spin and tilt

In addition to measuring velocity the LADCP also measures heading and tilt. This data primarily provides the vector direction of the measured velocities, but it can also be useful in determining the behaviour of the frame in the water during the cast. Too much rotation can damage the cable, especially at the termination where the cable is most vulnerable to failure. Bad data can be caused by a excessive tilt, particularly on the upcast where a beam from the tilted transducer head may be looking straight down and can be contaminated by wake interference. Figure 2.6 shows the behaviour of the frame on station 10 which is in the core of the Agulhas Current and on station 4 where velocities are very small. Generally, when the current shear is high the frame rotates slowly at the beginning of the cast but then becomes steady. In the core of the current, such as at station 10 (figure 2.6a), the frame stops spinning after only a few hundred meters and remains steady until the package is stationary at the bottom of the cast. During bottle stops the frame twists only a fraction of a turn and is gradually twisted back as the frame accelerates back to the standard winch speed of $1ms^{-1}$. On station 10 the tilt angle of the frame peaks at a depth of 1000m, corresponding not with the maximum vertical shear of the horizontal velocity, but with the fastest change in the shear (figure 2.7). The tilt of the instrument only exceeded 20° on station 11, in the core of the current, where shears are over $3\times10^{-3}s^{-1}$. When the tilt of the instrument exceeds 20° the top bin of data is assumed to be contaminated by wake interference and is automatically discarded.

Away from the high currents of the Agulhas Current (figure 2.6b) the frame generally spins clockwise once or twice during a downcast and then many times on the upcast during the bottle stops, in an anti-clockwise direction. The magnitude of the tilt of the instrument is small, about 2°, and mostly consistent with depth.

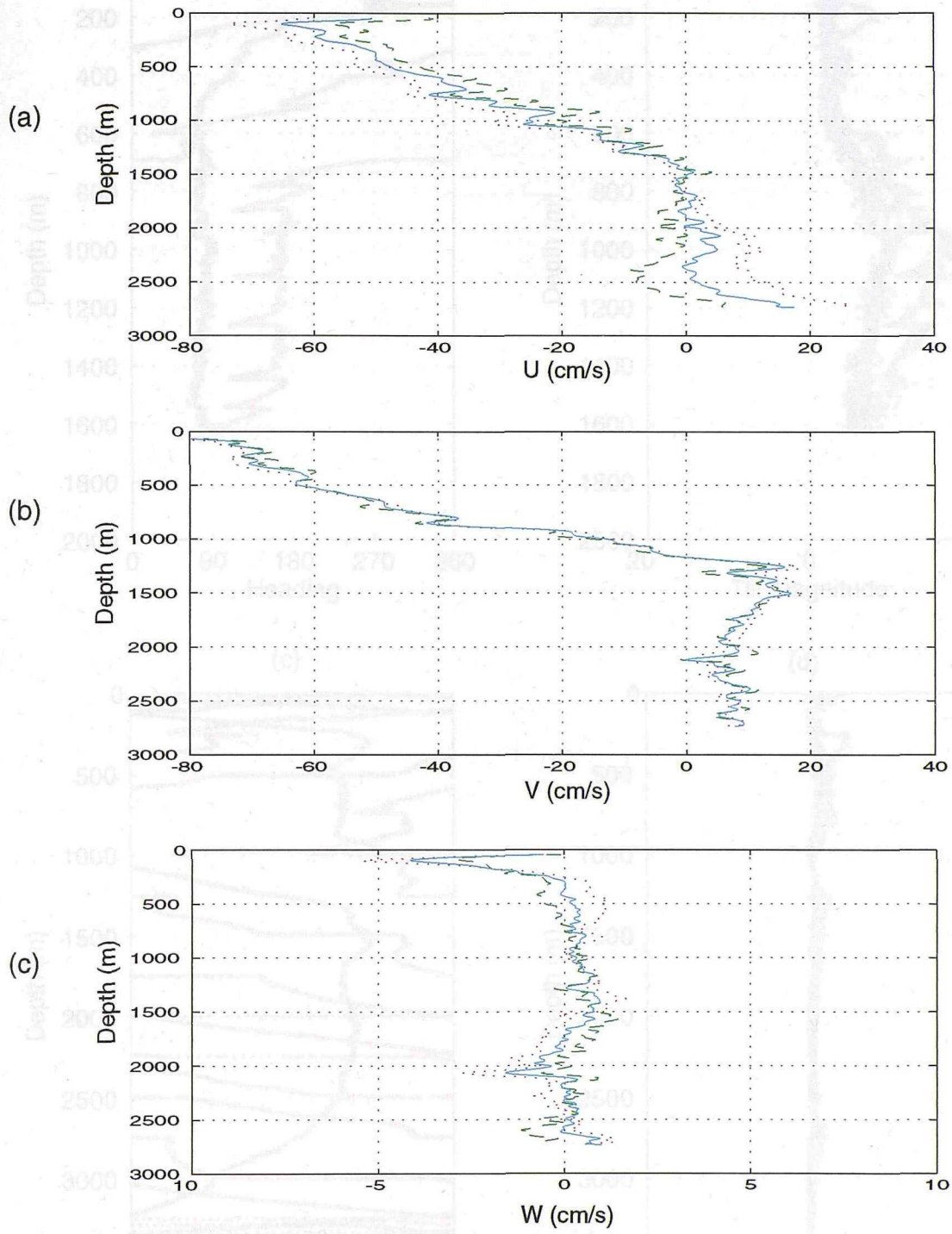


Figure 2.5 Second pass LADCP data from station 9. Green is downcast data, pink is upcast data and blue is the mean of the up and downcast velocities. (a) absolute eastward velocities, (b) absolute northward velocities, (c) vertical velocities. Notice that removing the on-station ship drift from the relative velocities (figure 2.4) acts to enhance the south-westward WBC flow, as would be expected. Although vertical velocity is shown here as an example of LADCP output the signal to noise ratio is so small that the data has not been considered during this work.

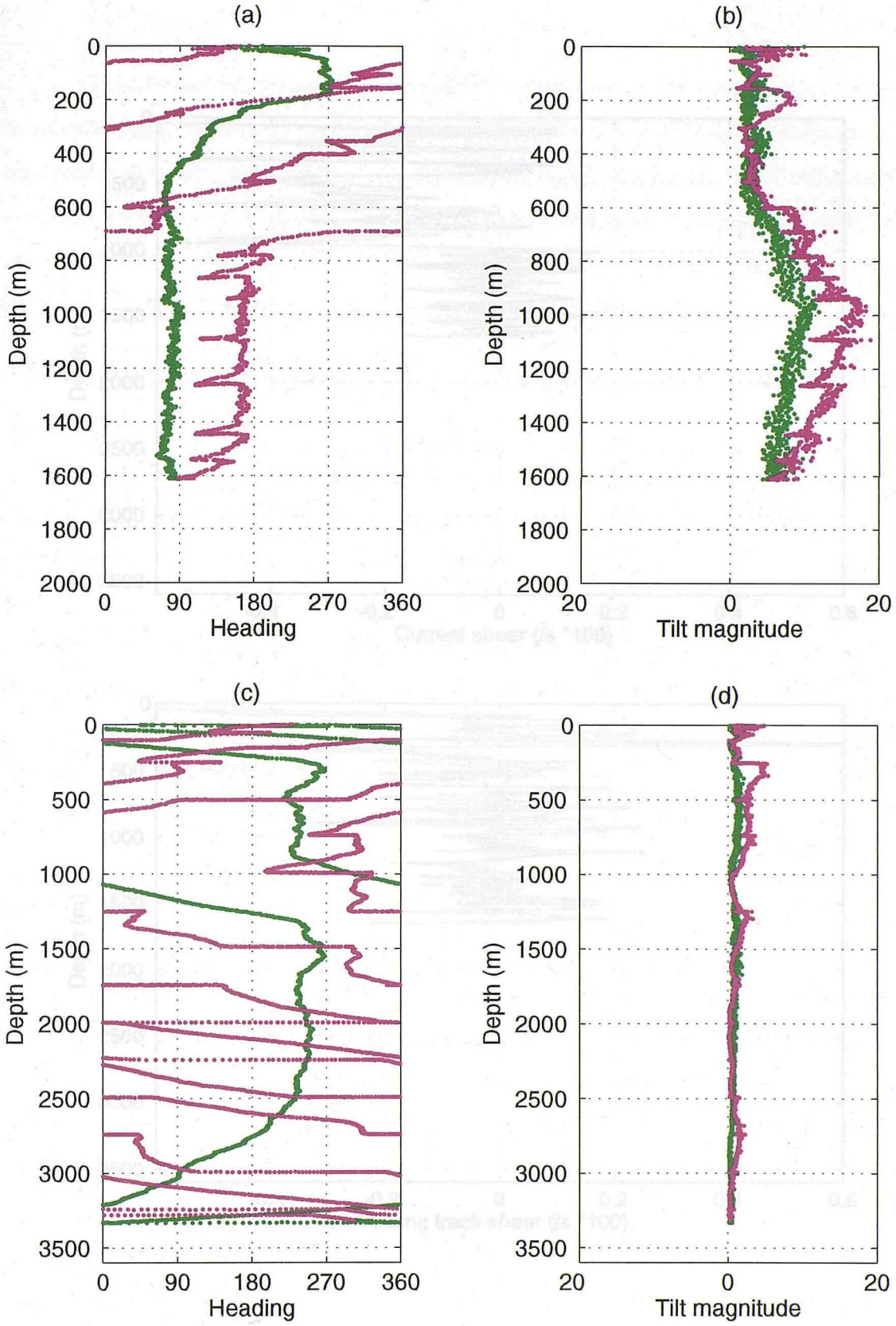


Figure 2.6 Spin and tilt of the LADCP during the downcast (green) and the upcast (pink). Heading and tilt are given in degrees. (a) station 10 heading, (b) station 10 tilt angle, (c) station 4 heading and (d) station 4 tilt angle.

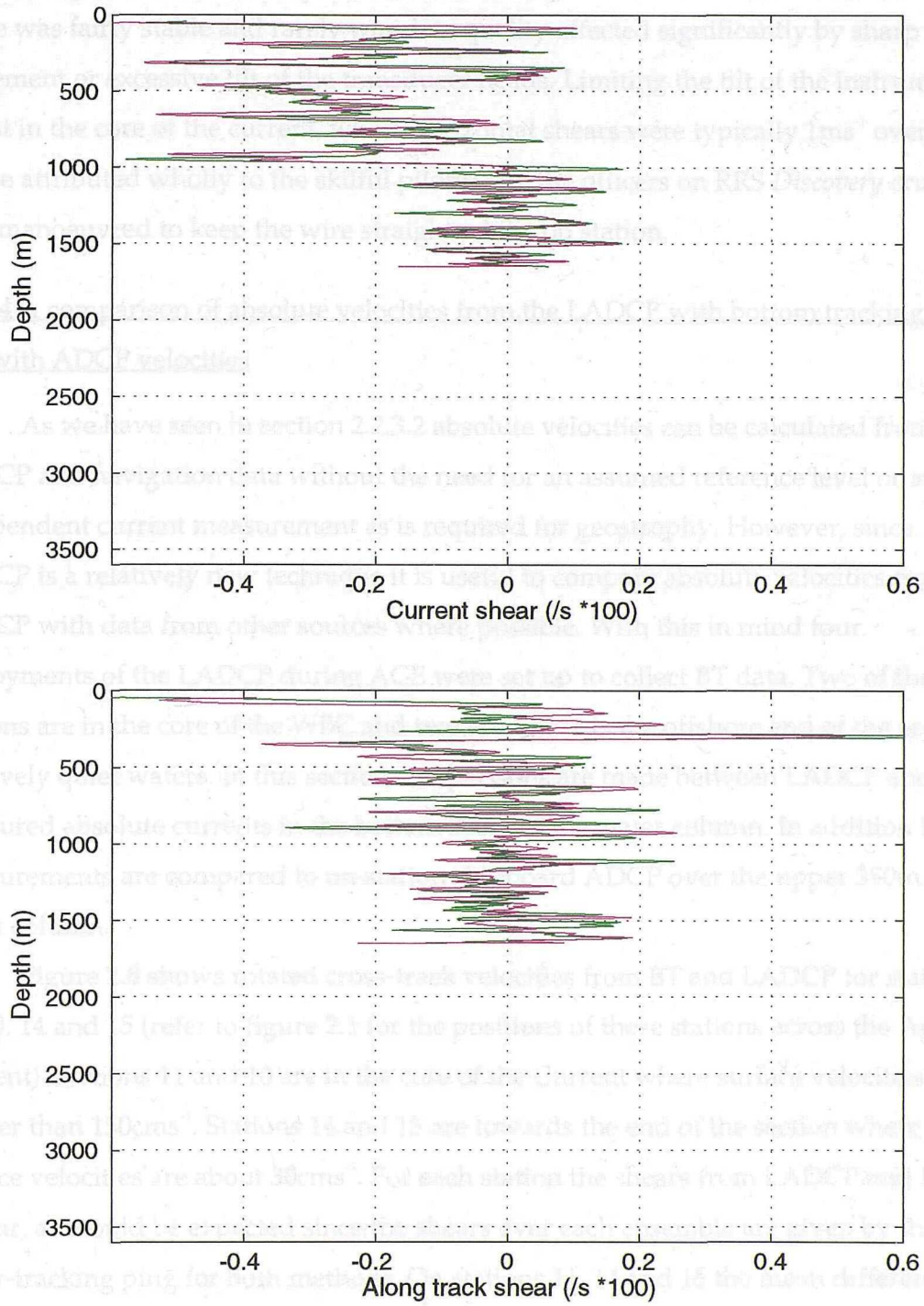


Figure 2.7 LADCP shears from station 10 rotated to cross-track (130°T, positive offshore) and along-track (220°T, positive downstream) components. The green line is the downcast shear, pink is the upcast shear.

Considering the dynamic environment encountered in the Agulhas Current the frame was fairly stable and rarely was data quality affected significantly by sharp movement or excessive tilt of the transducer heads. Limiting the tilt of the instrument whilst in the core of the current, where horizontal shears were typically $1ms^{-1}$ over 300m can be attributed wholly to the skilful piloting by the officers on RRS *Discovery* cruise 214 who manoeuvred to keep the wire straight whilst on station.

2.2.3.4 A comparison of absolute velocities from the LADCP with bottom tracking data and with ADCP velocities

As we have seen in section 2.2.3.2 absolute velocities can be calculated from LADCP and navigation data without the need for an assumed reference level or an independent current measurement as is required for geostrophy. However, since LADCP is a relatively new technique it is useful to compare absolute velocities from LADCP with data from other sources where possible. With this in mind four deployments of the LADCP during ACE were set up to collect BT data. Two of the stations are in the core of the WBC and two are towards the offshore end of the section in relatively quiet waters. In this section comparisons are made between LADCP and BT measured absolute currents in the bottom 300m of the water column. In addition LADCP measurements are compared to on-station shipboard ADCP over the upper 350m of the water column.

Figure 2.8 shows rotated cross-track velocities from BT and LADCP for stations 11, 10, 14 and 15 (refer to figure 2.1 for the positions of these stations across the Agulhas Current). Stations 11 and 10 are in the core of the Current where surface velocities are greater than $150cms^{-1}$. Stations 14 and 15 are towards the end of the section where surface velocities are about $30cms^{-1}$. For each station the shears from LADCP and BT are similar, as would be expected since the shears over each ensemble are given by the same water-tracking ping for both methods. On stations 11, 14 and 15 the mean difference, *ie* the barotropic displacement, has magnitude less than $4cms^{-1}$, but station 10 shows a mean difference between LADCP and BT of $9.6cms^{-1}$. There seems to be no obvious reason why the error in the LADCP absolute velocities should be larger for station 10. The GPS data for station 10 has no jumps or gaps and the down and up LADCP profiles are very similar. There are three stations (7, 8 and 9) that have bottom velocities from down and up profiles more than $10cms^{-1}$ apart and six in all, including station 14, that have a jump of more than $5cms^{-1}$ between down and up bottom velocities. However on

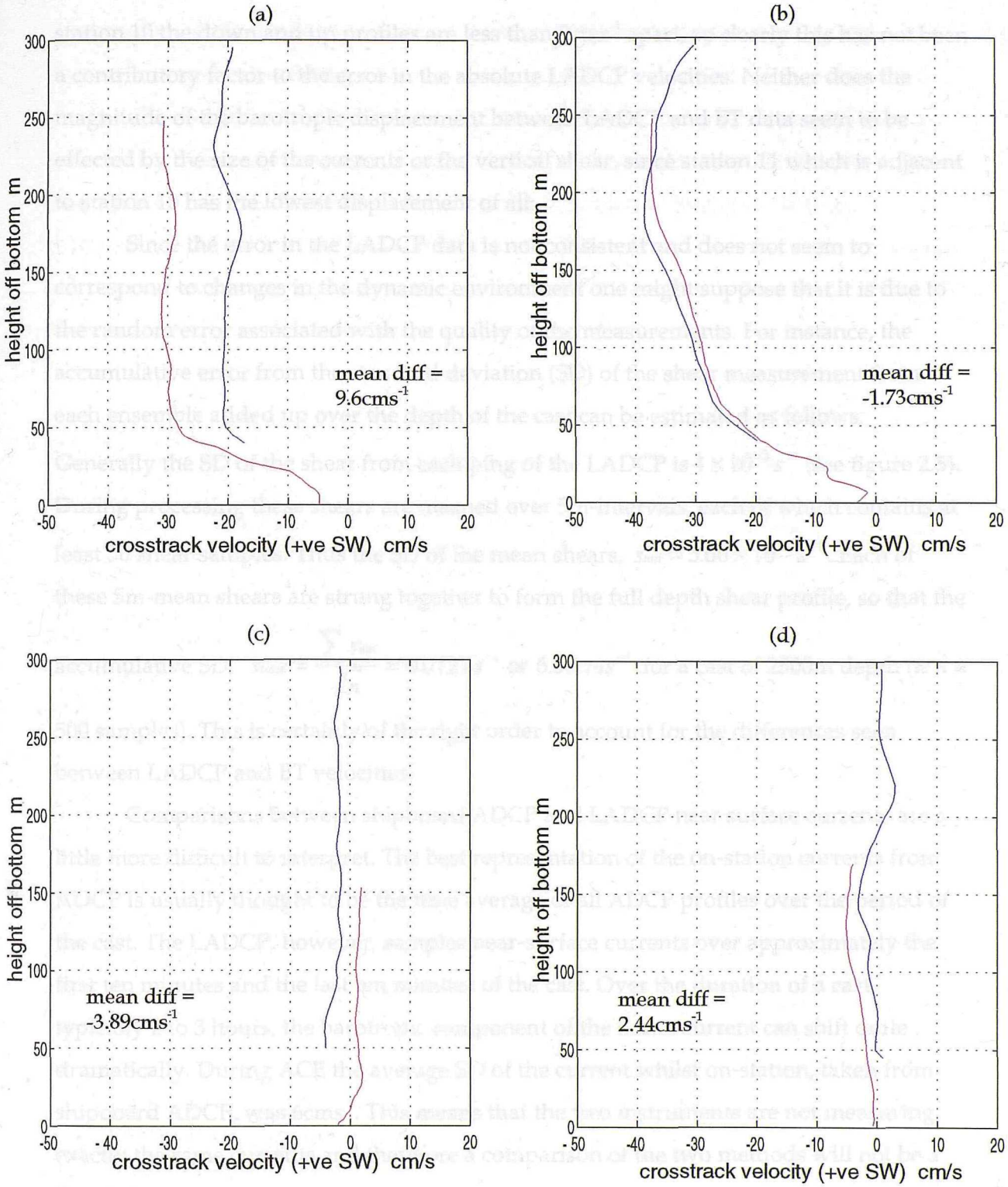


Figure 2.8 Cross-track component of LADCP and bottom-tracked absolute velocities. Blue data is LADCP, pink data is bottom-tracking data. (a) Station 10, (b) station 11, (c) station 14, (d) station 15. The depth-averaged difference or offset between the two techniques is given on each graph.

station 10 the down and up profiles are less than 2cms$^{-1}$ apart, so clearly this has not been a contributory factor to the error in the absolute LADCP velocities. Neither does the magnitude of the barotropic displacement between LADCP and BT data seem to be effected by the size of the currents or the vertical shear, since station 11 which is adjacent to station 10 has the lowest displacement of all.

Since the error in the LADCP data is not consistent and does not seem to correspond to changes in the dynamic environment one might suppose that it is due to the random error associated with the quality of the measurements. For instance, the accumulative error from the standard deviation (SD) of the shear measurement from each ensemble added up over the depth of the cast can be estimated as follows. Generally the SD of the shear from each ping of the LADCP is $4 \times 10^{-3} s^{-1}$ (see figure 2.5). During processing these shears are meaned over 5m-intervals, each of which contains at least 50 shear samples. Thus the SD of the mean shears, $s_{mn} = 5.66 \times 10^{-4} s^{-1}$. Each of these 5m-mean shears are strung together to form the full depth shear profile, so that the accumulative SD, $s_{total} = \frac{\sum s_{mn}}{\sqrt{n}} = 0.0127 s^{-1}$ or $6.33 cms^{-1}$ for a cast of 2500m depth (*ie* $n$ = 500 samples). This is certainly of the right order to account for the differences seen between LADCP and BT velocities.

Comparisons between shipboard ADCP and LADCP near surface currents are a little more difficult to interpret. The best representation of the on-station currents from ADCP is usually thought to be the time average of all ADCP profiles over the period of the cast. The LADCP, however, samples near-surface currents over approximately the first ten minutes and the last ten minutes of the cast. Over the duration of a cast, typically 2 to 3 hours, the barotropic component of the ocean current can shift quite dramatically. During ACE the average SD of the current whilst on-station, taken from shipboard ADCP, was 6cms$^{-1}$. This means that the two instruments are not measuring exactly the same currents and therefore a comparison of the two methods will not be a direct one.

A mean from the first and last on-station ADCP profiles may provide a more direct comparison to the LADCP profiles. However this would be a comparison of two techniques, rather than an evaluation of the performance of the LADCP in measuring 'real' currents. Of course, the ADCP is not error free and does not provide the 'real' current, but there is one reason why it should produce more accurate data than the LADCP. Whilst on station the ADCP can take about 12 ten-minute averaged profiles

(depending on the depth and therefore duration of the cast) thus improving any errors in the measured velocities by a factor of $\sqrt{12}$.

The shears from LADCP and ADCP are no longer exactly equivalent as was the case for LADCP and BT. Figure 2.9 shows cross-track LADCP and ADCP near-surface currents for the same four stations as appear in figure 2.8 so that the barotropic displacement of the LADCP from both BT and ADCP can be compared easily. However, all stations were considered to examine the differences between LADCP and ADCP absolute velocities and the results are summarised in table 2.1.

| | cross-track | | | along-track | | |
|---|---|---|---|---|---|---|
| **station number** | LADCP - ADCP | LADCP - BT | difference | LADCP - ADCP | LADCP - BT | difference |
| **11** | -1.4 | -1.7 | 0.3 | 5.2 | -11.4 | 16.6 |
| **10** | 5.8 | 9.6 | 3.8 | 1.8 | -10.4 | 12.2 |
| **9** | 1.5 | | | 1.8 | | |
| **8** | -2.3 | | | 4.1 | | |
| **7** | 3.4 | | | -0.3 | | |
| **6** | 2.4 | | | 1.1 | | |
| **5** | -0.1 | | | -0.6 | | |
| **14** | 3.6 | -3.9 | 7.5 | 3.5 | -3.6 | 7.1 |
| **4** | 4.0 | | | -2.5 | | |
| **3** | 3.9 | | | 3.2 | | |
| **15** | 2.2 | 2.4 | 0.2 | -4.4 | 8.6 | 13 |
| **2** | -2.4 | | | -0.2 | | |

Table 2.1 Mean difference between LADCP and ADCP velocity profiles and between LADCP and BT velocity profiles where available, both in $cms^{-1}$. Cross-track and along-track differences are shown.

With the exception of station 10 all stations show that the depth-mean difference between the two techniques is $4cms^{-1}$ or less. Station 10 has a mean difference of $5.8cms^{-1}$. Of the four BT stations three indicate that the barotropic displacement of the LADCP from both BT close to the bottom and ADCP close to the surface are similar. However on station 14, although the magnitudes are very similar the signs of the offsets are opposite. When one considers the assumption that the down and up profiles of the LADCP

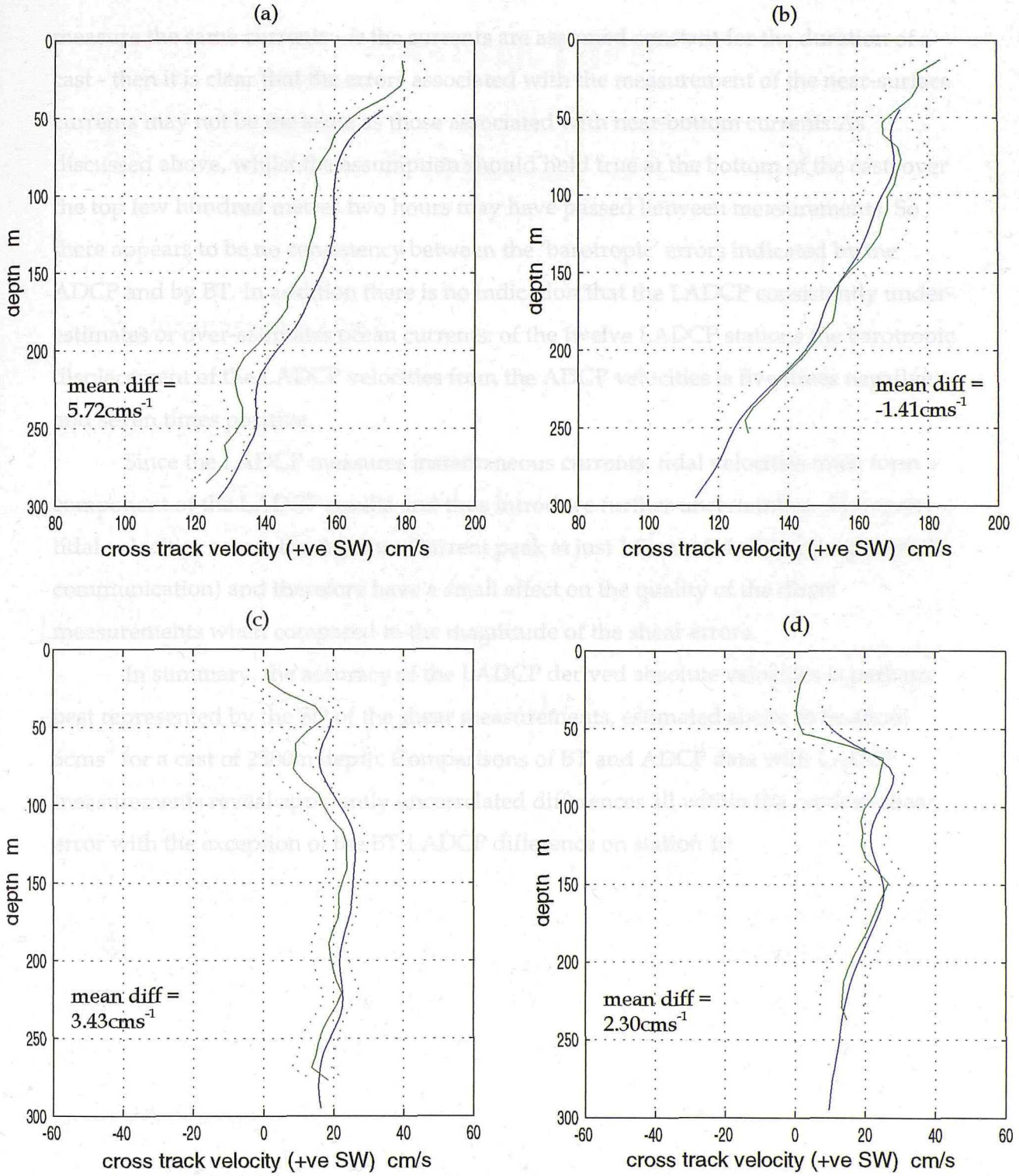


Figure 2.9 Cross-track component of LADCP and ADCP absolute velocities. Blue line is LADCP, green line is time-averaged, on-station ADCP. The green dotted line is the standard deviation of the ADCP time-averaged profile. (a) Station 10, (b) station 11, (c) station 14, (d) station 15. The depth-averaged difference or offset between the two sets of data is given in each graph.

measure the same currents - *ie* the currents are assumed constant for the duration of a cast - then it is clear that the errors associated with the measurement of the near-surface currents may not be the same as those associated with near-bottom currents.As discussed above, whilst the assumption should hold true at the bottom of the cast, over the top few hundred metres two hours may have passed between measurements. So there appears to be no consistency between the 'barotropic' errors indicated by the ADCP and by BT. In addition there is no indication that the LADCP consistently under-estimates or over-estimates ocean currents: of the twelve LADCP stations the barotropic displacement of the LADCP velocities from the ADCP velocities is five times negative and seven times positive.

Since the LADCP measures instantaneous currents, tidal velocities must form a component of the LADCP results and thus introduce further uncertainties. However, tidal velocities across the Agulhas Current peak at just 1.5cms$^{-1}$ (M. Tsimplis, personal communication) and therefore have a small effect on the quality of the direct measurements when compared to the magnitude of the shear errors.

In summary, the accuracy of the LADCP derived absolute velocities is perhaps best represented by the SD of the shear measurements, estimated above to be about 6cms$^{-1}$ for a cast of 2500m depth. Comparisons of BT and ADCP data with LADCP measurements reveal apparently uncorrelated differences all within the random shear error with the exception of the BT-LADCP difference on station 10.

# CHAPTER THREE

# *HYDROGRAPHY*

## 3.1 Water mass structure

### 3.1.1 General features

The hydrographic section across the Agulhas Current (figure 3.1) exhibits a density structure typical of that found in a WBC, with isopycnals sloping sharply upwards towards the coast marking strong poleward velocities. The gradient of the upward slope of the isopycnals doubles at about 40km from the coast, coincident with the foot of the continental slope, to a maximum rise of 1m in 100m. The mixed layer is very thin, less than 20m deep and surface temperatures are high, over 26°C (figure 3.2); these features are the result of vigorous heating of surface waters during the southern hemisphere summer combined with the swift flow of the WBC which carries warm water southward along the coast. The thermocline, as defined by the 4°C isotherm, is 1500m thick at the offshore end of the section (230km from the coast) and 1100m thick next to the continental slope. These features are consistent with the findings of Toole & Warren (1993) (TW), except for the temperature of the surface waters which were about 2°C cooler during their crossing of the Agulhas Current which took place in early summer, November 1987.

### 3.1.2 Upper ocean

There is a subsurface salinity maximum of 35.6 in the ACE section (figure 3.3) positioned at about 200m depth indicative of subtropical surface waters (STSW) (Wyrtki, 1973). This salinity distribution is typical of more northerly waters where STSW made salty by evaporation, advects northward in the interior flow and is capped, through surface warming and excess precipitation, by a warmer, fresher layer of tropical surface water (TSW). The presence of TSW here is an indication of the fast southward advection of upper waters in the WBC. Oxygen concentration also exhibits a subsurface maximum (figure 3.4), this time at about 100m depth and between distances of 70 and 180km along

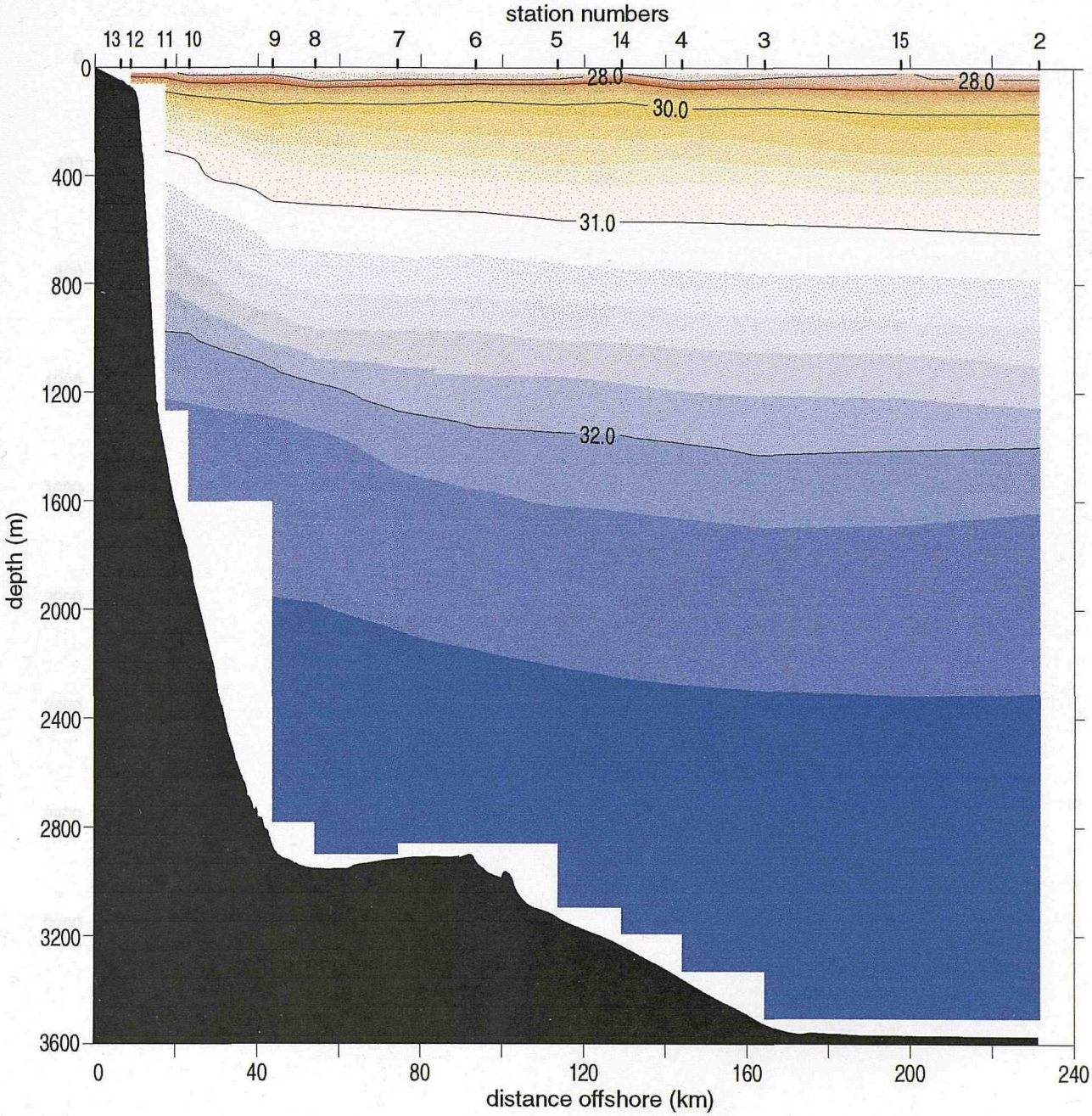


Figure 3.1 Section of density surfaces across the Agulhas Current at 32°S, from the Agulhas Current Experiment (ACE) in February and March 1995. The contours are sigma-1 surfaces, that is density relative to 1000db, and density transitions are indicated by colour changes at intervals of 0.2kgm$^{-3}$. Bathymetry is shaded in black. The x axis shows distance along the section (the origin is at the coast) which is oriented at 130°T so as to cross bathymetric contours perpendicularly.

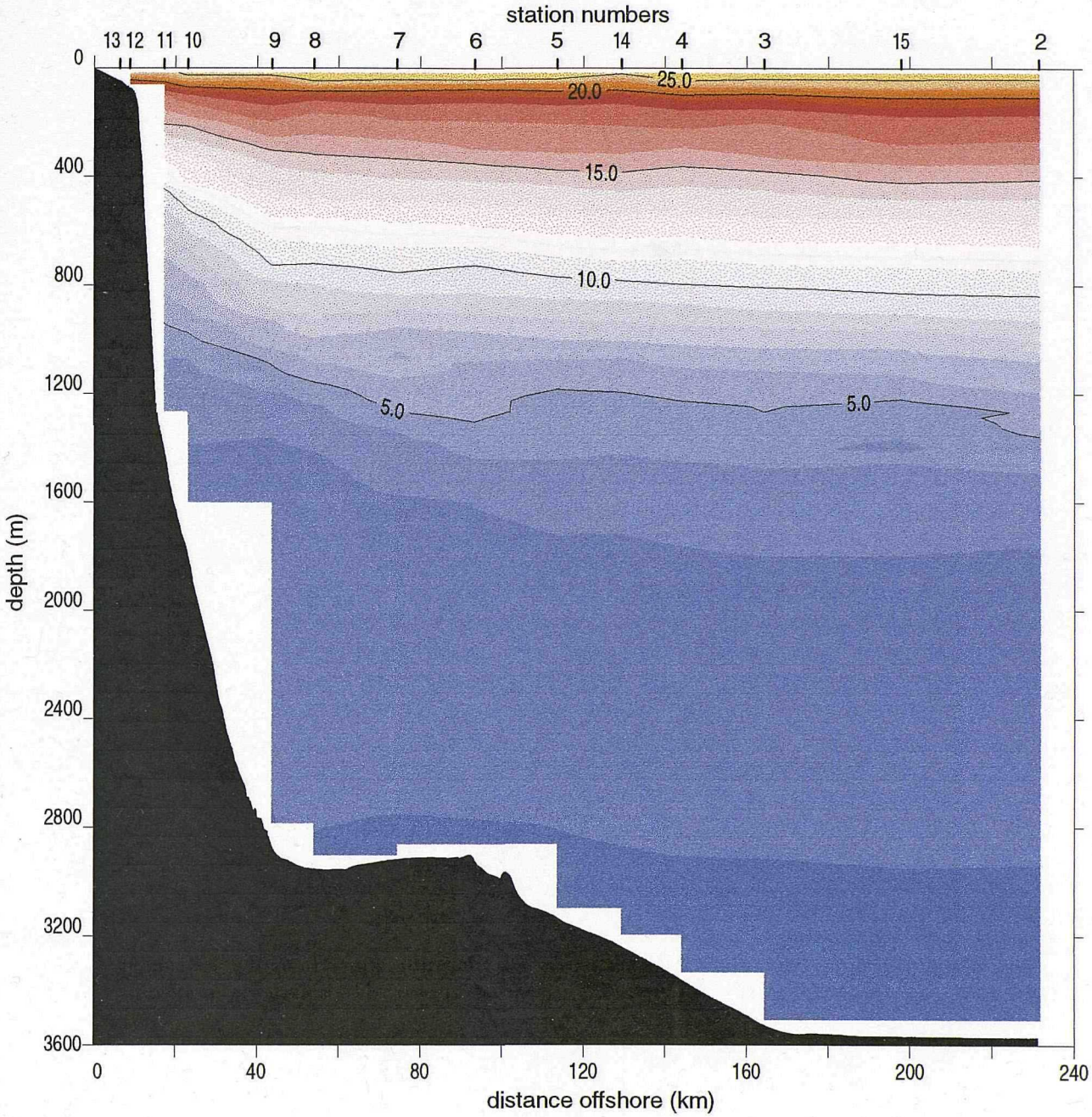


Figure 3.2 Potential temperature surfaces across the Agulhas Current at 32°S. Temperature transitions are indicated by colour changes at 1°C intervals below 20°C and by 2.5°C intervals above 20°C.

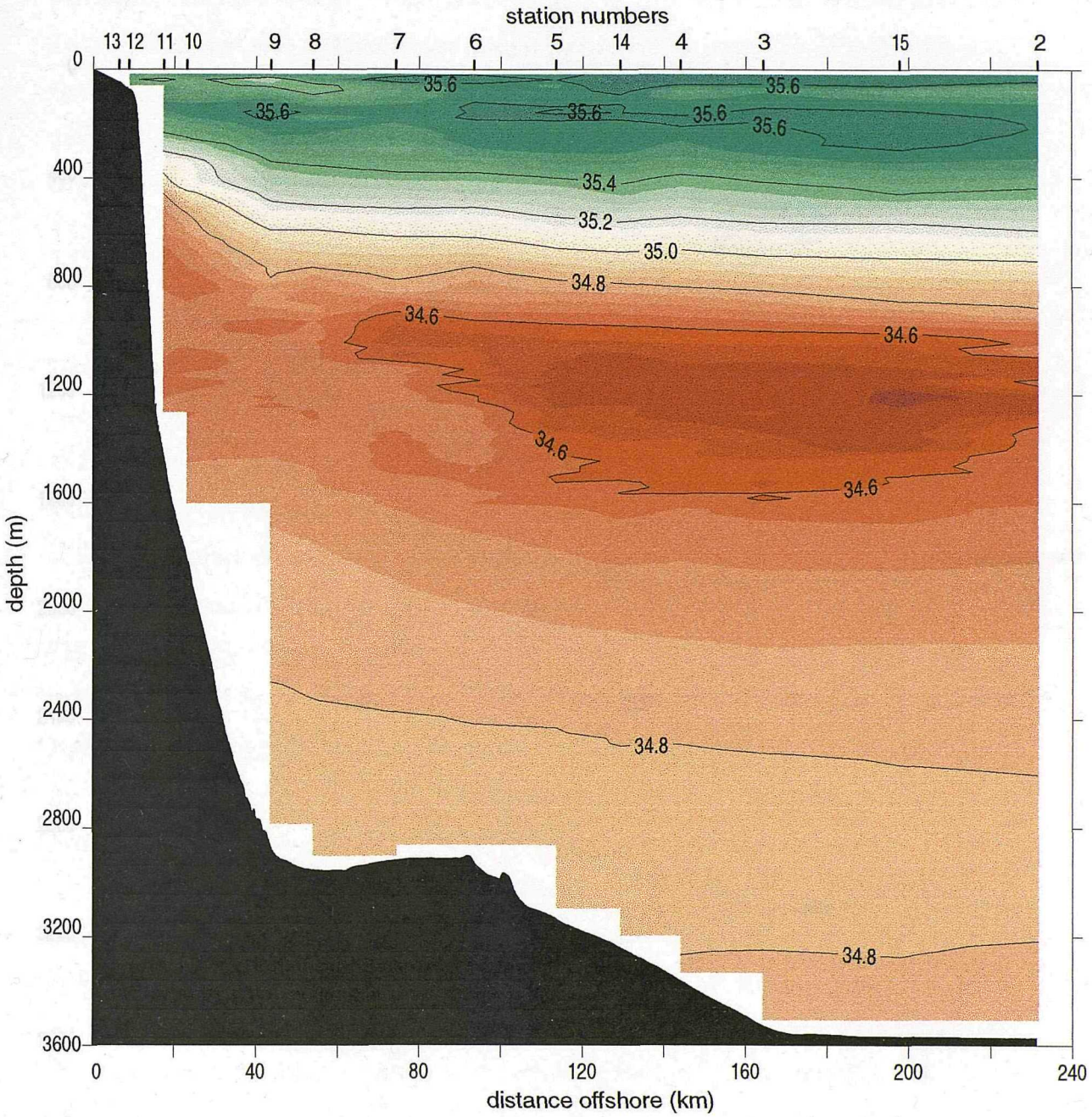


Figure 3.3 Section of salinity surfaces across the Agulhas Current at 32°S. Changes in salinity are indicated by colour changes at intervals of 0.05.

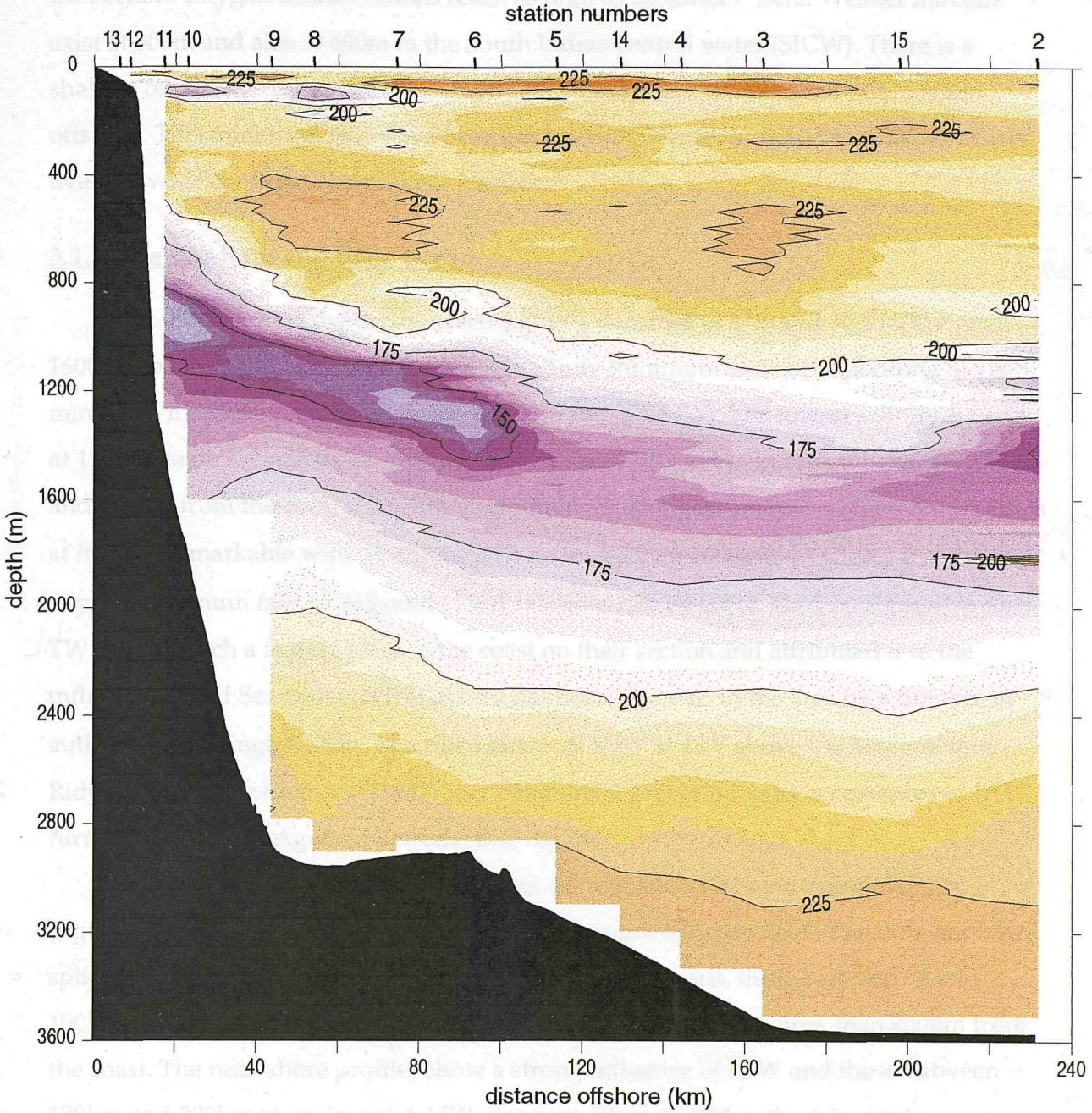


Figure 3.4 Oxygen concentration across the Agulhas Current at 32°S. Transitions in oxygen concentration are indicated by changes in colour at intervals of 5µmol $l^{-1}$.

the section. Oxygen concentrations reach as high as 235μmol $l^{-1}$ here. Weaker maxima exist at 300m and also at 600m in the South Indian central water (SICW). There is a shallow oxygen minimum at 150m depth which extends from the shelf out to 80km offshore. This minimum may have been advected downstream from the shallow waters over the wide continental shelf near Durban.

### 3.1.3 Intermediate and deep ocean

At intermediate depths, between sigma-1 densities of 31.6 and 32.1 (600m and 1600m next to the slope), there is a strong salinity minimum and corresponding oxygen minimum indicating Antarctic intermediate waters (AAIW). The lowest salinity is 34.45 at 1200m depth on station 15, about 200km offshore. In the broad region between 100km and 200km from the coast the salinity minimum is strongest and the oxygen minimum is at its least remarkable with concentrations no lower than 160μmol $l^{-1}$. Closer inshore the oxygen minimum falls to 135μmol $l^{-1}$ and salinities rise by 0.2 to 34.65 on sigma-1 = 32.1. TW noticed such a feature close to the coast on their section and attributed it to the influence of Red Sea water (RSW), which has been reported in the area by a number of authors. Grundlingh (1985b) described lenses of RSW at 28°S above the Mozambique Ridge and both Gordon *et al* (1987) and Valentine *et al* (1993) report occurrences of RSW further south in the Agulhas Retroflection region.

Plots of potential temperature versus salinity and of oxygen versus salinity (figure 3.5) highlight the areas of AAIW which are modified by RSW. The data has been split into four sets of profiles: those within 50km of the coast, those between 50 and 100km, those between 100km and 200km and finally one profile more than 200km from the coast. The near-shore profiles show a strong influence of RSW and those between 100km and 200km show 'pure' AAIW. Between 50km to 100km there is much interleaving of RSW and AAIW (figure 3.6). Beyond 200km, at station 2, there is an indication of another intrusion of saltier, oxygen poor water, suggesting more RSW may be present offshore of the WBC. Grundlingh (1985b) found similar patterns of RSW intrusions further to the east, suggesting that RSW was present in discrete filaments or lenses which interleave with the surrounding AAIW at their edges.

Below sigma-1 = 32.4, water mass characteristics are those of North Atlantic deep water (NADW) which rounds Cape Agulhas to flow from the Southeast Atlantic into the Southwest Indian Ocean at depths below 2000m. The NADW exhibits a very strong

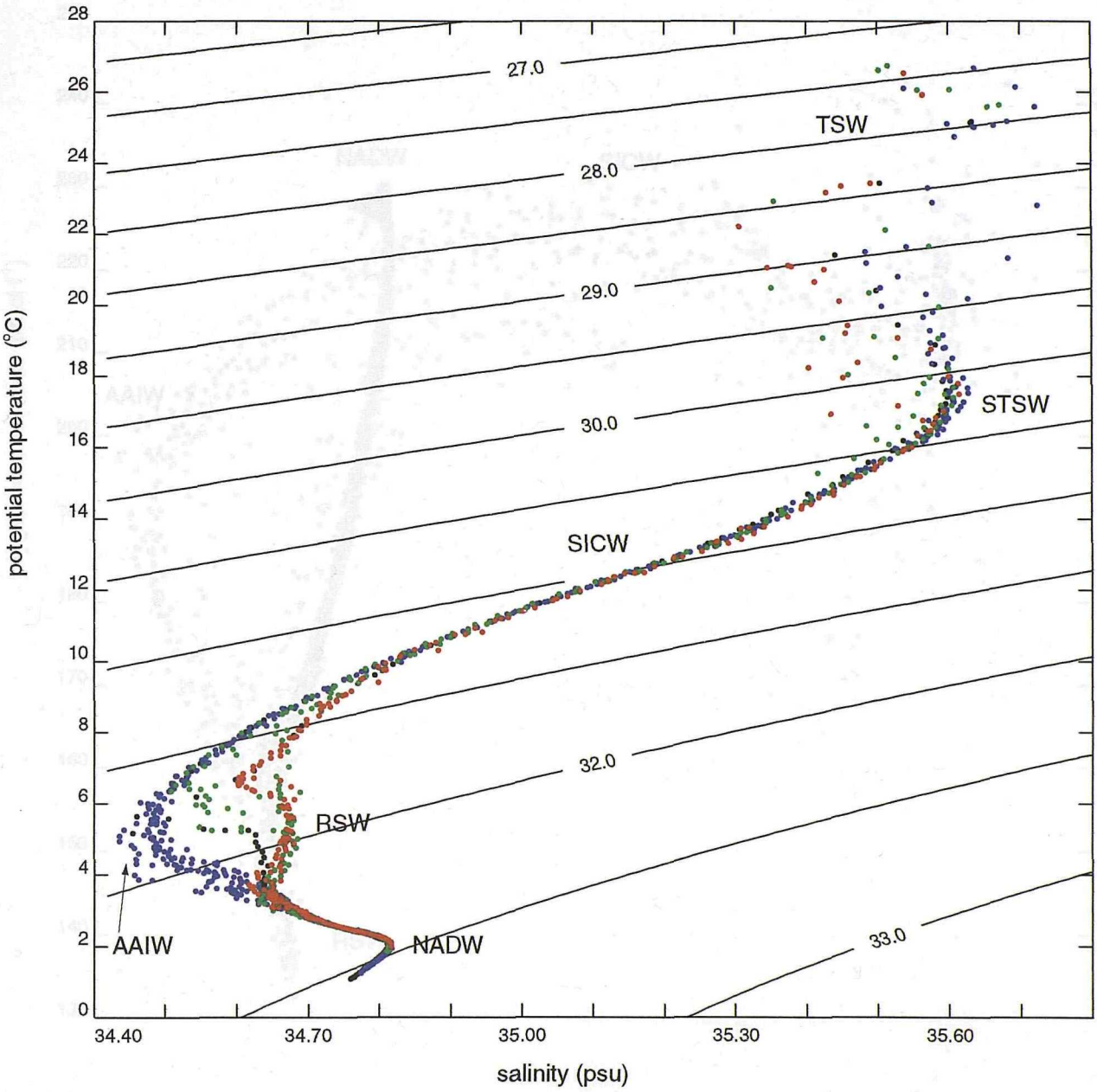


Figure 3.5a Temperature-salinity relationship of water masses in the Agulhas Current. Contours indicate sigma-1 surfaces (density relative to 1000db). Red dots represent water masses within 50km of the coast, green dots denote water masses between 50km and 100km offshore, blue dots are water masses between 100km and 200km offshore and black dots indicate water masses more than 200km from the coast. The labelled water masses are TSW, Tropical Surface Water; STSW, SubTropical Surface Water; SICW, South Indian Central Water; RSW, Red Sea Water; AAIW , AntArctic Intermediate Water and NADW, North Atlantic Deep Water.

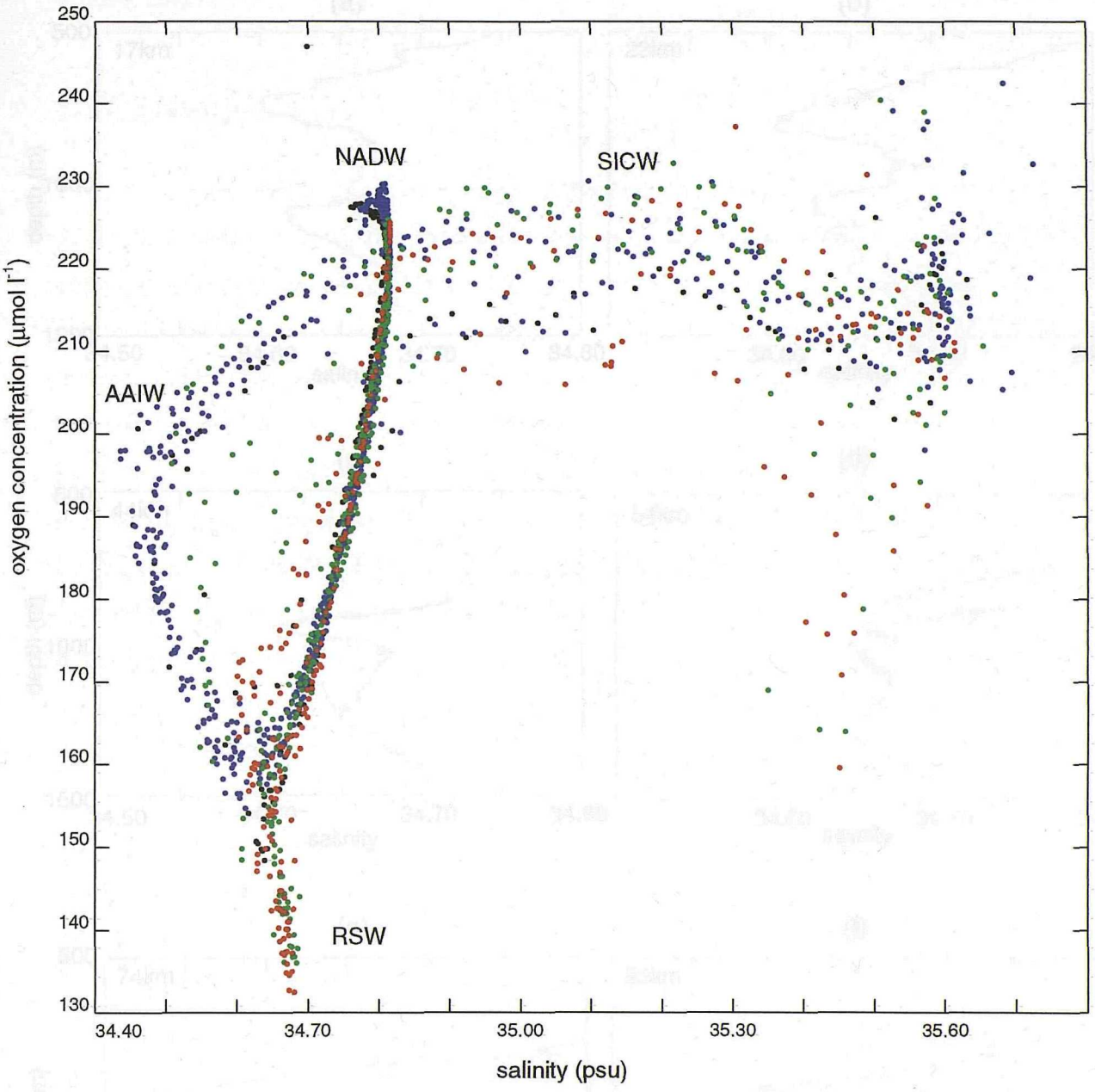


Figure 3.5b Oxygen-salinity relationship of water masses in the Agulhas Current. Red dots represent data within 50km of the coast, green dots are data between 50km and 100km offshore, blue dots indicate data between 100km and 200km offshore and black dots represent data more than 200km from the coast. The labelled water masses are: SICW, South Indian Central Water; RSW, Red Sea Water; AAIW, AntArctic Intermediate Water and NADW, North Atlantic Deep Water.

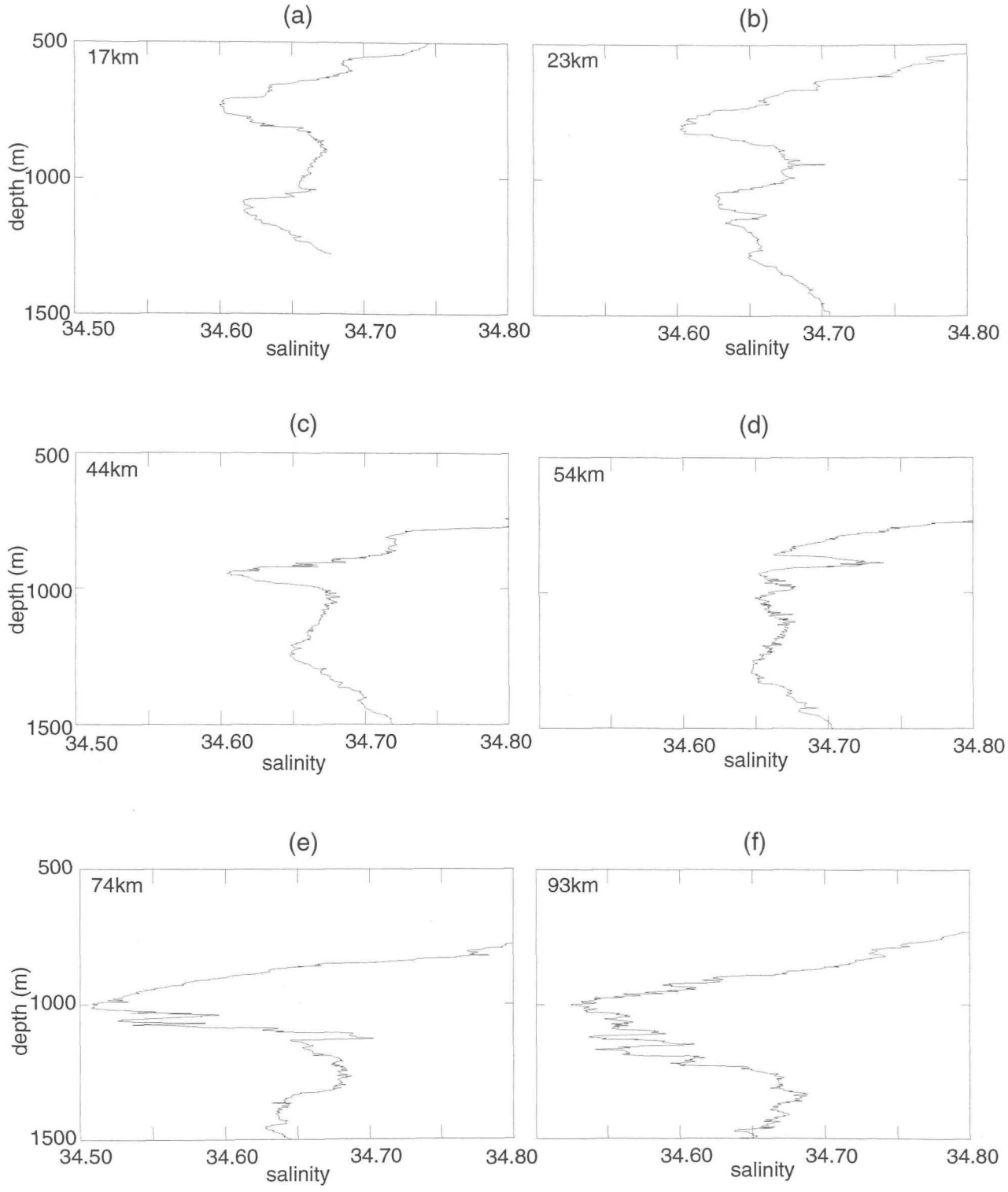


Figure 3.6 Interleaving and mixing of layers of different salinities at intermediate depths. (a) station 11, (b) station 10, (c) station 9, (d) station 8, (e) station 7 and (f) station 6. The distance of each station from the coast is shown in each plot. Stations 6 and 7 exhibit the most fine structure. Station 8 has the strongest influence of Red Sea Water (RSW) with salinities over 34.65 throughout the intermediate layer. Stations 9, 10 and 11 show one layer of RSW of thickness 200m at around 1000m depth .

potential temperature - salinity relationship with a salinity maximum of 34.83 at 2°C (figure 3.5a).

## 3.2 Geostrophy

Absolute geostrophic velocities are calculated from the ACE hydrographic (CTDO2) data by studying the juxtaposition of water masses and choosing an appropriate level of no motion. The idea that overlying water masses of different properties move more or less independently of one another and in contrasting ways has come about through much observational evidence (Worthington, 1976 and Reid, 1981), and using a zero velocity surface (ZVS) based on water mass distribution is a well established method for determining absolute geostrophic velocities and thereby estimating volume transports. However, as discussed in chapter 1, volume transport estimates are hugely dependent on the position of the ZVS so that this method must be implemented with care. As a result the ZVS used here is the one chosen by TW in their study of the Agulhas Current. The results are presented in the next section as well as a comparison with the TW data. An estimate of the error in geostrophic velocity is described in section 3.2.2 and in section 3.2.3 the geostrophic volume transport of the Agulhas Current is estimated using TW's reference level. Finally, section 3.2.4 is a discussion on the Rossby number of the flow and on the validity of the geostrophic approximation in the Agulhas Current.

### 3.2.1 Geostrophic currents

The water below 2000m in the Agulhas Current is essentially NADW whilst the water above 2000m shows some extreme characteristics of RSW. TW argued that the flow of these waters away from their sources should be concentrated toward the western boundary. They also noted that the Natal Valley is closed to the north below depths of 2500-3000m so that continuity requires the net transport across the section to be small below 2500-3000m. As a result of these criteria they placed the ZVS at 2000db for station pairs west of 89km offshore (station pair 3-12 inclusive). For those station pairs over the continental slope and in water shallower than 2000db, the ZVS was placed at the deepest common level (DCL) of each station pair. East of 89km offshore the ZVS was moved deeper to minimise the transport of deep waters, to 2500db between 89km and 137km offshore (station pair 12-13) and to 3000db east of 137km offshore (station pair 13/14). A

section of geostrophic velocities from the RRS *Charles Darwin*, reproduced using the ZVS described by TW is shown in figure 3.7.

The ZVS devised by TW was followed closely to provide absolute geostrophic velocities from the ACE data, as shown in figure 3.8. Inshore and inclusive of station pair 7-6 (84km offshore) the ZVS was placed at 2000db or at the DCL of each station pair. Station pairs 6-5 to 14-4 have a ZVS at 2500db (between 84km and 137km offshore) and east of 137km offshore the remaining three station pairs (4-3 to 15-2) have a ZVS at 3000db.

Since both the TW data and the ACE data (figures 3.7 & 3.8) are referenced to essentially the same ZVS then any changes between the two sections must occur as a result of the change in the density structure of the Agulhas Current from that in November 1987 to that in March 1995. Generally the two crossings of the current seem dynamically similar and the width of the current between the $0.5ms^{-1}$ isotachs is about 70km in both cases. There are some differences however: TWs data implies the core of the current is situated farther offshore than during ACE and maximum surface velocities are only 60% the size of the velocity maximum in the ACE section.

Looking more closely at the geostrophic velocity structure of the ACE section, the main jet of the Agulhas Current appears to be confined within 100km of the coast. Maximum velocities of up to $240cms^{-1}$ are found in the surface core of the current (at station pair 11-10) which is positioned 20km offshore. The core of the current, as defined by the position of the velocity maximum, moves offshore with increasing depth, for example at 1000m depth where maximum velocities in the current have reduced to $50cms^{-1}$ the core is 55km offshore. The width of the current between the $50cms^{-1}$ isotachs is about 70km as compared to the 90-100km estimated by Pearce (1977). In the upper 100m horizontal shears peak at $2.8\times10^{-4}s^{-1}$ (or $28cms^{-1}$ over 1km, corresponding to a Rossby number of 3.7) between station pairs 12-11 and 11-10 on the cyclonic edge of the current. Vertical shears reach a maximum of $2.5\times10^{-3}s^{-1}$ (or $25cms^{-1}$ over 100m) close to the slope between 500m and 700m depth on station pair 11-10 in the core of the current. None of the peak shears discussed above are over the upper 50m of the water column since there is likely to be a large effect of wind forcing close to the sea surface.

Offshore of the main current, at station pair 14-4 about 137km from the coast is a small lens of water above 100m depth with velocities greater than $30cms^{-1}$. Stations 4 and 14 were sampled several days apart and these high surface velocities are most likely due to the movement of isopycnals in the time elapsed between stations and not

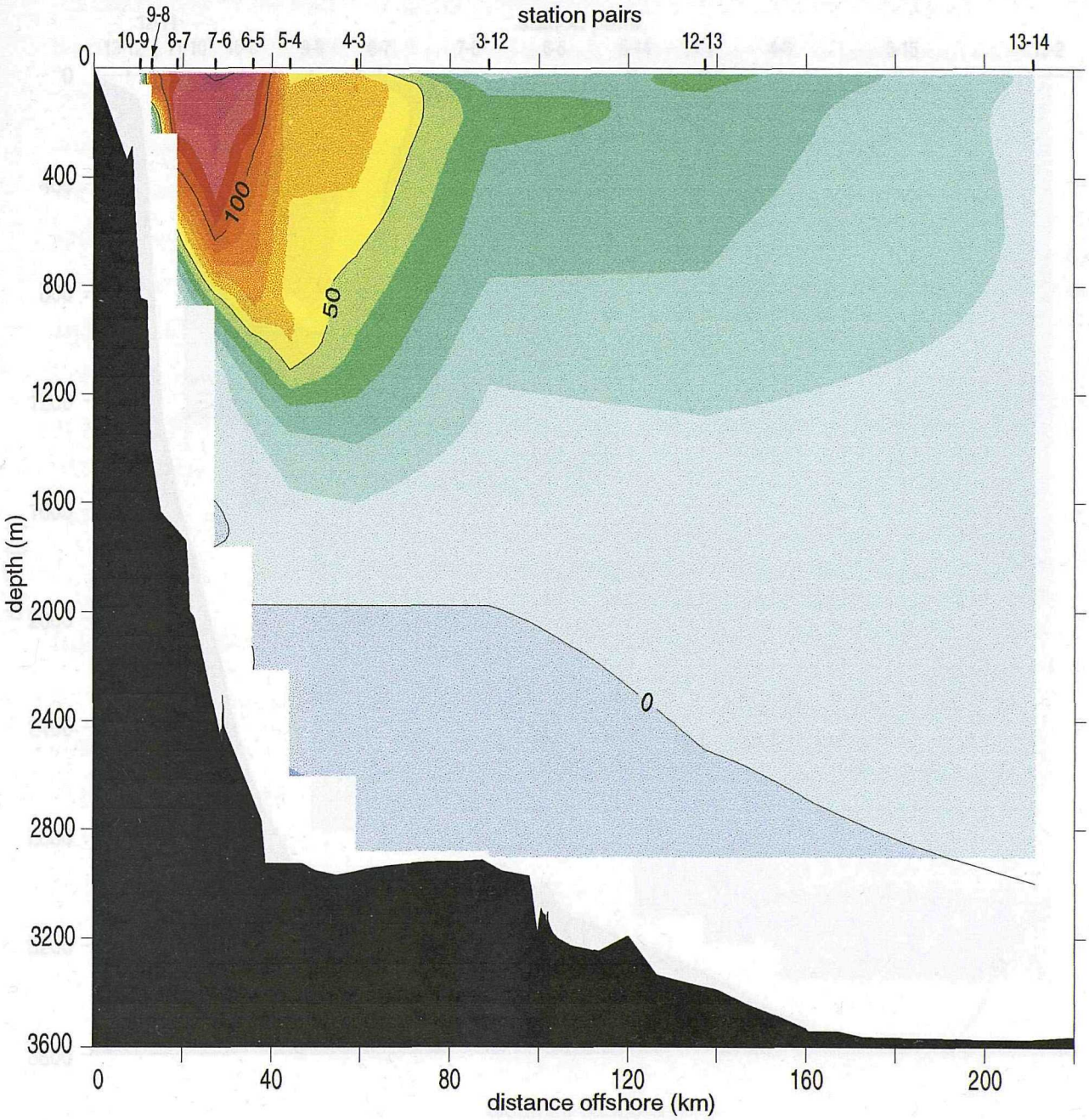


Figure 3.7 Absolute geostrophic velocities in the Agulhas Current at 32°S in November 1987. Transitions in velocity are marked by colour changes at intervals of 10cms$^{-1}$. Note that the velocity is positive to the south-west (in the direction of the WBC). The level of no motion has been approximated by considering the juxtaposition of water masses across the section and by assuming that each water mass be flowing away from its source near a western boundary (Toole & Warren, 1993). The geostrophic volume transport of this section is estimated to be 85Sv.

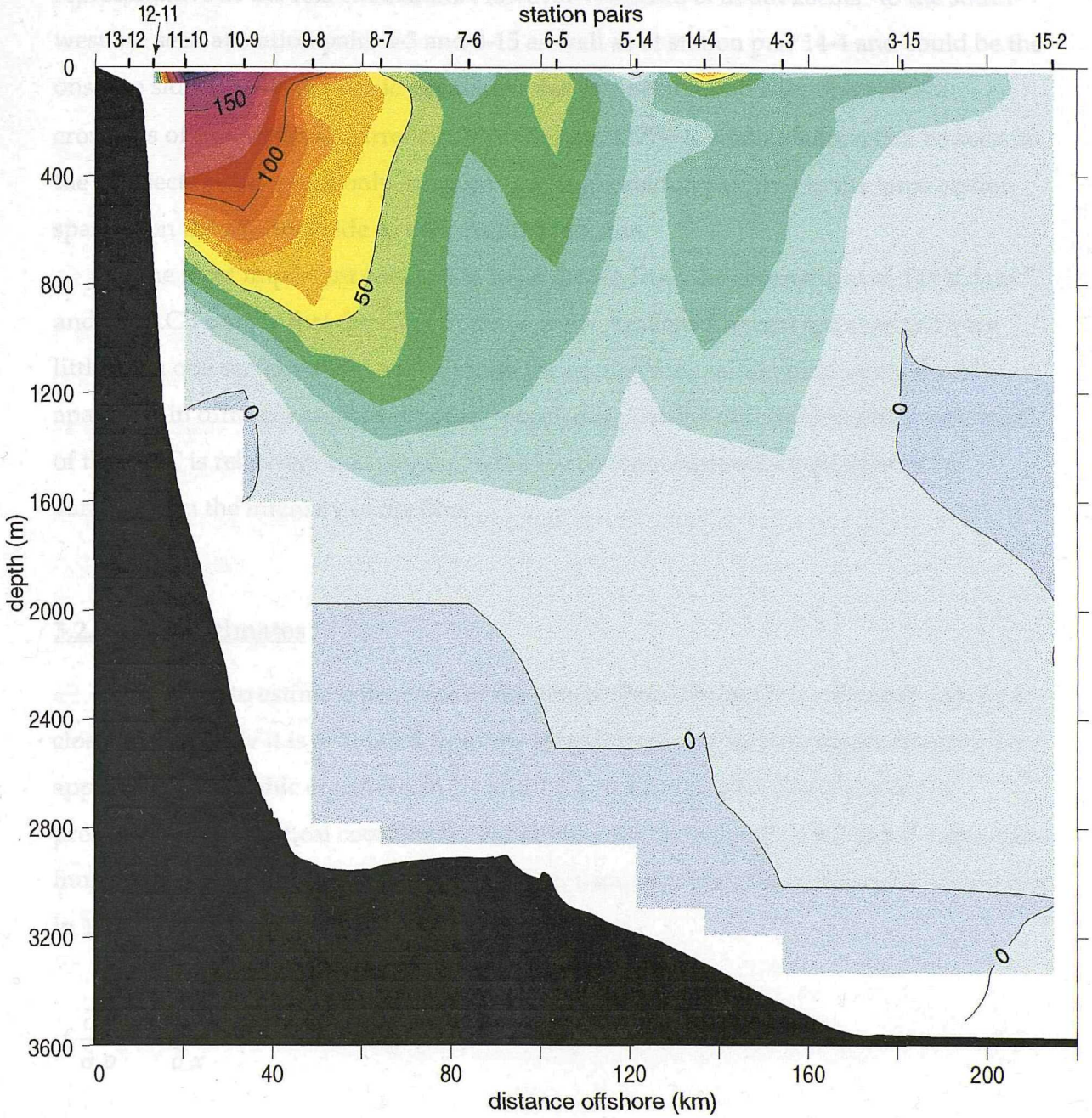


Figure 3.8 Absolute geostrophic velocities across the Agulhas Current at 32°S in February-March 1995. Transitions in velocity are indicated by colour changes at intervals of 10cms$^{-1}$. Velocities are positive to the south-west. The level of no motion is the same as that described in figure 3.7. The geostrophic volume transport of the Agulhas Current is estimated to be 82Sv from this section.

representative of the real circulation. However velocities of about 20cms$^{-1}$ to the south-west are seen at station pairs 4-3 and 3-15 as well as at station pair 14-4 and could be the onshore side of an anticyclonic circulation that has been found here on previous crossings of the Agulhas Current at 32°S (Pearce, 1977). A similar feature can be seen on the TW section, although only sampled at a single station pair due to the large station spacing on the offshore side of their Agulhas section.

The most important conclusion to be drawn from the comparison of TW's data and the ACE data is that density structure of the Agulhas Current has changed very little from one section to the next, despite the occupations taking place several years apart and in different seasons. In other words it is possible that the baroclinic structure of the WBC is relatively unchanging, whilst barotropic currents cause most of the variability in the intensity of the flow.

### 3.2.2 Error estimates

In order to estimate the error in the geostrophic velocity it is necessary to take a closer look at how it is evaluated from the temperature and salinity measurements. To apply the geostrophic equations in 1.4 and 1.5 to oceanographic data there is the problem that the vertical coordinate $z$ cannot be directly measured. Instead the equations must be re-expressed in pressure coordinates, using the hydrostatic approximation given in 1.3, so that 1.4 becomes,

$$f\frac{\partial v}{\partial p} = -\frac{\partial \alpha}{\partial x} \qquad 3.1$$

where $\alpha = 1/\rho$ is the specific volume and $\partial/\partial x$ is taken along constant pressure surfaces. The dynamic method consists of integrating 3.1 vertically,

$$\int_{p_{ref}}^{p} \frac{\partial v}{\partial p} dp = -\frac{1}{f}\frac{\partial}{\partial x}\int_{p_{ref}}^{p} \alpha \, dp \qquad \text{or} \qquad v - v_{ref} = -\frac{1}{f}\frac{\partial}{\partial x}\int_{p_{ref}}^{p} \delta \, dp \qquad 3.2$$

where $\delta = \alpha - \alpha(35,0,p)$ is the specific volume anomaly relative to a "standard ocean" specific volume for which $S$ and $T$ are constants (35psu and 0°C) and hence $\alpha(35,0,p)$ is constant along pressure surfaces (Johns *et al*, 1989). It is numerically most accurate to

deal with this last integral, defined as the "dynamic height anomaly", $\Delta D$. The expression in 3.2 is usually evaluated by first differences,

$$v = \frac{1}{f}\frac{\partial}{\partial x}(\Delta D) + v_{ref} = \frac{1}{fL}(\Delta D_2 - \Delta D_1) + v_{ref} \qquad 3.3$$

where $(\Delta D_2 - \Delta D_1)$ is the difference in dynamic height anomaly between, for instance, stations 1 and 2 separated by distance $L$. Overall then, the geostrophic velocity at any pressure level may be determined relative to the velocity at the reference level using the lateral gradient in the dynamic height anomaly field.

The error in the geostrophic velocity can be estimated by taking the total differential of equation 3.3 and assuming that the three sources of error are uncorrelated (Johns *et al*, 1989),

$$dv = \sqrt{\underset{1}{\left(\frac{d\Delta D}{fL}\right)^2} + \underset{2}{\left(\frac{dL}{L}v\right)^2} + \underset{3}{\left(dv_{ref}\right)^2}} \qquad 3.4$$

So the measurement errors in geostrophic velocity arise from uncertainties in the station spacing (2), the dynamic height measurements (1) and the reference velocity (3). Johns *et al* (1989) found that by far the most important source of error when measuring geostrophic velocities in the Gulf Stream was the station spacing term. Their reference velocity was measured using a Pegasus profiler with an estimated error of only $\pm 1 cms^{-1}$. The error in dynamic height anomaly, based on the measurement error in temperature and salinity, was taken to be at most ±0.004dyn m. Stating that the greatest uncertainty in the station positioning is not due to navigational accuracy but due to ship drift whilst on station Johns *et al* (1989) estimated this uncertainty as ±0.5km, giving an error in the station spacing, $dL = (0.5^2 + 0.5^2)^{1/2} = \pm 0.7$km, assuming random drift. Using this value of $dL$ across the Gulf Stream they found geostrophic velocity errors as large as $12 cms^{-1}$ in the surface core of the current.

In assessing these errors for the Agulhas Current, the ship drift, which contributes so strongly to the station spacing error in the analysis by Johns *et al* (1989), was found to be far from random. In fact most station pairs exhibited an on-station drift

of similar magnitude and direction (with the Current) so that the drift ultimately makes little contribution to station spacing error. Table 3.1 shows the ship drift (in magnitude and direction) for each ACE station. The vector-averaged drift direction is 245° with a standard deviation of 24°.

| stn | 11 | 10 | 9 | 8 | 7 | 6 | 5 | 14 | 4 | 3 | 15 | 2 |
|---|---|---|---|---|---|---|---|---|---|---|---|---|
| drift | 5.38 | 6.51 | 5.19 | 4.36 | 3.38 | 3.52 | 2.57 | 3.40 | 0.10 | 1.60 | 2.27 | 1.37 |
| angle | 218° | 221° | 239° | 232° | 224° | 248° | 265° | 252° | 241° | 225° | 289° | 290° |

Table 3.1 Ship drift given in magnitude (km) and direction (degrees true) for stations across the Agulhas Current. From left to right the stations progress away from the coast.

Approximating that the ship drift is always down-stream (a good assumption for all but stations 15 and 2 at the far end of the section) and that the station spacing is measured across-stream, then the error in station spacing for a single station pair will be,

$$dL = \sqrt{L^2 + \Delta d^2} - L \qquad 3.5$$

where $\Delta d$ is the difference between the ship drift at the two stations. Using this equation the error from ship drift is very much smaller; on average $dL$ is one tenth that estimated by Johns *et al* (1989). Using their estimate for a standard error in dynamic height anomaly we find that term 1 of equation 3.4 is of more significance than term 3, except at station pair 11-10, where the station spacing is just 5.8km and surface velocities are greater than 150cms$^{-1}$. Overall, the maximum baroclinic geostrophic velocity error across the Agulhas Current (terms 1 and 2 of equation 3.4) is 0.6 cms$^{-1}$, excluding station pair 11-10 where the error is 3cms$^{-1}$. The error in reference velocity, based on the subjective reference level used in this chapter is much larger, possibly 10cms$^{-1}$ in regions of high shear, but can be improved upon later using direct measurements (see chapter 4).

### 3.2.3 Geostrophic volume transport

The volume transport is estimated for the ACE and TW data by a simple integration across the sections shown in figures 3.7 and 3.8, where the velocity at each station pair is assumed to be representative of the flow for the distance between those two stations. On the ACE section this is an integration out to the last station pair 15-2, at

230km from the coast. The closest equivalent TW section runs out to 245km offshore at station pair 13-14. There is no attempt to deal with bottom triangles on either section.

Using TWs ZVS the geostrophic volume transport of the Agulhas Current is estimated to be 82Sv from the ACE data and 85Sv from the TW data. These transports fall within 5% of one another - a remarkable agreement. The transport contribution from each station pair is shown in figure 3.9. Unfortunately in the case of the ACE section the inshore side of the current is poorly resolved because during the experiment the core of the current was so close to the coast. The two stations west of the core were taken in water shallower than 100m and hence their transport contribution is negligible. However the anticyclonic side of the WBC is better represented in the ACE section than in the TW section where the station spacing towards the end of the section extends to 58km and then 90km. The distribution of transport per unit width is similar in both sections with a roughly exponential decrease in transport per unit distance going east from the core of the current (more on the lateral shape of the current in chapter 4 when looking at the underway ADCP data). It is interesting to note that the cumulative transport of the two sections is more or less equivalent out to 140km offshore (72Sv). Due to the large station spacing at the end of the TW section there is an extra 15km over which the geostrophic velocities at station pair 13-14 are integrated, producing about 2Sv extra contribution to the transport there (see figure 3.9). Disregarding the volume transport beyond 230km (where the last ACE station is positioned) therefore reduces the geostrophic transport of the TW section to 83Sv, suggesting that the two sections are essentially equivalent in their density structure.

### 3.2.4 Is the Geostrophic Approximation valid in the Agulhas Current?

The geostrophic velocity section across the Agulhas Current has revealed very strong horizontal shears (of order $10^{-4}$ $s^{-1}$), particularly on the inshore edge of the current. In light of this is it appropriate to assume that the flow in the WBC is dominated by rotation, especially within 20km of the boundary? Or should we take into account velocity shear and eddy viscosity effects? The first indicator for the importance of rotation in a flow is the Rossby number, $R_o$ which is often determined by considering the comparative scales of the shear and the Coriolis parameter of a flow:

$$R_o = \frac{v_x}{f} = \frac{1 \times 10^{-4}}{7.5 \times 10^{-5}} = O(1) \qquad 3.6$$

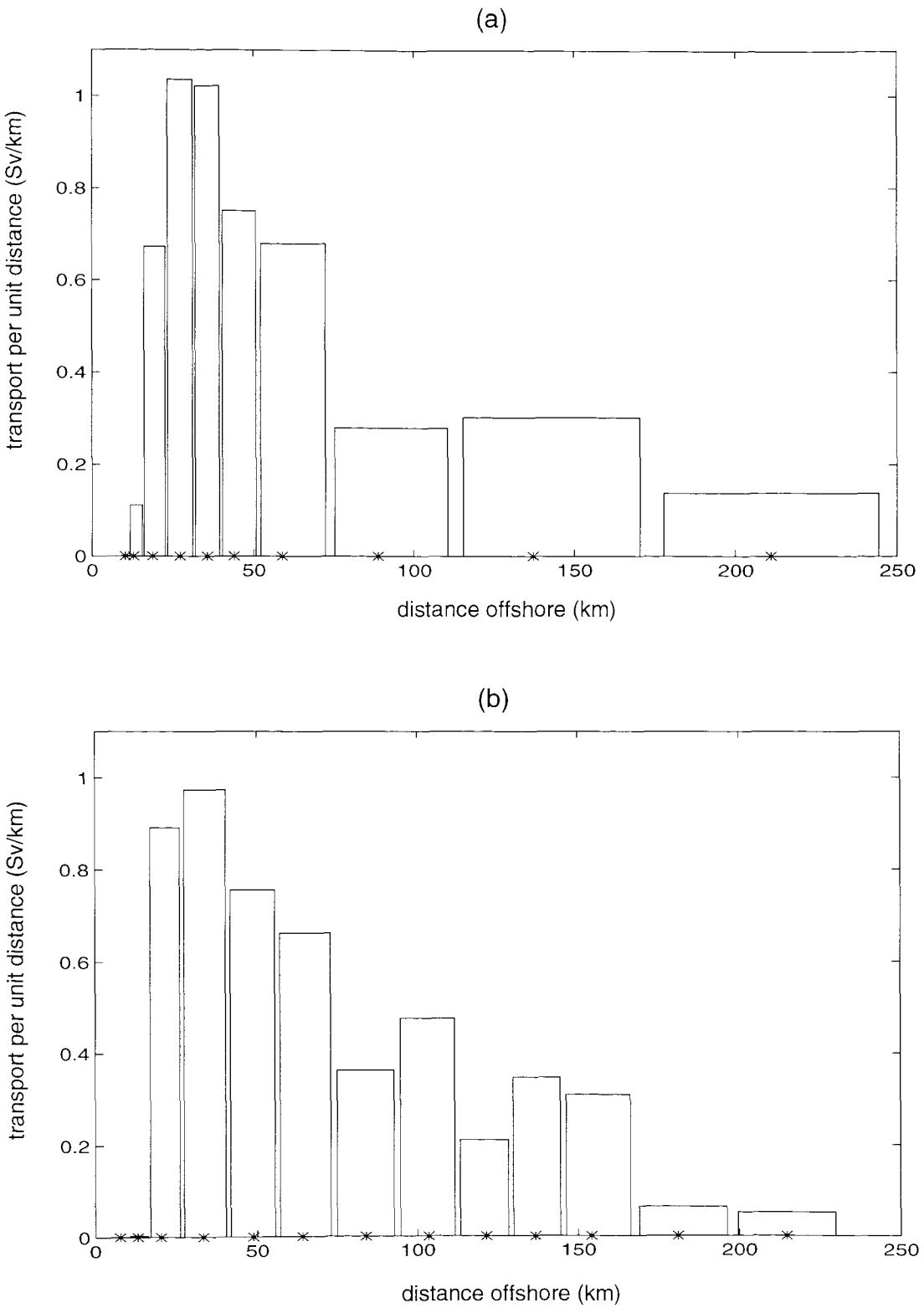


Figure 3.9 Distribution of transport across the Agulhas Current. (a) Geostrophic transport from RRS *Charles Darwin* cruise in November 1987, (b) Geostrophic transport from ACE, February-March 1995. Stars indicate the positions of station pairs.

This implies that non-linear effects may be important in the core of the current and farther inshore and that the geostrophic approximation may not hold true. So let us look more closely at the equations of motion to determine which terms are important in the Agulhas Current. Assuming a steady flow the horizontal momentum equations for an incompressible fluid can be written as,

$$u\frac{\partial u}{\partial x}+v\frac{\partial u}{\partial y}+w\frac{\partial u}{\partial z}-fv=-\frac{1}{\rho}\frac{\partial p}{\partial x}-A_H\left(\frac{\partial^2 u}{\partial x^2}+\frac{\partial^2 u}{\partial y^2}\right)-A_V\frac{\partial^2 u}{\partial z^2} \qquad 3.7$$

$$u\frac{\partial v}{\partial x}+v\frac{\partial v}{\partial y}+w\frac{\partial v}{\partial z}+fu=-\frac{1}{\rho}\frac{\partial p}{\partial y}-A_H\left(\frac{\partial^2 v}{\partial x^2}+\frac{\partial^2 v}{\partial y^2}\right)-A_V\frac{\partial^2 v}{\partial z^2} \qquad 3.8$$

where $y$ is the along-stream distance, $x$ is the cross-stream distance, $v$ is along-stream velocity, $u$ is cross-stream velocity and $A$ is a parameter for eddy viscosity. The order of magnitude of each parameter in the equation of motion for the Agulhas Current can be approximated as follows:

$V = O(1)$, $U = O(0.1)$, $W = O(0.01)$ all in $ms^{-1}$

$X = O(10^4)$, $Y = O(10^5)$, $Z = O(10^3)$ all in m

$f = O(10^{-4})$ and $A_H = O(10^3)$, $A_V = O(10^1)$ $m^2s^{-1}$

where the cross-stream length scale is taken as 10km to represent the strongest shears on the onshore side of the WBC. Below are the characteristic scales for equations 3.1 and 3.2 with the corresponding order of magnitude written below each term.

$$\frac{U^2}{X} \quad \frac{UV}{Y} \quad \frac{UW}{Z} \quad fV = \quad \frac{P}{\rho X} \quad A_H\frac{U}{X^2} \quad A_H\frac{U}{Y^2} \quad A_V\frac{U}{Z^2} \qquad 3.9$$

$10^{-6}$ $10^{-6}$ $10^{-6}$ $10^{-4}$ ? $10^{-9}$ $10^{-8}$ $10^{-6}$

$$\frac{UV}{X} \quad \frac{V^2}{Y} \quad \frac{VW}{Z} \quad fU = \quad \frac{P}{\rho Y} \quad A_H\frac{V}{X^2} \quad A_H\frac{V}{Y^2} \quad A_V\frac{V}{Z^2} \qquad 3.10$$

$10^{-5}$ $10^{-5}$ $10^{-5}$ $10^{-5}$ ? $10^{-5}$ $10^{-7}$ $10^{-5}$

It is clear that even accounting for the strongest shears on the cyclonic side of the WBC the along-stream momentum balance (equation 3.9) is satisfied geostrophically: the Coriolis force associated with the along-stream flow is balanced by a pressure gradient

across the current. Although $V$ reduces rapidly with increasing depth, implying that the geostrophic balance may be disrupted deeper in the current, the core of the WBC moves offshore with depth (figure 3.8) thereby increasing the cross-stream scale of the flow and helping to maintain the geostrophic balance. The effective Rossby number for the along-stream flow in the x-momentum equation is O(0.01).

In the y-momentum equation (equation 3.10) the strong shears in along-stream velocity mean that the cross-stream flow is not geostrophic. In fact horizontal and vertical shear, rotation and eddy viscosity all seem to be important terms and the Rossby number is O(1).

So whilst all terms in the y-momentum equation are important, the along-stream flow is geostrophic to order $10^{-2}$:

$$fv = \frac{1}{\rho}\frac{\partial p}{\partial x} \text{ to } O(10^{-2}).$$

# CHAPTER FOUR

# *DIRECT MEASUREMENTS OF THE AGULHAS CURRENT*

## 4.1 General features of the Agulhas Current as revealed by LADCP

The LADCP data reveals a strong south-westward flowing boundary current with a surface core situated about 20km from the coast. Stations 10 and 11 are in the core of the WBC and their LADCP velocity vectors are shown in figure 4.1. Perhaps the most striking feature in both profiles, apart from the large surface velocities of the Agulhas Current is the extremely high vertical shears which occur between 300m and 800m depth on station 11 (closest to the slope) and between 500m and 950m depth on station 10. The shear is so strong that the flow of the WBC is reversed at about half the water depth on both stations and again on station 9 (figure 4.2). There is almost no rotation of flow direction with depth at these three stations until the speed passes through zero, at which point the flow direction flips from south-west to north-east. The LADCP velocity vector profiles for the remaining stations are shown in figure 4.2. Proceeding offshore the velocity of the Agulhas Current gradually reduces and turns slightly towards the west. Stations 15 and 2 at the offshore end of the section are exhibiting mainly westward currents close to the surface and there is much rotation of the flow with depth suggesting that these stations may be beyond the anti-cyclonic edge of the WBC.

The barotropic component of the flow is estimated using a combination of LADCP measurements and ship drift (table 3.1), as described in chapter 2 (equation 2.3). No adjustments have been made to match LADCP velocities to on-station ADCP or bottom tracked velocities. Table 4.1 shows the along-stream depth-averaged or barotropic velocity at each station. It is very large in the core of the current, at stations 11 and 10 and from there on reduces fairly steadily towards the offshore end of the section.

A contoured section of the rotated cross-track LADCP velocities is shown in figure 4.3 and, like the geostrophic velocity section of figure 3.8, velocities are shown

(a)

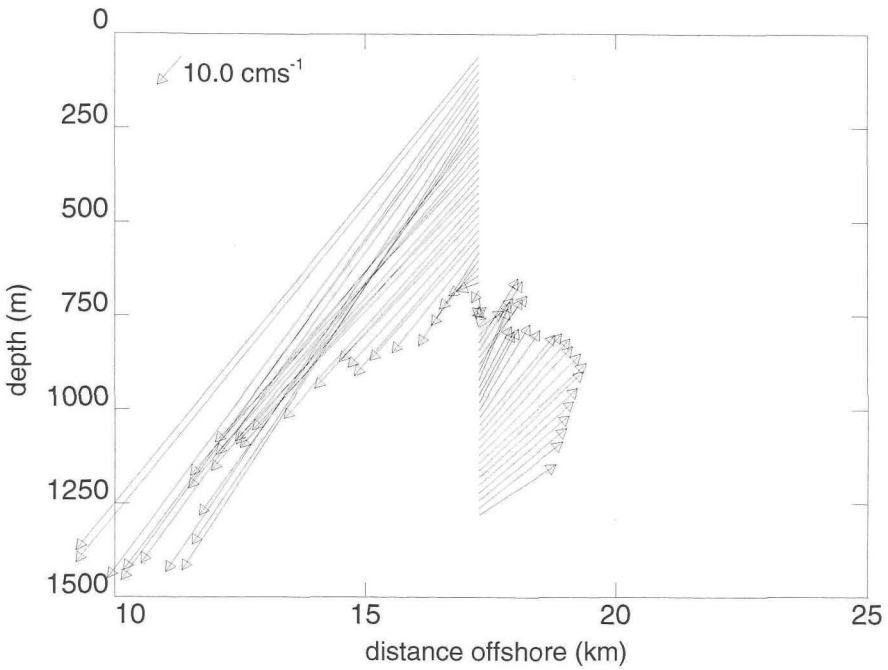


(b)

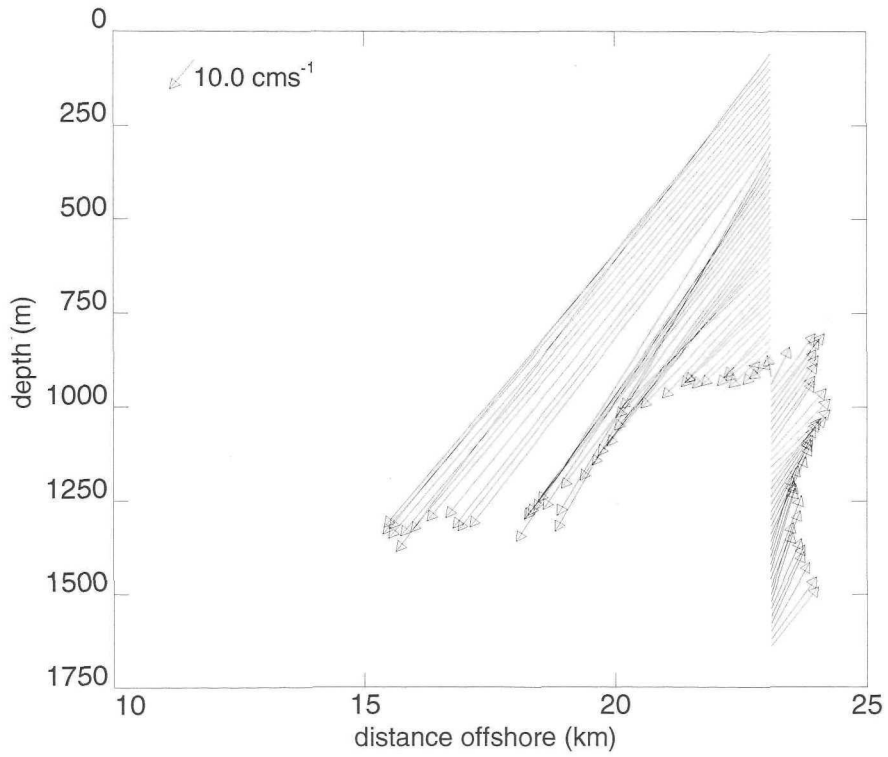


Figure 4.1 LADCP velocity vectors at (a) station 11, and (b) station 10. Vector scales are shown on each plot pointing to 220°T. Northward flow is vertically upward, eastward flow is to the right. The scales of (a) and (b) are identical.

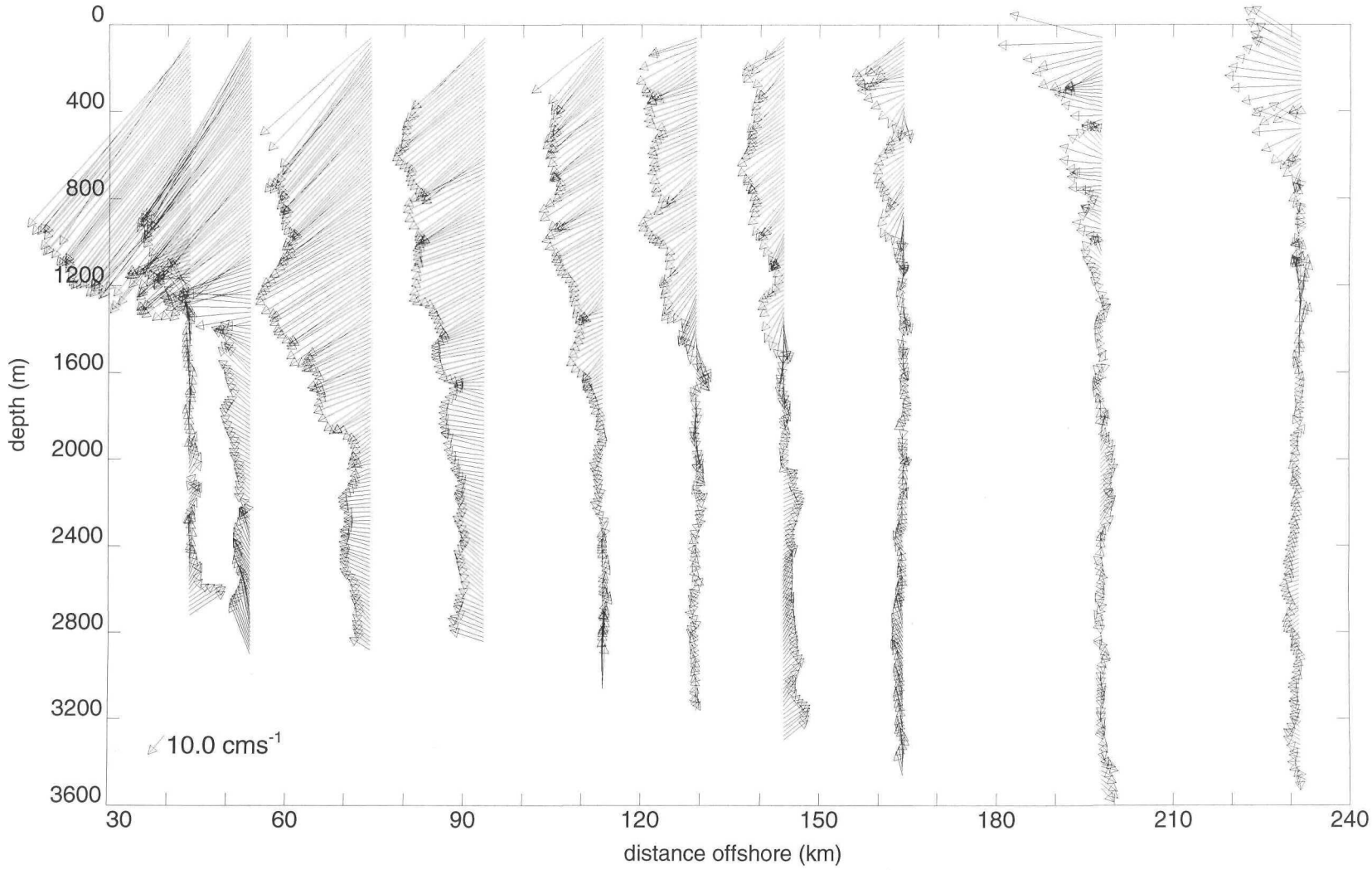


Figure 4.2 LADCP velocity vectors. From left to right, stations 9, 8, 7, 6, 5, 14, 4, 3, 15 and 2. The vector scale is shown with the arrow pointing to 220°T. Northward flow is vertically upward, eastward flow is to the right.

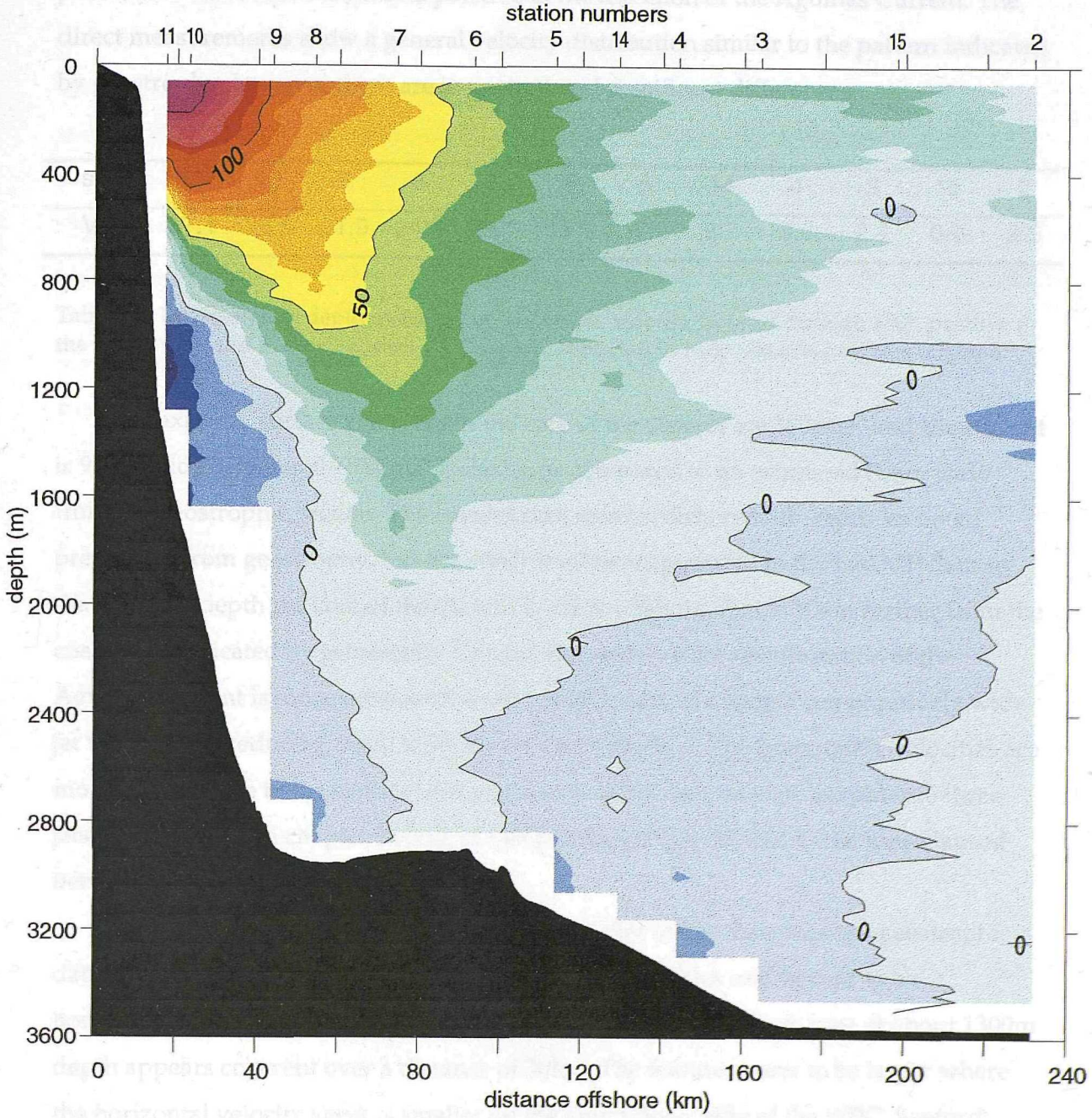


Figure 4.3 Along-stream LADCP velocities contoured across the ACE section. Velocities have been rotated through 130° so that along-stream flow is positive to the south-west (220°T). Velocity transitions are indicated by colour changes at intervals of 10cms$^{-1}$.

positive to the south-west, that is positive in the direction of the Agulhas Current. The direct measurements show a general velocity distribution similar to the pattern indicated by geostrophy, however there are important and significant differences.

| stn | 11 | 10 | 9 | 8 | 7 | 6 | 5 | 14 | 4 | 3 | 15 | 2 |
|---|---|---|---|---|---|---|---|---|---|---|---|---|
| $V_{ref}$ | 37.1 | 36.5 | 21.9 | 24.5 | 28.1 | 18.9 | 10.0 | 8.7 | 3.8 | 2.1 | 0.9 | 2.5 |

Table 4.1 Down-stream depth-averaged or barotropic velocity (rotated through 130°, positive to the south-west and in $cms^{-1}$) at each ACE station. From left to right stations progress offshore.

Maximum surface velocities in the core of the current are $180cms^{-1}$ and the current is 90km wide between the $50cms^{-1}$ isotachs, as compared to an estimated 70km wide from the geostrophic section. The current core moves offshore with depth, as noted previously from geostrophy, but the effect is more exaggerated in the LADCP data so that at 900m depth the core of the current is 65km offshore, that is 10km further from the coast than indicated by geostrophy. Overall the near-surface manifestation of the Agulhas Current is more consistent in the LADCP data, showing a comparatively wide jet with speeds reducing away from the centre of the flow. The geostrophic velocities are more patchy close to the surface with some indication that the WBC is split into three jets. As discussed in chapter 3 some of this patchiness may be due to the time elapsed between stations.

The LADCP data exhibits structure on smaller scales than does the geostrophic data. These features are of order a few hundred metres thick and appear to be horizontally coherent, for instance the feature across the high shear zone at about 1300m depth appears coherent over a distance of 30km. The features seem to be larger where the horizontal velocity shear is smaller on the anticyclonic side of the WBC. Sanford (1975) used repeat profiles taken half an inertial period apart to demonstrate that similar small scale velocity features were due to inertial oscillations. In the ACE data there are no repeat stations and therefore we can only guess at what these features may represent.

One of the most obvious differences between the LADCP velocities and geostrophy is the vertical structure of velocity in the deep waters. In chapters 1 and 3 we showed that it is common when calculating geostrophic velocities to assume that the ZVS is generally deep and horizontal. Now we can see that choosing such a level of no motion in the Agulhas Current imposes a very different shape to the velocity jet at depth (figure 3.8) than the shape revealed by the direct measurements (figure 4.3). The LADCP

data shows that the jet is distinctly V-shaped (in the vertical) throughout the water column and so is the level of no motion. In fact at the coastal end of the section the ZVS leaves the continental slope at a depth of just 700m and then falls off towards the continental rise at an angle almost parallel to the slope of the topography, reaching a depth of 2900m some 80km offshore. Thereafter it rises steadily until it reaches 1000m depth about 200km from the coast.

Comparing this velocity structure to geostrophy the result of the V-shaped ZVS is to increase the shears on the cyclonic side of the current but elsewhere to decrease them, thus allowing the jet to widen and strengthen in the deeper waters. Where the shears are large on the cyclonic side of the current the LADCP data reveals a counter-current flowing next to the continental slope beneath the WBC. This undercurrent has velocities larger than $30cms^{-1}$ to the north-east, is centred around a depth of 1200m and is positioned directly below the surface core of the south-westward flowing Agulhas Current. Recall that in chapter 2 the uncertainties associated with the absolute LADCP velocities were found to be large at station 10, which is one of only three stations that sampled the Agulhas Undercurrent. However, the suggestion from both the bottom tracking derived velocities near the sea bed and the ADCP velocities near the sea surface was that the barotropic component at station 10 may be in error by about 5 to $10cms^{-1}$, and therefore any adjustment would only serve to increase the magnitude of the undercurrent.

The observation of an Agulhas Undercurrent during ACE raises several questions which are addressed in the next part of this chapter (section 4.2). Perhaps the most obvious question is how reliable are the measurements, since the LADCP technique has not previously been used in a WBC and the Undercurrent has never been observed before. Moreover, if the Undercurrent does exist could it be a persistent DWBC driven by basin-wide thermohaline processes (Stommel, 1958) or is it a local feature driven by topography (Gill & Schumann, 1979)? These questions are addressed by examining further observational evidence of the Agulhas Undercurrent. In addition there is a particular question associated with the water mass structure of the Undercurrent. In chapter 3 it was shown that RSW is present at intermediate depths close to the continental slope, in fact it is in a position apparently coincident with the Undercurrent. If the Undercurrent is transporting RSW equatorward this would mean a flow of waters towards their source, which seems unlikely. An attempt is made to shed light on the dynamics of the Undercurrent and the intermediate water masses by

examining the potential vorticity of the Agulhas Current. To complete the discussion, the volume transport of the Agulhas Undercurrent is estimated.

In the second half of this chapter the whole Agulhas Current is once more considered and LADCP results are compared more closely to geostrophy. Section 4.3 looks at the differences between geostrophic velocities and direct velocities from LADCP and attempts to explain them in terms of sampling errors, measurement errors and possible real dynamical effects. Finally in section 4.4 the volume transport of the Agulhas Current is estimated in a number of different ways using a combination of direct measurements and geostrophic estimates.

## 4.2 The Agulhas Undercurrent

### 4.2.1 Persistence

There is evidence that the Agulhas Undercurrent may have been measured before by Toole & Warren (1993) during the RRS *Charles Darwin* 32°S transindian section in November 1987. In chapter 3 we saw that TW estimated a ZVS that reflected their requirements on the flow direction of the deep and intermediate waters in the Agulhas Current. However, using their ADCP measurements as a reference for geostrophic shears on stations 5 to 8 TW found that the resulting velocity profiles had a zero crossing around 1000m depth, below which there was equatorward flow. On the basis of the intermediate water mass characteristics, specifically the flow of RSW towards its source, TW rejected the possibility of an undercurrent below 1000m depth and chose to retain a deeper ZVS.

Further measurements of the Agulhas Undercurrent were made in April 1996, when the ACE section across the Agulhas Current at 32°S was repeated during a mooring recovery cruise aboard RV *Algoa* (a South African vessel belonging to the Sea Fisheries Research Institute in Cape Town). The experiment was named ACE Recovery (ACER). Having observed an Undercurrent during ACE, ACER provided a timely opportunity to take the LADCP back to the Agulhas Current and attempt to sample the Undercurrent again. However, whilst the RV *Algoa* is more than adequate for a mooring recovery operation (as was originally planned) the vessel is not well suited to deep sea hydrography. Thus there were two limitations: the maximum length of cable available

with which to lower equipment was just 2000m, and a lack of clearance above the starboard deck meant that CTD and LADCP operations could not be carried out simultaneously.

Despite these limitations the Agulhas Undercurrent was observed during ACER and in much the same position as it was found the previous year. Figure 4.4 is a contoured section of rotated, absolute LADCP velocities in the Agulhas Current from the RV *Algoa*. Since no simultaneous CTD measurements were taken the depth of the LADCP and the in situ speed of sound could not be determined from local pressure, temperature and salinity. Instead the depth of the LADCP was calculated by integrating the vertical component of the measured velocity. The resultant error in the depth is estimated to be about 10m in every 1000m from differences in the LADCP estimates of the sea surface at the end of each cast. As for variations in the speed of sound, the LADCP standard sound speed is 1500ms$^{-1}$, and the in situ speed of sound varies by no more than 2% from this standard. Therefore a further depth error of 1% may be contributed, making a total possible depth error in the ACER LADCP data of 2%. The ACER section consists of nine LADCP velocity profiles out to 116km offshore (figure 4.4). With the exception of the two most inshore stations, 4 and 5, all LADCP measurements during ACER were taken with the instrument set up in configuration 4 (see appendix 1), but with bottom tracking mode switched off. Stations 4 and 5 were set-up with 20 bins of length 4m (rather than 16m) since the stations were relatively shallow. However such a short binlength increases the shear standard deviation from about $4\times10^{-3}$ s$^{-1}$ (see chapter 2) to $10\times10^{-3}$ s$^{-1}$.

The overall structure of the Agulhas Current as revealed by the ACER data is similar to the structure found in the ACE LADCP section and in particular the Agulhas Undercurrent is clearly evident. Stations 4 and 5 are further inshore than the innermost station (11) on the ACE section so that the cyclonic edge of the Agulhas Current is much better determined in 1996 than it was in 1995. The Agulhas Current in the ACER section runs shallower and narrower than in the ACE section and there is evidence that the core of the WBC is even closer to the coast. The 50cms$^{-1}$ isotach indicates a current width of 75km, compared to 90km during ACE. The Agulhas Undercurrent is similarly situated in both sections where at 20km offshore the depth of the zero crossing point is 800m. The core of the Undercurrent appears to be 300m deeper in 1996, however it extends to between 60 and 70km from the coast in both sections, although this observation is limited to the upper 2000m in the ACER section. In the ACER data the peak velocity in

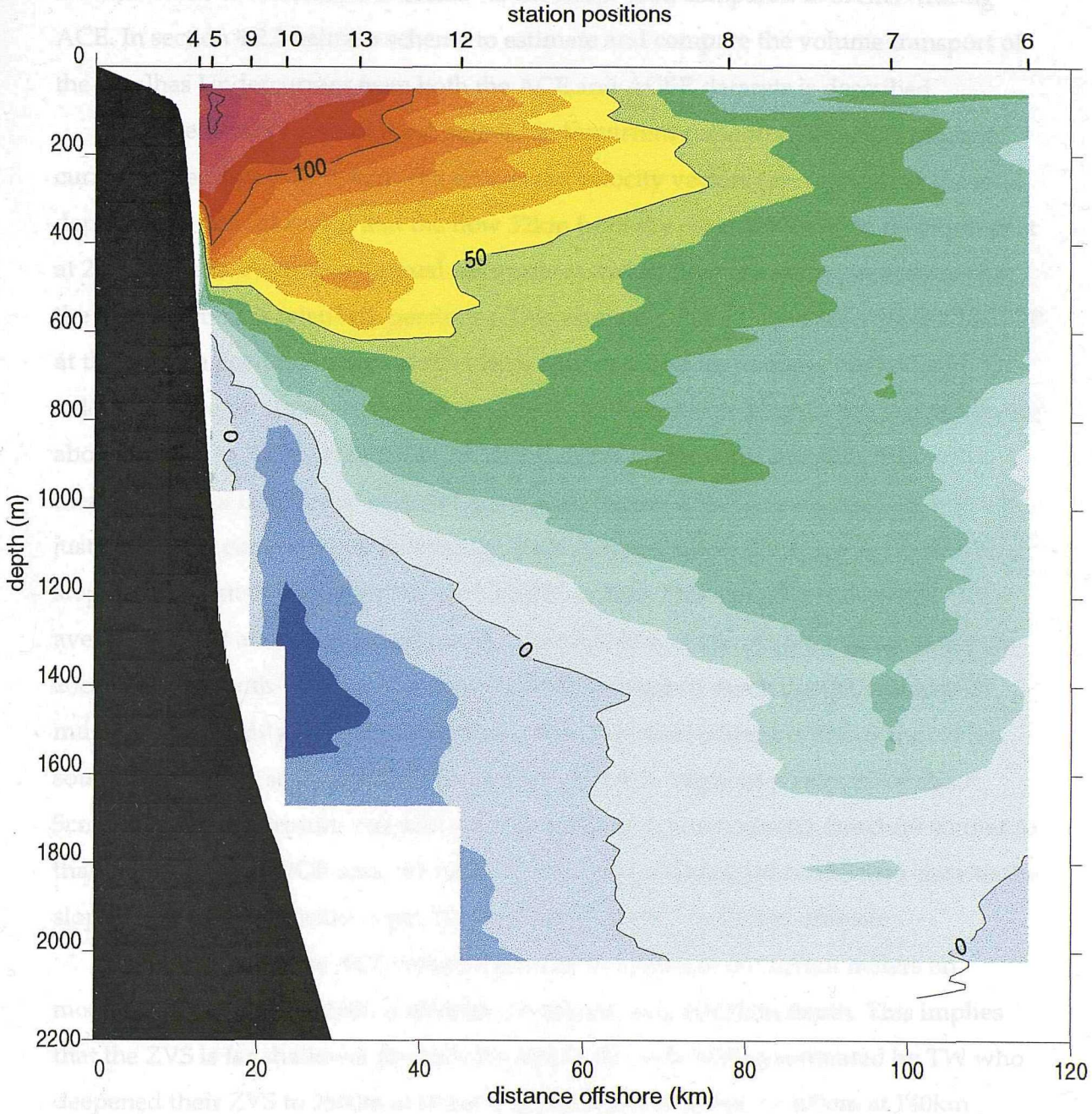


Figure 4.4 Contoured LADCP velocity data from ACER, April 1996. (The ACER section has the same position and orientation as the ACE section). LADCP north and east velocities have been rotated through 130° so that the flow is positive to the south-west (220°T). Velocity transitions are indicated by colour changes at intervals of 10cms$^{-1}$(colour scale same as figure 4.3). Note that the depth and distance scales are different from those of figure 4.3.

the core of the undercurrent is 28cms$^{-1}$ to the north-east, compared to 39cms$^{-1}$ during ACE. In section 4.2.3 below a scheme to estimate and compare the volume transport of the Agulhas Undercurrent from both the ACE and ACER datasets is described.

More observations of the Agulhas Undercurrent come from the ACE moored current meter data (figure 4.5). The time mean velocity vectors (averaged over the total deployment period) reveal that the flow 32km from the coast is 10cms$^{-1}$ to the north-east at 2000m depth. Finding an annual net north-eastward flow is a strong indication that the undercurrent is relatively persistent. Unfortunately there is no data from the LADCP at this precise position in the Undercurrent (due to a bottom triangle) but LADCP velocities close by also indicate that the flow is of the order of 10cms$^{-1}$. The current meter above the one in the Undercurrent, at 1200m depth on the same mooring line, shows a mean current of only 1cms$^{-1}$ directed northward (figure 4.5). The zero crossing is clearly just above this current meter on average, indicating a shallow ZVS near the continental slope as suggested from the synoptic LADCP section. This should be compared to the average current at the same depth on the next mooring 63km offshore which is almost 20cms$^{-1}$ to the south-west, so that here the ZVS has dipped much deeper and indeed must be significantly deeper than 2000m where the mean current is still 6cms$^{-1}$ to the south-west. At the same position the LADCP data also suggests a velocity of about 5cms$^{-1}$. Again these results support the hypothesis of a deep velocity structure similar to that resolved by LADCP data, where the ZVS is very shallow (above 1000m) close to the slope, but deepens quickly to reach to sea bed at about 70 or 80km offshore.

Farther along the ACE section the mean velocities from current meters on moorings at 102km and 160km offshore are almost zero at 2000m depth. This implies that the ZVS is far shallower towards the end of the section than estimated by TW who deepened their ZVS to 2500m at about 90km offshore and then to 3000m at 140km offshore. In fact, the velocity structure from the time series data supports the LADCP results convincingly right across the section (figure 4.5).

To summarise, an Agulhas Undercurrent has been observed along the ACE section at 32°S in February-March 1995 and again in April 1996 using an LADCP. On each occasion the Undercurrent exhibited maximum velocities of about 30cms$^{-1}$ to the north-east, counter to the direction of the Agulhas Current above it. The Undercurrent exists below 800m depth under the core of the Agulhas Current (20km offshore), and over the continental slope out to a distance of about 70km offshore. The existence of an undercurrent was inferred in the same position in November 1987 when ADCP

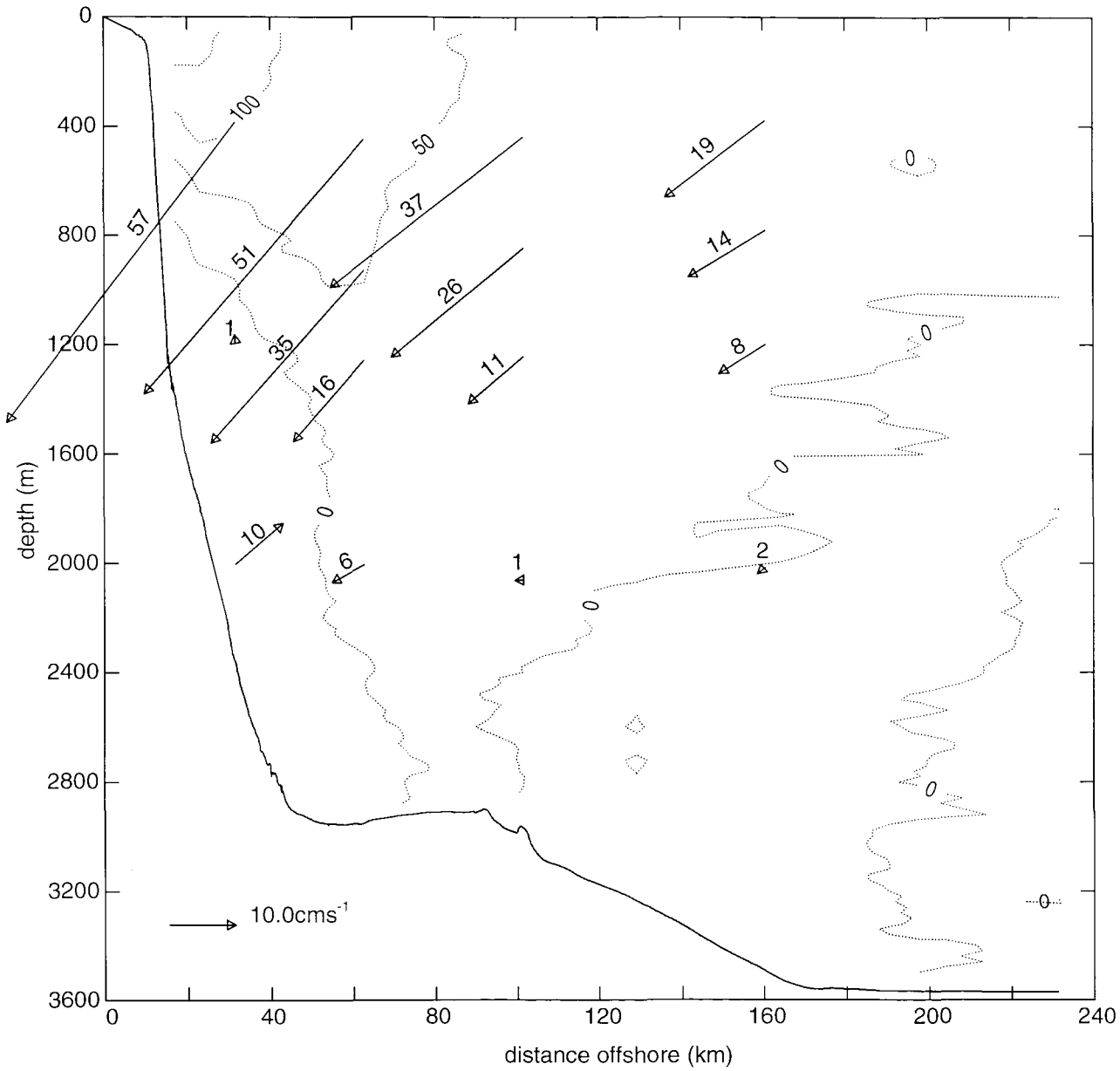


Figure 4.5 Mean velocity vectors from moored current meters. The mean is taken as the vector average over the full period of available data from each current meter. Northward flow is vertically upward, eastward flow is to the right. The vector scale is shown at the bottom and the numbers on the vectors represent speed in $cms^{-1}$. Dotted lines are contours of LADCP along-stream velocity in $cms^{-1}$ (see figure 4.3). The solid line represents bathymetry.

referenced, geostrophic velocities suggested north-eastward flow below 1000m depth (TW). Velocity time series data collected along the ACE section over the period February 1995 to April 1996 also indicate an Undercurrent. Results from moored current meters positioned 30km offshore show mean velocities of $10cms^{-1}$ to the north-east at 2000m depth and about $1cms^{-1}$ to the north at 1200m depth. These results concur with the position and magnitude of the Undercurrent as revealed in the synoptic LADCP results. On the basis of these observations we conclude that the Agulhas Undercurrent is a persistent feature of the circulation of the Southwest Indian Ocean.

### 4.2.2 A discussion on the presence of Red Sea Water in the Agulhas Undercurrent

The previous section presented much evidence of a relatively persistent Agulhas Undercurrent and yet it still seems unlikely that RSW should be flowing towards its source on average. In this section several hypotheses that attempt to resolve this dilemma are discussed.

The first possibility is that the relatively salty, anoxic water mass identified as Red Sea Water is in fact from an alternative source. The water could flow around the Cape from the South Atlantic, hugging the continental slope and passing beneath the Agulhas Current as it separates from the continental shelf off Port Elizabeth. WOCE section A11 crosses the Angola Basin near 30°S, heading for the African coast perpendicular to the underlying topography. Hydrographic data from the last twelve stations on section A11 is shown in figure 4.6. There is no evidence of modification of AAIW by relatively saline waters in the A11 data, in fact the intermediate waters are 0.15 psu fresher than AAIW in the Indian Ocean and 0.35psu fresher than the supposed RSW. Thus there seems to be no source or flux of such salty waters through the Southeast Atlantic. Indeed the only source of saline intermediate waters in the Atlantic is the Mediterranean outflow which sinks over the Gibraltar sill and begins to spread at a depth of 1000m with a salinity of 36.5, but Mediterranean water has not been observed crossing the equator. This evidence combined with other sightings of RSW in the Southwest Indian Ocean (see chapter one) and the indications of a possible path in Wyrtki's atlas of the Indian Ocean (Wyrtki, 1971) lead to the conclusion that the relatively saline and oxygen depleted intermediate waters found in the ACE section can have no other source than the Red Sea.

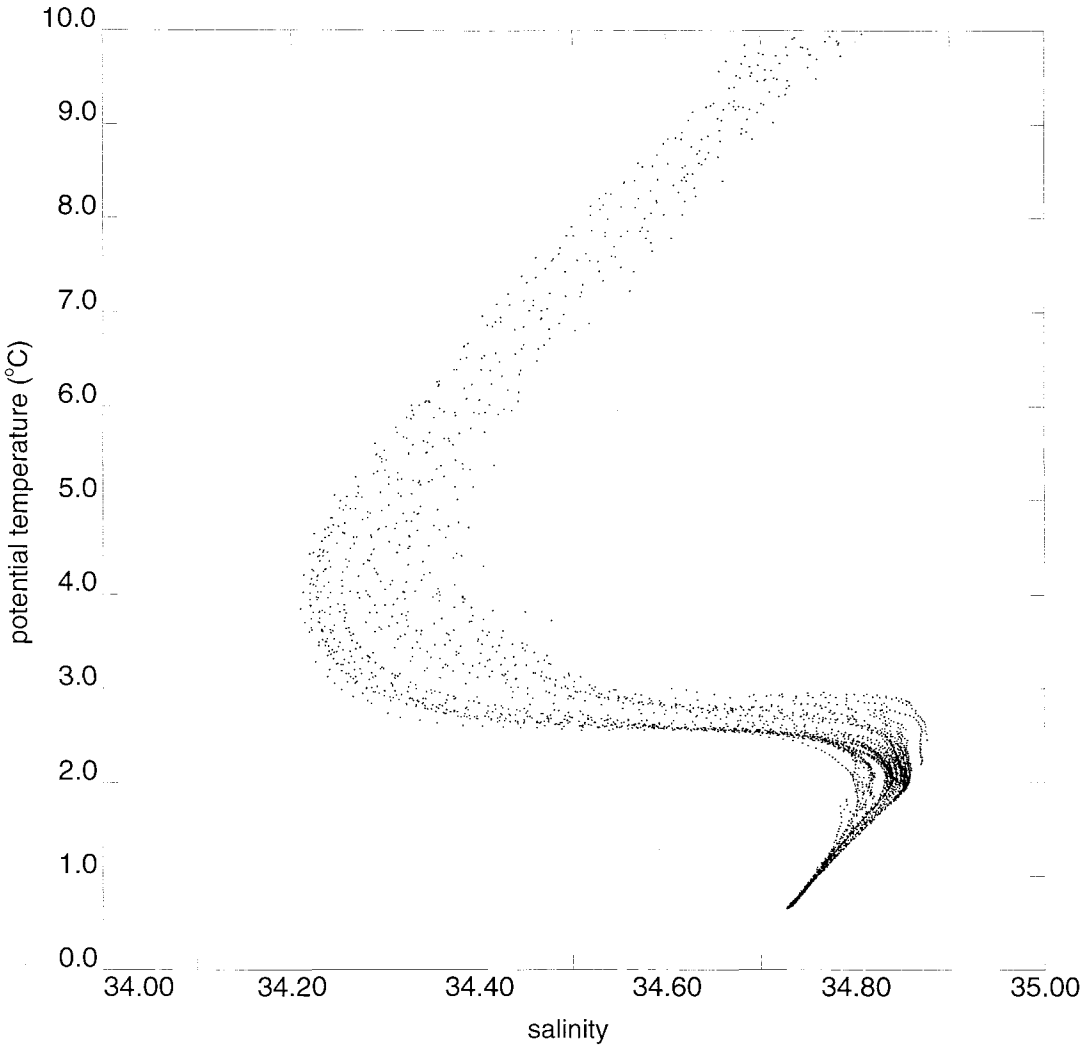


Figure 4.6 Temperature - salinity relationship of water masses in the eastern basin of the South Atlantic, from WOCE cruise A11 (data from 44°S, 12°W to 30°S, 15.5°E). There is no evidence of high salinity intermediate waters of Atlantic origin.

Having established the presence of RSW, perhaps the Undercurrent is highly variable at depths above 1500m and thus there may be no net flow of RSW towards the equator. In chapter one it was mentioned that large meanders propagate downstream along the Agulhas Current several times a year pushing the current far off course. These meanders are believed to originate at about 29°S in the Natal Bight and are known as Natal Pulses. At 32°S a Natal Pulse can cause the Agulhas Current to meander more than 100km offshore. When the Agulhas Current moves offshore and the velocity shear on the cyclonic edge of the WBC reduces, it is possible that the north-eastward flow either vanishes or moves offshore as well.

Results from the ACE moored current meter array show four events between March and the end of December 1995 which indicate the passing of a Natal Pulse. At 400m depth and 32km offshore the velocity weakens and turns cyclonically through 360° during each of these events (figure 4.7). The events are anywhere between 5 and 20 days long and occur in April (around Jday 125), at the beginning of August (Jday 225), at the end of September (Jday 280) and in mid November (Jday 340). These four events can also be seen in the near-surface (400m) velocity time series 63km offshore, but here the current does not weaken so significantly and during two of the events there is no complete spin of the velocity vector. Instead the current turns cyclonically to the north-west and then turns back, anti-cyclonically to the south-west again. What happens in the Undercurrent during these events?

The current meter at 1200m depth, 30km offshore shows a highly fluctuating velocity with little correlation to the flow above (figure 4.8a). This is perhaps because the current meter is in the edge of the undercurrent where shears are high, but it could also indicate that the Undercurrent is highly variable at this depth. If the Undercurrent is highly variable at intermediate depth then the net transport of RSW to the north may be negligible. However, at 2000m depth on the same mooring the velocity time series (figure 4.8b) shows a persistent Undercurrent with only a few isolated reversals which are not coincident with events in the flow above. During each of the seven events the Undercurrent reverses and flows towards the south-west and during three of the events the velocity vector circles cyclonically 360°. These results indicate that although there are similar reversals present in the deep current record as those attributed to Natal Pulses close to the surface, there is little similarity between the variability in the Agulhas Current and the Undercurrent. Moreover the Undercurrent appears to be relatively

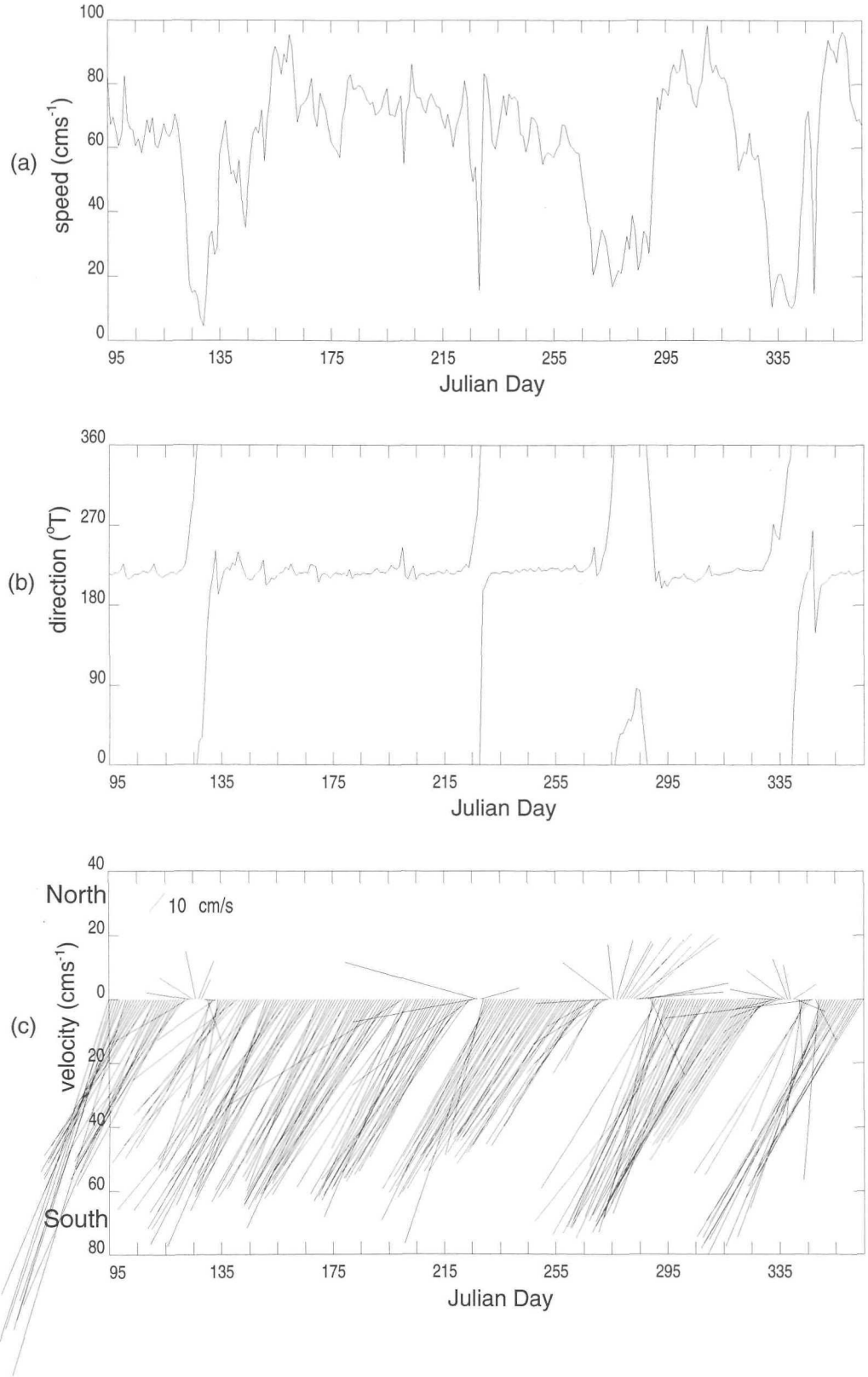


Figure 4.7 Time series data from ACE moored current meter situated 31.5km offshore and at 437m depth. Julian day is referenced to 1 Jan 1995. All data is daily averaged: (a) speed, (b) direction, (c) velocity vectors; scale of velocity vectors is shown rotated to 220°T. Time period shown is that of shortest current meter record so that figures 4.7(c) and 4.8(a) and (b) are all on same time scale.

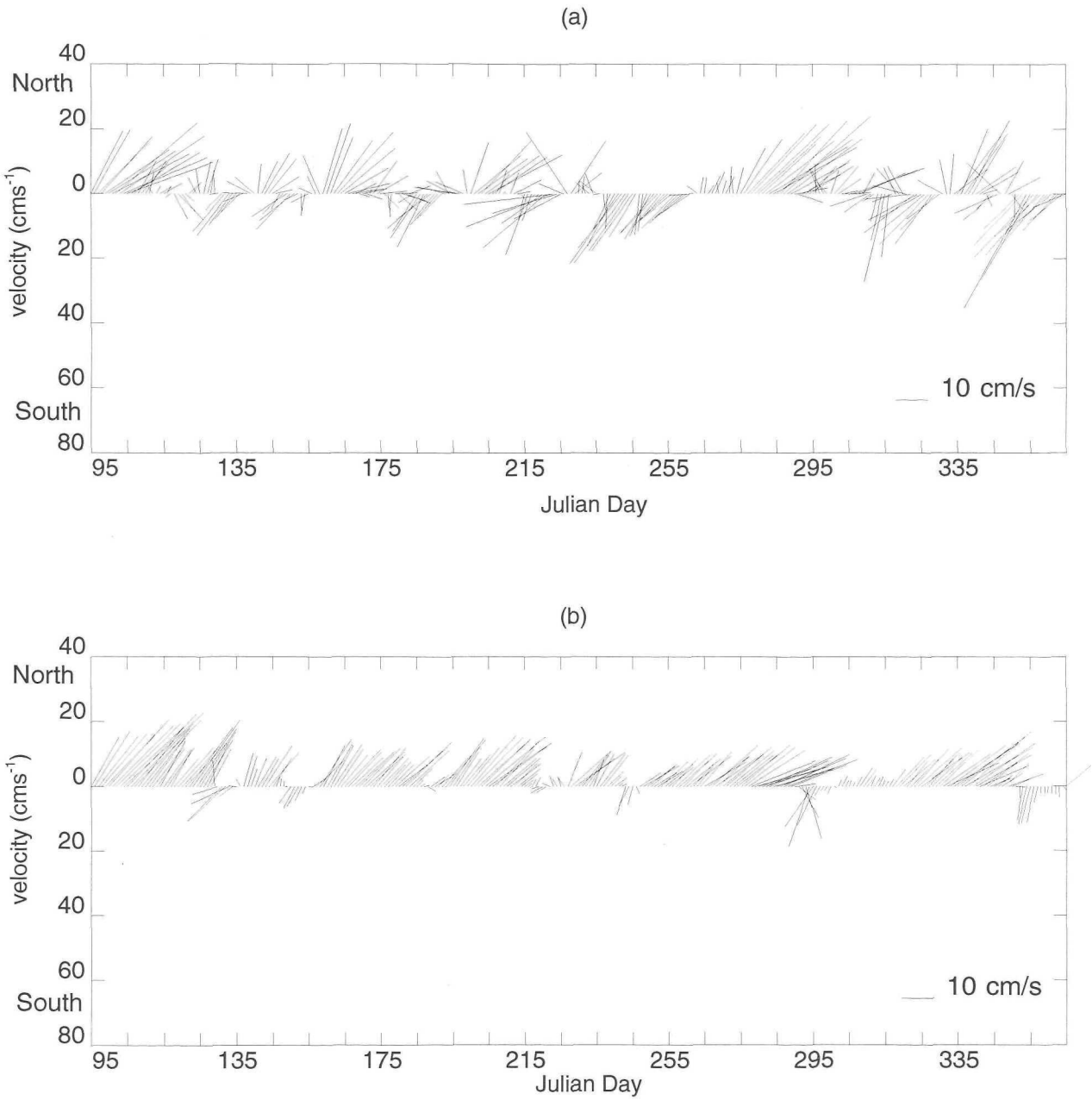


Figure 4.8 Vector time series data from ACE moored current-meters situated 31.5km offshore at (a) 1189m and (b) 2004m depth. Julian day is referenced to 1 Jan 1995. Scale of velocity vectors is shown on each plot.

steady which suggests that the flow variability seen from the current meter at 1200m is as a result of the instrument being sometimes in the Undercurrent and sometimes not. The frequency and duration of the events which interrupt the Undercurrent are not sufficient to significantly reduce any equatorward transport of RSW.

The problem still remains that RSW seems to be transported equatorward at intermediate depths in the Agulhas Undercurrent. Due to the presence of RSW it might be considered that the Undercurrent is part of a localised deep recirculation cell. The current at 32°S is at its narrowest and most swift as it makes its closest approach to the coast (Pearce, 1977; Gill & Schumann, 1979), so that boundary effects may become a significant forcing close to the steep continental slope. However, as figure 4.9 illustrates, the Undercurrent carries some of the most concentrated RSW as well as some of the most dilute so that a recirculation hypothesis seems unlikely. Examining more closely the juxtaposition of the Undercurrent and RSW (figure 4.9) it becomes apparent that the core of the Undercurrent is in fact generally deeper than the core of the RSW layer. In addition the most concentrated RSW is present on station 8 (figure 3.6) where the flow at intermediate depths is to the south-west. Overall the relationship of flow directionality and water mass distribution is muddled.

The best way to resolve the difficulty of RSW flow towards the equator is to estimate its overall volume transport. LADCP velocities can be combined with salinity and temperature data to give an estimate for the volume transport of RSW across the ACE section. Waters representative of RSW in the Agulhas Current were estimated to lie within three classes: water of salinities greater than 34.61 and with potential temperatures between 3.55 and 8°C, waters with salinities between 34.54 and 34.61 and potential temperatures between 4.5 and 6.93°C, and waters saltier than 34.68 and between 8 and 9°C (see figure 5.3). The volume transport of each of these classes is 5.5Sv, 1.7Sv and 2.8Sv respectively all towards the south-west. Therefore, the estimated volume transport of RSW across the whole section is 10Sv poleward and thus there is a net flow of RSW away from its source.

### 4.2.3 Volume transport of the Undercurrent

In order to estimate comparable volume transports for the Undercurrent measured in March 1995 and April 1996 it is necessary to fill in the data gaps between the velocity profiles and the continental slope. Two extrapolation techniques are used:

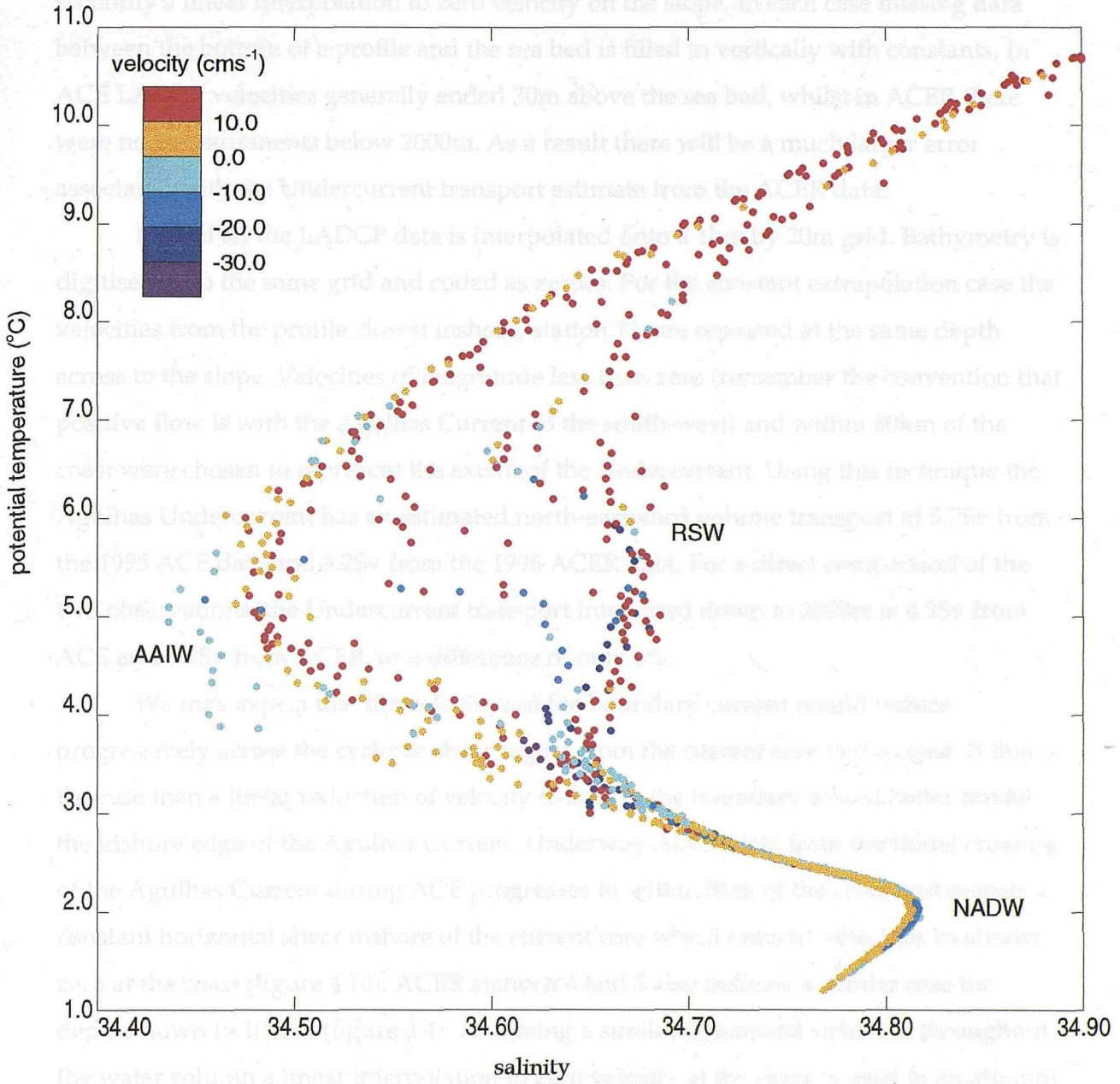


Figure 4.9 Temperature - salinity relationship of water masses in the Agulhas Current at 32°S. The temperature and salinity interval is chosen to emphasise the intermediate and deep water masses of AAIW: Antarctic intermediate water, RSW: Red sea water and NADW: North Atlantic deep water. The velocity (from LADCP) of the water masses is indicated with colours, as shown on the colour scale, with each colour transition marking a change of 10cms$^{-1}$. Undercurrent flow is depicted in shades of blue. Positive flows in red and orange represent south-westward flow in the direction of the Agulhas Current.

firstly a straightforward, horizontal extrapolation of constant velocities to the slope and secondly a linear interpolation to zero velocity on the slope. In each case missing data between the bottom of a profile and the sea bed is filled in vertically with constants. In ACE LADCP velocities generally ended 30m above the sea bed, whilst in ACER there were no measurements below 2000m. As a result there will be a much larger error associated with the Undercurrent transport estimate from the ACER data.

First of all the LADCP data is interpolated onto a 1km by 20m grid. Bathymetry is digitised onto the same grid and coded as zeroes. For the constant extrapolation case the velocities from the profile closest inshore, station 11, are repeated at the same depth across to the slope. Velocities of magnitude less than zero (remember the convention that positive flow is with the Agulhas Current to the south-west) and within 80km of the coast were chosen to represent the extent of the Undercurrent. Using this technique the Agulhas Undercurrent has an estimated north-eastward volume transport of 5.7Sv from the 1995 ACE data and 8.2Sv from the 1996 ACER data. For a direct comparison of the two observations, the Undercurrent transport integrated down to 2000m is 4.9Sv from ACE and 5.2Sv from ACER, or a difference of only 6%.

We may expect that the velocities in the boundary current would reduce progressively across the cyclonic shear region from the current core to the coast. If this is the case then a linear reduction of velocity to zero at the boundary would better model the inshore edge of the Agulhas Current. Underway ADCP data from the initial crossing of the Agulhas Current during ACE progresses to within 5km of the coast and reveals a constant horizontal shear inshore of the current core which reduces velocities to almost zero at the coast (figure 4.10). ACER stations 4 and 5 also indicate a similar case for depths down to 1000m (figure 4.4). Assuming a similar dynamical structure throughout the water column a linear interpolation to zero velocity at the slope is used in an attempt to crudely model for the horizontal shear. Using this technique to fill in the data gaps reduces the volume transport of the Undercurrent to 5.0Sv from the ACE data and 7.6Sv from ACER.

In chapter 2 the LADCP data collected aboard RRS *Discovery* during ACE was compared with the mean on-station ADCP velocities. The shear profile from each technique is very similar and the difference between the barotropic component of the LADCP and ADCP profiles was found to be within LADCP measurement error estimates, except on station 10. Adjusting the ACE LADCP measurements barotropically to match the ADCP measurements near the surface gives larger estimates for the volume

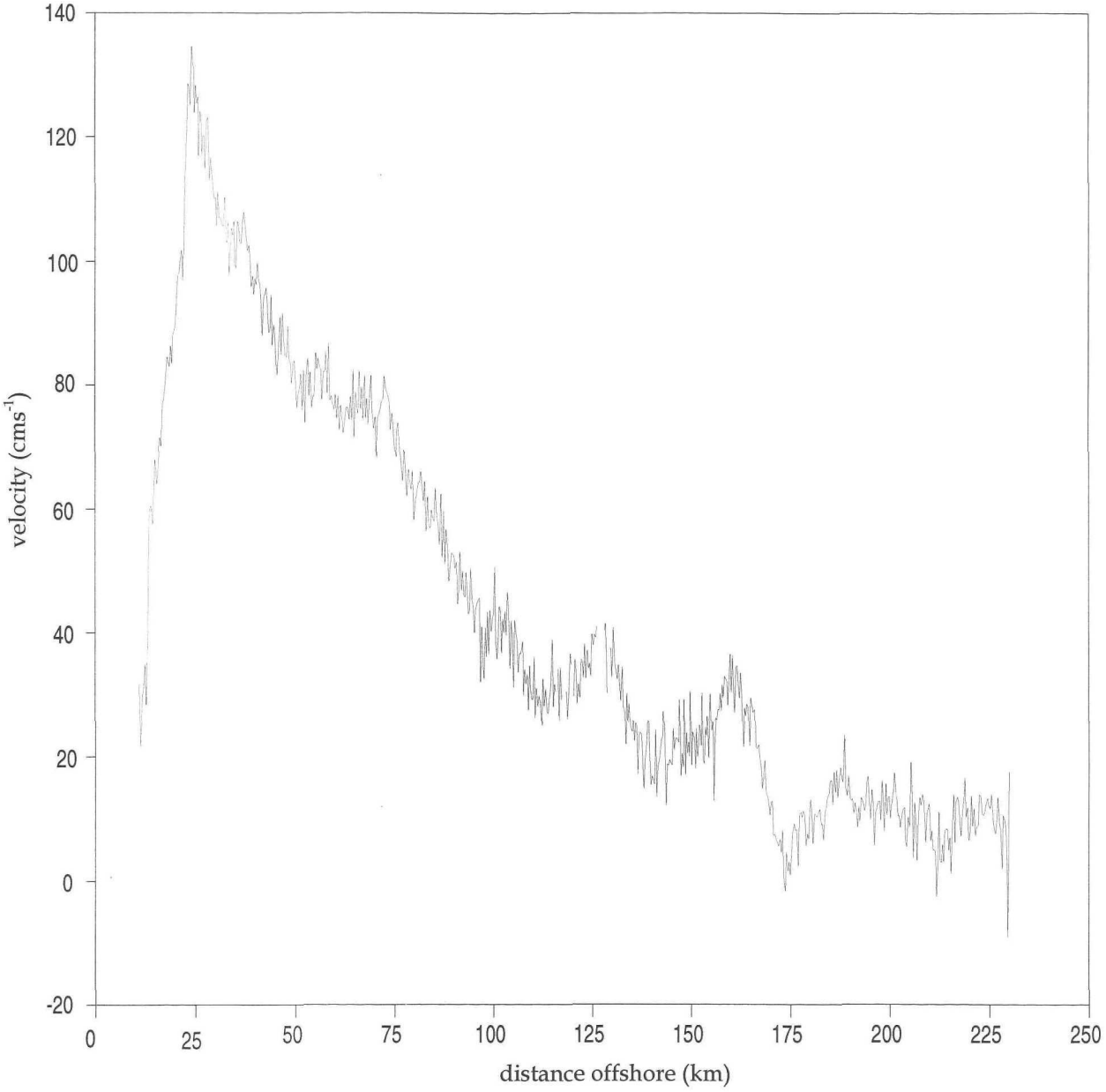


Figure 4.10 Underway ADCP velocity along the ACE section at 237m depth . Velocity has been rotated through 130° to give along-stream velocity positive to the south-west (220°). This data has been post-processed using differential GPS.

transport of the undercurrent. Constant extrapolation of the adjusted velocities gives a volume transport of 6.6Sv and linear interpolation to a no slip boundary gives an estimate of 5.8Sv. In conclusion the Agulhas Undercurrent has a volume transport of 6±1Sv to the north-east.

### 4.2.4 Potential Vorticity

Potential vorticity (PV) is an important quantity in ocean dynamics because it combines two basic laws: the conservation of mass and the conservation of angular momentum. If dissipation and diabatic processes are insignificant then PV is conserved and can be used as a tracer of large scale ocean circulation (Liu & Rossby, 1993; McDowell *et al*, 1982). In chapter 3 a scale analysis of the terms in the x-momentum equation suggested that dissipative effects were negligible even in the cyclonic edge of the current. Certainly geostrophy should hold as far onshore as station 11, the innermost LADCP profile from ACE. In this case we may expect that the distribution of potential vorticity across the Agulhas Current will reflect the very different origins of the water masses present.

PV can be expressed in a natural co-ordinate system that reflects the geometry of the Agulhas Current. Using Ertel vorticity (Pedlosky, 1986) and neglecting unimportant terms by scale analysis PV can be written:

$$Q = -\frac{1}{\rho}\left\{ f\frac{\partial \rho}{\partial z} + \left( \frac{\partial v}{\partial x}\frac{\partial \rho}{\partial z} - \frac{\partial v}{\partial z}\frac{\partial \rho}{\partial x} \right) \right\} \qquad 4.1$$

where $x$ is the cross stream co-ordinate (positive offshore) and $z$ is depth (positive downwards). The first term on the right hand side is the planetary vorticity multiplied by the stratification, the second term is the shear vorticity (including stratification) along an isopycnal. Since the density surfaces in a WBC are far from horizontal the shear vorticity normal to an isopycnal has contributions from both the vertical and horizontal shear of the current. The vertical density gradient can be expressed in terms of the buoyancy frequency, N and the horizontal density gradient can be expressed in terms of the vertical shear using the thermal wind balance:

$$\frac{N^2}{g} = -\frac{1}{\rho}\frac{\partial \rho}{\partial z} \qquad 4.2 \qquad\qquad \frac{f}{g}\frac{\partial v}{\partial z} = -\frac{1}{\rho}\frac{\partial \rho}{\partial x} \qquad 4.3$$

So that the potential vorticity equation becomes:

$$Q = Q_p + Q_{hs} + Q_{vs} = \frac{fN^2}{g}\left\{1 \quad + \quad \frac{1}{f}\frac{\partial v}{\partial x} \quad - \quad \frac{1}{N^2}\left(\frac{\partial v}{\partial z}\right)^2\right\} \qquad 4.4$$

Rossby no. Richardson no.

Three contoured, full depth sections of the three components of Q are shown in figure 4.11. Typical contributions from each of the terms in equation 4.4 are: planetary vorticity, $Q_p \approx 1.5\times10^{-10}\,\mathrm{m^{-1}s^{-1}}$; relative vorticity from horizontal shear, $Q_{hs} \approx -1\times10^{-10}\,\mathrm{m^{-1}s^{-1}}$ and relative vorticity from vertical shear, $Q_{vs} \approx -1\times10^{-10}\,\mathrm{m^{-1}s^{-1}}$ on the cyclonic side of the current. On the anticyclonic (offshore) side of the WBC the relative vorticity contributions are small. Although $Q_{hs}$ and $Q_{vs}$ are of similar magnitude their distributions are different and they do not negate each other. At intermediate depths and within 80km of the coast the relative vorticity plays a significant role in shaping the PV field (figure 4.12).

Across most of the width of the Agulhas Current the total PV at a given depth is more or less independent of cross stream distance (figure 4.12). However, at depths between 400m and 1400m and within about 80km of the coast the horizontal PV gradients are high and the magnitude of PV becomes large. Schmitz (1969) found a similar pattern of small, uniform PV offshore and high PV onshore in the Gulf Stream. In the Agulhas Current the transition between relatively uniform PV in the eastern end of the section and the inshore region of large lateral PV gradients is located just to the west of the current core and moves offshore with depth, as does the current core. This transition occurs at a PV value of about $1.3\times10^{-10}\mathrm{m^{-1}s^{-1}}$ and between the 14°C and 4°C isotherms, above and below which the PV is more or less uniform along an isotherm across the whole section. The PV structure suggests that at intermediate depths there is a tendency for the PV distribution to behave like a barrier between the high velocity cyclonic core of the Agulhas Current and water farther offshore, which impedes lateral mixing of intermediate water masses. Such a barrier perhaps goes some way to

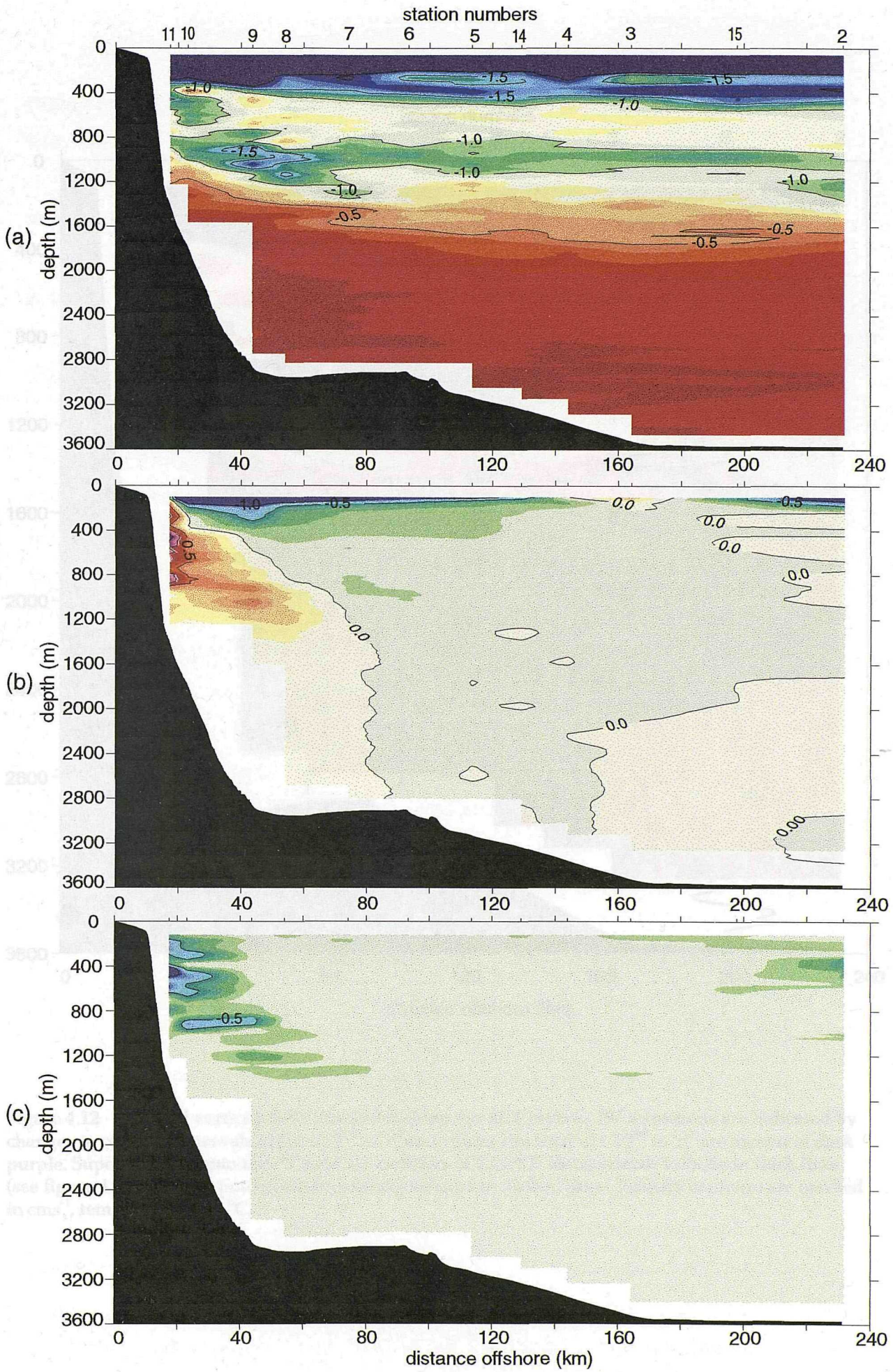


Figure 4.11 Contoured sections of (a) planetary vorticity, (b) relative vorticity from horizontal shear and (c) relative vorticity from vertical shear. Vorticity transitions are indicated by colour changes at intervals of $0.1 \times 10^{-10} m^{-1}s^{-1}$. Colour scales are the same for (b) and (c), but NOT for (a) where all colours indicate negative vorticity. In (a) values less than $-2 \times 10^{-10} m^{-1}s^{-1}$ are shown in dark purple.

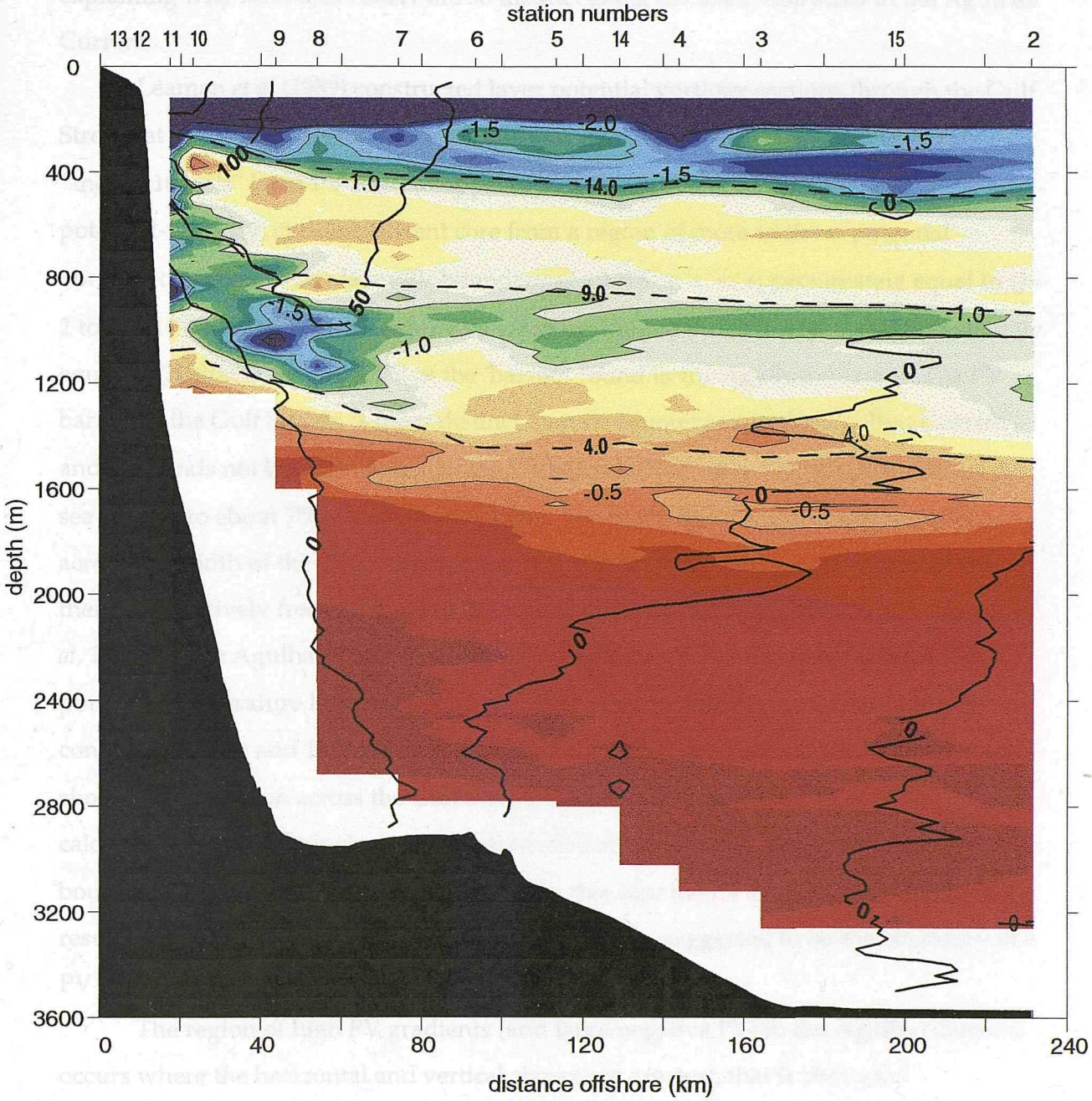


Figure 4.12 Potential vorticity (PV) contoured along the ACE section. PV transitions are indicated by changes in colour at intervals of $0.1 \times 10^{-10}$ $m^{-1}s^{-1}$ and values less than $-2 \times 10^{-10}$ $m^{-1}s^{-1}$ are shown in dark purple. Superimposed onto the PV field are contours of LADCP along-stream velocity in thick lines (see figure 4.3) and three potential temperature surfaces in dashed lines. Velocity contours are marked in $cms^{-1}$, temperature is in °C.

explaining why RSW and AAIW are so distinct along the same isopycnal in the Agulhas Current.

Leaman *et al* (1989) constructed layer potential vorticity sections through the Gulf Stream at 27°N, 29°N and off Cape Hatteras at 75°W. At each section they found that "the $10\times10^{-7}m^{-1}s^{-1}$ layer PV contour appears as a distinctive boundary separating the high-potential-vorticity, cyclonic current core from a region of more uniform potential vorticity offshore." Their layer PV boundary of $10\times10^{-7}m^{-1}s^{-1}$ is approximately equal to $Q\approx$ 2 to $2.5\times10^{-10}m^{-1}s^{-1}$ (since their layer PVs when multiplied by $10^{-3}\Delta\sigma_\theta/\rho_0$ are approximately equal to $Q$), that is twice the PV of the 'barrier' found in the Agulhas Current. The PV barrier in the Gulf Stream is more distinct than its counterpart in the Agulhas Current and it extends not between potential temperatures of 14°C and 4°C but from almost the sea surface to about 7°C (Leaman *et al*, 1989). Below 7°C the PV is practically uniform across the width of the Gulf Stream, supporting other work which has suggested that there is a relatively free exchange of fluid across the current in the deep layers (Bower *et al*, 1985). In the Agulhas Current such a free exchange may be expected in waters of potential temperature less than 4°C, that is below about 1100m depth next to the continental slope and 1500m depth at the eastern end of the section. McCartney (1982) showed a PV section across the Gulf Stream much farther downstream at 50°W, calculated without the inclusion of relative vorticity, which also shows a similar PV boundary at a value of about $2.0\times10^{-10}m^{-1}s^{-1}$. In this case the PV boundary cannot be as a result of increasing relative cyclonic vorticity, but was suggested to be the boundary of a PV plateau on the cyclonic side of the current core.

The region of high PV gradients (and large negative PV) in the Agulhas Current occurs where the horizontal and vertical shears are greatest, that is above the Undercurrent. However, as we saw from figure 4.11a, the component of PV resulting from planetary vorticity and stratification alone - i.e. no shear terms - also shows a region of high negative PV in much the same position. So this region of high PV gradients that seems to be coincident with the high-shear, cyclonic side of a WBC as seen by Schmitz (1969), by McCartney (1982) and by Leaman *et al* (1989) in the Gulf Stream and here in the Agulhas Current appears to be primarily a result of increased stratification and not of increased relative cyclonic vorticity. Leaman *et al* (1989) suggest that the high PV encountered in the Gulf Stream at 27°N and 29°N may not be surprising since the current is bounded in the west by the continental slope. Perhaps in the Agulhas Current at 32°S there is also some generation of PV (in this case negative PV) next to the

slope. However, neither Leaman *et al's* second section off Cape Hatteras nor the McCartney (1982) section at 50°W are bounded by topography, although the high PVs may have been advected from upstream. In the Agulhas Current it still seems that the low PVs are largely a result of decreased layer depth over the continental slope. In the Agulhas sigma-1 section (figure 3.1) the slope of the isopycnals doubles at about 40 to 50km offshore and this is about the same region that the PV 'boundary' occurs. The effect is particularly evident at sigma-1 densities between 30.8 and 32.0, in other words at mid-depths.

Various investigators have attempted to use PV as a conservative tracer to follow types of 'mode' waters (e.g., McDowell *et al*, 1982; Talley & McCartney, 1982; Talley & Raymer, 1982). Talley & McCartney (1982) found that in the Northwest Atlantic at mid depths Labrador Sea Water (LSW) can be traced as a PV minimum due to its vertical homogeneity, whilst the relatively high PV in the Northeast Atlantic can be attributed to the Mediterranean salt tongue. The PV distribution on the ACE section is shown again in figure 4.13 using potential density as the vertical co-ordinate. Also shown are the salinity and oxygen distributions against potential density. High negative PV in the Agulhas Current close to the coast at intermediate depths is coincident with the relatively high salinities that indicate RSW next to the continental slope and is just above the oxygen minimum. This may suggest that the mid-depth negative PV maximum is acting as a tracer of RSW, much like the salty, mid-depth Mediterranean water outflow in the North Atlantic can be seen as a relative PV maximum (Talley & McCartney, 1982) (note that a PV maximum in the northern hemisphere is equivalent to a minimum in the southern hemisphere - both are related to high stratification). There are traces of a weaker PV minimum all the way across the ACE section at intermediate depths which could be the result of current meandering - the RSW leaving a trace of low PV as the current meanders offshore. A similar effect was noted by Talley & McCartney (1982) when they saw a patch of low PV, indicating LSW, to the east of the North Atlantic Current and deduced that the current had recently meandered to the east. However, the Natal Pulses at this latitude rarely take the Agulhas Current as far as 200km off course. On the other hand there is evidence of the beginnings of another patch of low PV at the eastern end of the section. This patch once again coincides with evidence of relatively high salinities and low oxygens on station 2 (which may, or may not develop into another lens of RSW a little way beyond the end of the ACE section), thus inferring that the PV in the Agulhas may be useful as a tracer.

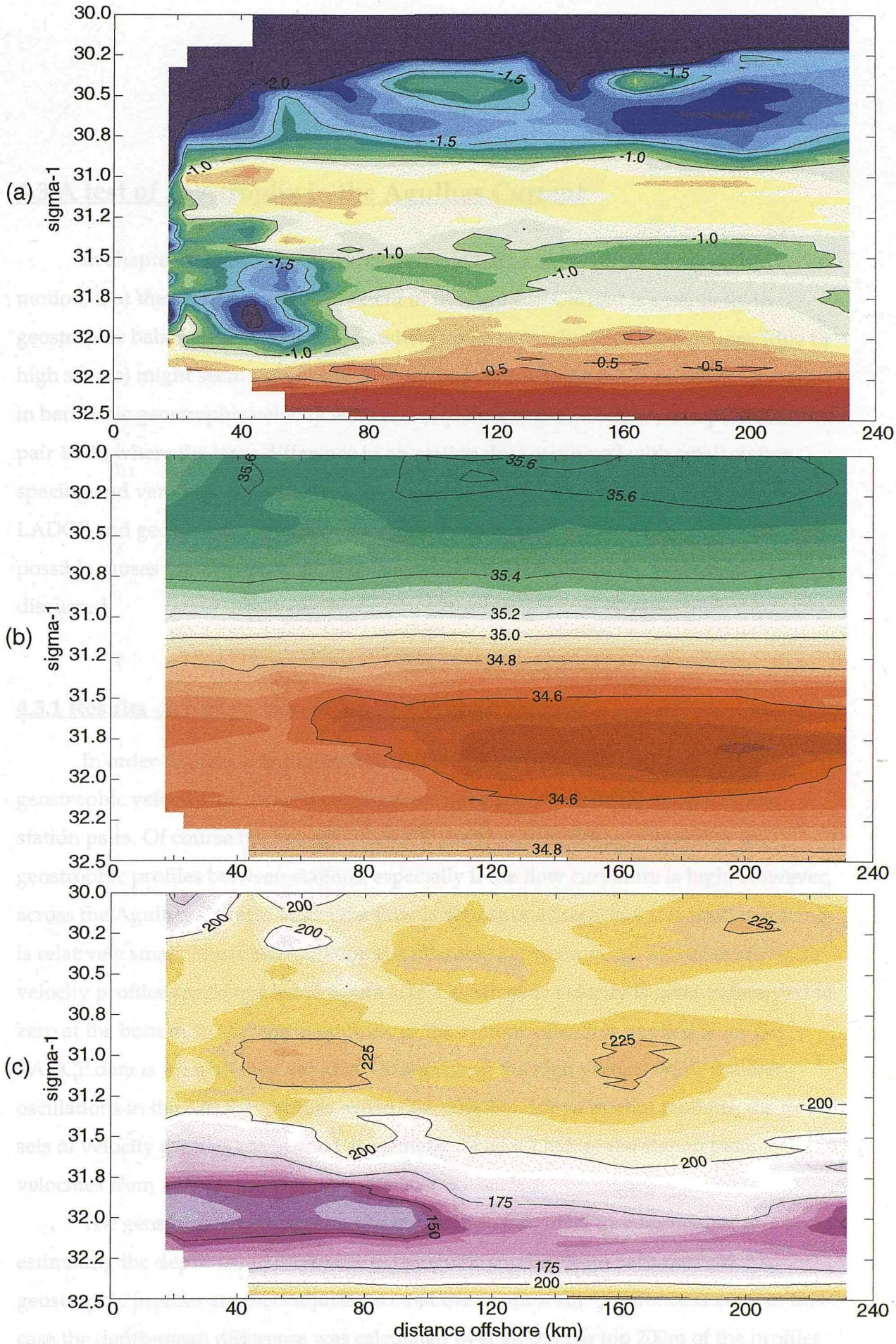


Figure 4.13 Contoured sections against potential density of (a) potential vorticity, where colour changes indicate intervals of 0.1 x $10^{-10}$ $m^{-1}s^{-1}$ and values less than -2.0 x $10^{-10}$ $m^{-1}s^{-1}$ are shown in dark purple, (b) salinity, where colour changes indicate intervals of 0.05 and (c) oxygen, where colour changes indicate intervals of 5μmol $l^{-1}$. Sigma-1 is density ($kgm^{-3}$) referenced to 1000dbar.

## 4.3 A test of geostrophy in the Agulhas Current

In chapter 3 (section 3.2.4) it was estimated, by scale analysis of the equations of motion, that the along-stream component of the Agulhas Current is essentially in geostrophic balance even at station 11, where non-linear advective accelerations (due to high shears) might seem significant. Also in chapter 3 (section 3.2.2) measurement errors in baroclinic geostrophic velocity were found to be less than $0.6cms^{-1}$, except at station pair 11-10 where the large difference in on-station drift combined with small station spacing and very high velocities causes a measurement error of $3cms^{-1}$. In this section LADCP and geostrophic velocities are carefully compared everywhere in the WBC and possible causes for any apparent departures from geostrophy in the velocity field are discussed.

### 4.3.1 Results - a comparison of LADCP and geostrophy

In order to make comparisons between profiles of LADCP velocity and geostrophic velocity the direct measurements have been linearly interpolated onto station pairs. Of course the averaged LADCP profiles need not correspond to the geostrophic profiles between stations, especially if the flow curvature is high. However, across the Agulhas Current where the flow is almost unidirectional and station spacing is relatively small, linear interpolation is a tolerable approximation. Eleven station-pair velocity profiles are compared in figure 4.14. Geostrophic velocity is given referenced to zero at the bottom so that the magnitude of the bottom velocities implied from the LADCP data is immediately obvious. Disregarding the high vertical wave number oscillations in the LADCP profiles, which are possibly due to inertial motions, the two sets of velocity profiles are in good agreement. At about half of the station pairs, velocities from the two methods diverge near the surface.

The geostrophic velocities can be matched to the direct measurements by estimating the depth-mean difference between the profiles from each method. The geostrophic profiles are then adjusted so that the depth-mean difference is zero. In this case the depth-mean difference was calculated over all but the top 200m of the profiles since here it is apparent that the direct and geostrophic velocities are dissimilar. The

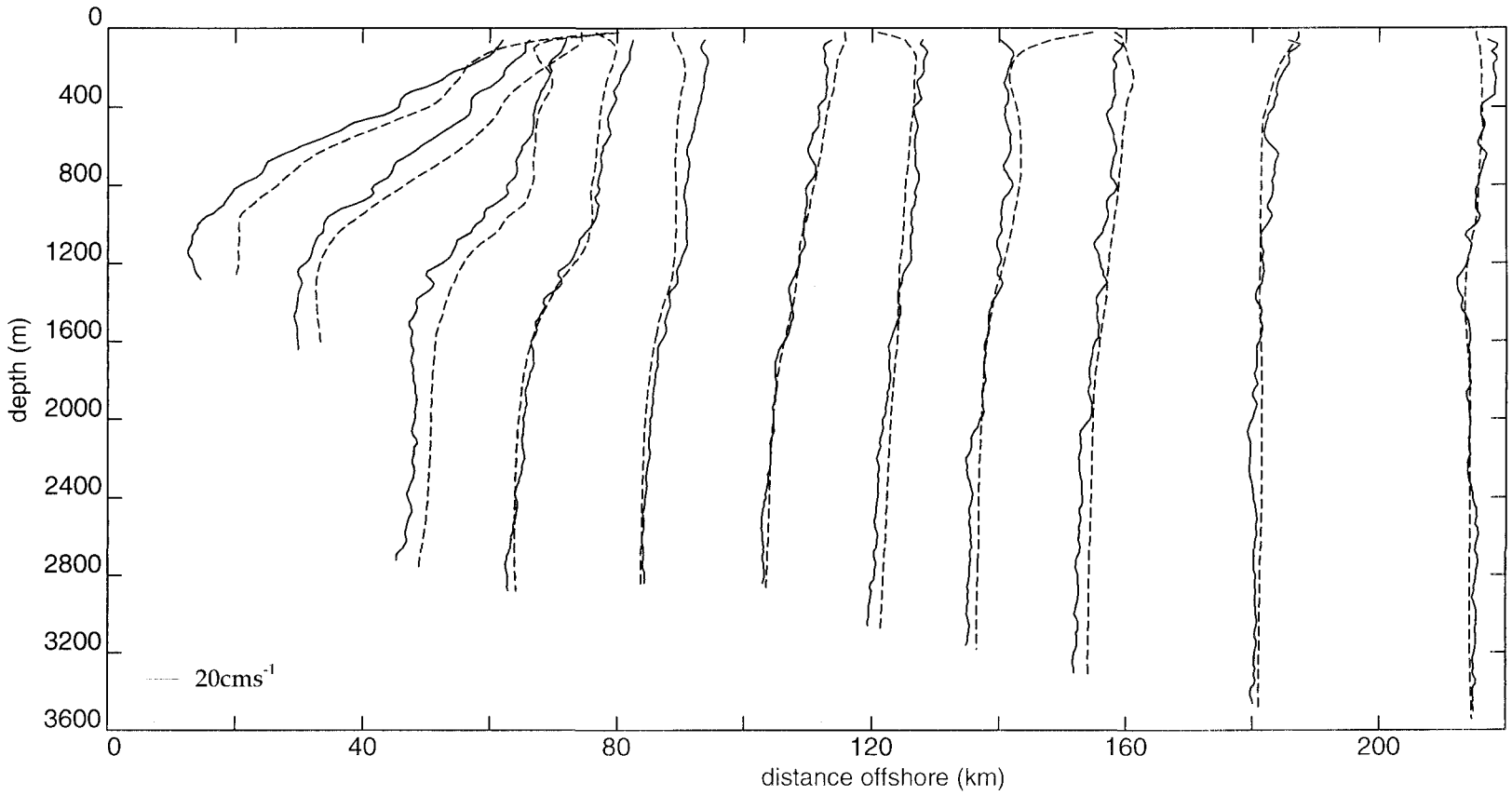


Figure 4.14 Station profiles of along-stream LADCP velocity (solid line) and geostrophic velocity referenced to the bottom (dashed line).

matched profiles are shown in figure 4.15. The standard deviation about the depth-mean difference and the matched geostrophic bottom velocities are given in table 4.2.

A summary of the comparison between LADCP and geostrophy is shown in figure 4.16, which contours $\Delta v = v_{LADCP} - v_g$, the difference between the direct LADCP measurements and matched geostrophic velocities. The highest values of $\Delta v$ occur in the upper 300m in the core of the Agulhas Current, where the direct velocities exceed geostrophic velocities by 10 to 25cms$^{-1}$. The highest negative values of $\Delta v$ are found in the upper 150m at station pair 10-9 in the core of the current and station pair 5-14, where geostrophic velocities exceeds direct measurements by 10 to 25cms$^{-1}$. Below 300m the ageostrophic flow is everywhere less than 10cms$^{-1}$.

| station pair | standard deviation (cms$^{-1}$) | bottom velocity (cms$^{-1}$) |
|---|---|---|
| 11-10 | 8.9 | -21.7 |
| 10-9 | 6.6 | -16.4 |
| 9-8 | 7.1 | -11.5 |
| 8-7 | 4.2 | 1.5 |
| 7-6 | 5.4 | 6.6 |
| 6-5 | 2.9 | -2.0 |
| 5-14 | 5.3 | -1.2 |
| 14-4 | 4.1 | -4.3 |
| 4-3 | 2.7 | -6.0 |
| 3-15 | 4.5 | -1.0 |
| 15-2 | 3.2 | 1.2 |

Table 4.2 The standard deviation about the depth-mean difference (below 200m) between profiles of direct and geostrophic velocity on each station pair (see figure 4.15) and geostrophic bottom velocities are given in cms$^{-1}$ for each station pair.

### 4.3.2 Discussion

The results show that for the most part LADCP and geostrophic shears are similar. Only over the top 200 to 300m do the results indicate that measurable geostrophic departures occur; that is, geostrophic departures of magnitude greater than the estimated measurement error of the LADCP (see chapter 2) and of geostrophy. The geostrophic departure in the upper waters at station pair 5-14 is almost certainly due to temporal variability, since the stations were occupied 5 days apart. Still to consider are the patchy departures from geostrophy closer to the core of the Agulhas Current.

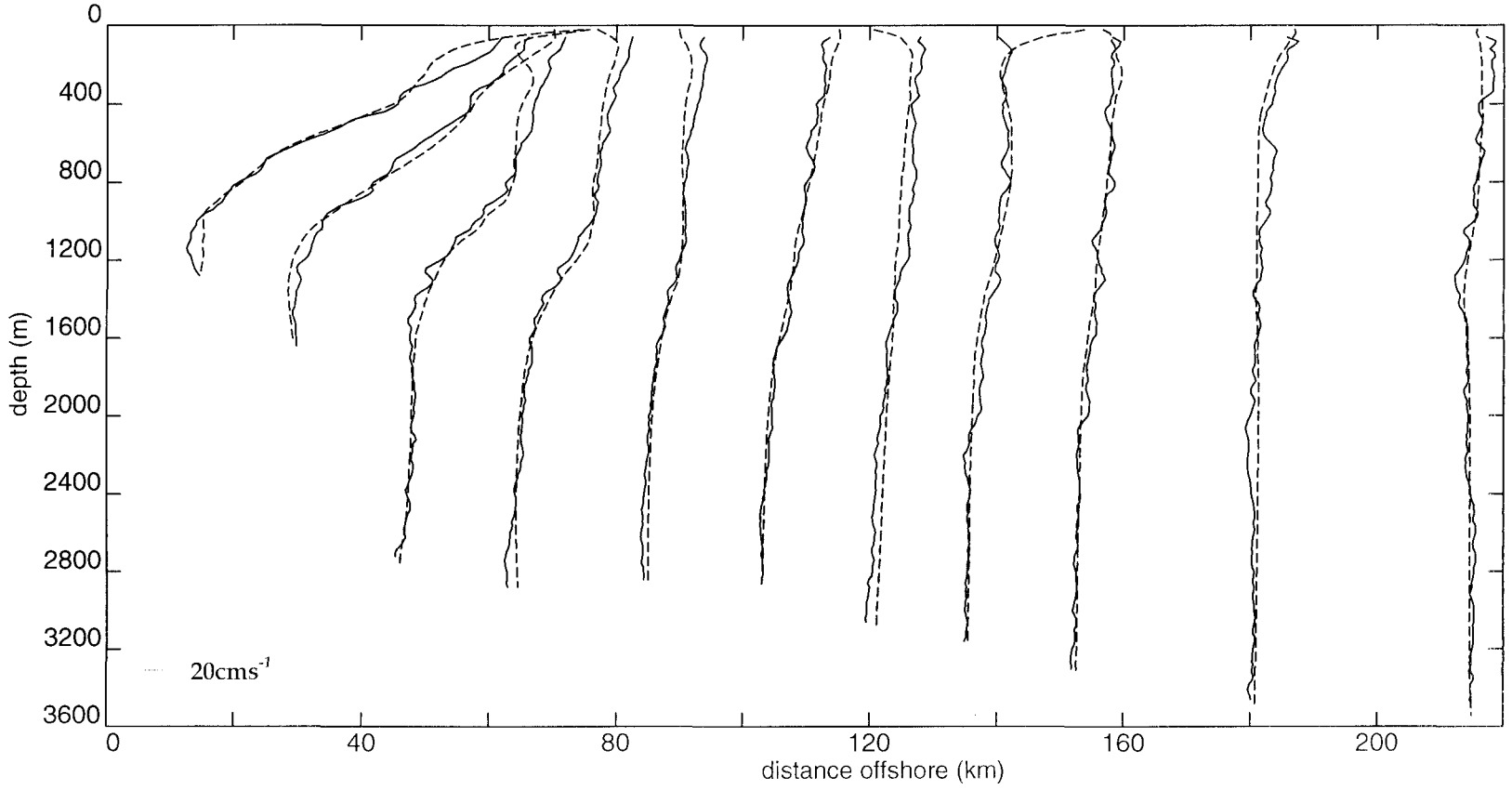


Figure 4.15 Station profiles of along-stream LADCP velocity (solid line) and geostrophic velocity referenced to the LADCP data using a depth-averaged-difference fit that excludes the upper 200m of the water column (dashed line).

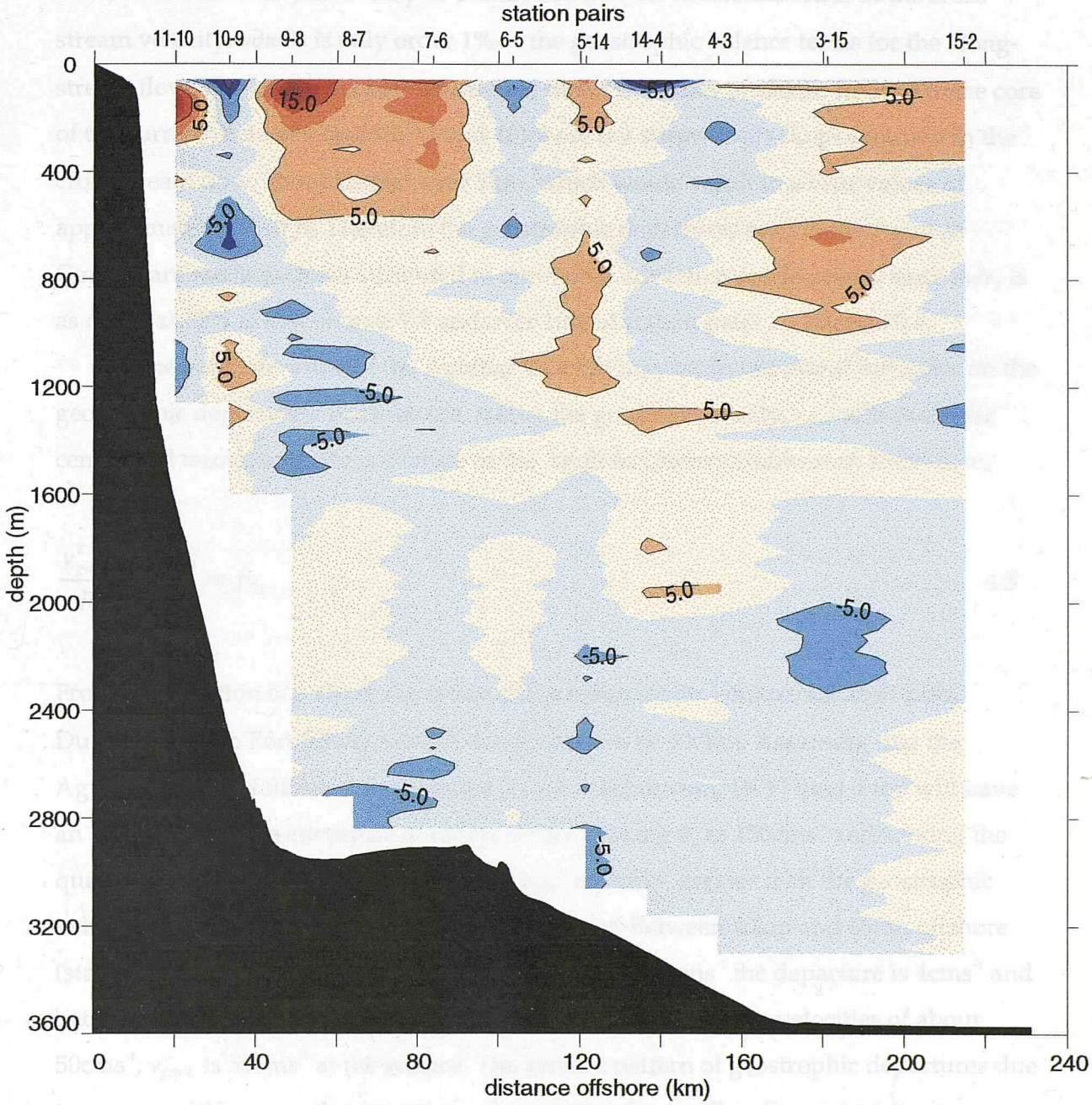


Figure 4.16 Apparent ageostrophic velocity contoured along the ACE section. Transitions of velocity are indicated by colour changes at intervals of 5cms$^{-1}$.

The scale analysis of chapter 3 indicates that the horizontal shear of the cross-stream velocity, $u\partial u/\partial x$ is only order 1% of the geostrophic balance terms for the along-stream flow. The LADCP observations give direct estimates of $u\partial u/\partial x$. In the surface core of the current (between stations 11 and 10) there is a surprisingly large variation in the cross stream flow, about 10cms$^{-1}$ over 5km, which would result in $u\partial u/\partial x$ values of approximately 2% of $fv$. Therefore the geostrophic departures seen in the Agulhas Current are too large to be attributed to non-linear advective accelerations, since $dv/v_g$ is as much as 25% at station pair 9-8 and over 10% at station pairs 11-10 and 10-9.

The path curvature of the Agulhas Current may be an important influence on the geostrophic departures. For instance, taking the gradient velocity, $v_{grad}$ to include the centripetal term due to the curvature of the Agulhas Current (Johns *et al*, 1989) then,

$$\frac{v_{grad}^2}{R} + fv_{grad} = fv_g \quad . \qquad 4.5$$

From examination of a chart, the radius of curvature of the continental shelf from Durban (30°S) to Port Edward (31°S) is estimated to be 400km. Assuming that the Agulhas Current follows the topography (Gill & Schumann, 1979) then it too will have an anticyclonic path curvature of radius 400km. Taking $v_g$ as 150cms$^{-1}$ and solving the quadratic equation in 4.5 gives values for $v_{grad}$ as 8cms$^{-1}$ greater than the geostrophic velocity in the surface core of the Agulhas Current. Between 40km and 60km offshore (station pair 9-8), where surface velocities are about 100cms$^{-1}$ the departure is 4cms$^{-1}$ and between 60km and 80km offshore, corresponding to geostrophic velocities of about 50cms$^{-1}$, $v_{grad}$ is 51cms$^{-1}$ at the surface. The general pattern of geostrophic departures due to $v_{grad}$ would be a swath of positive values across the Agulhas Current with a maximum in the current core and values reducing away from the coast and with depth, consistent with the velocity field of the WBC. This pattern of a super-geostrophic flow does not seem consistent with the pattern of geostrophic departures seen in figure 4.16 which are patchy, sometimes negative and do not appear to increase as the geostrophic velocity increases. This implies that there must be additional factors causing geostrophic departures near the surface, which superimpose patchiness onto the expected smooth pattern of supergeostrophic flow caused by the curvature of the current path.

In addition to the measurement errors already discussed, there are sampling biases which can result from the time taken to complete a station pair. ACE combined

CTDO2/LADCP stations with mooring deployment, so that the synopticity of the hydrographic measurements had to be compromised. If the Agulhas Current shifted laterally during the seven day occupation of the ACE section then a large scale broadening or narrowing of the apparent current structure may occur, depending upon whether the ship traverses with or against the direction of path shift. If the current should shift between the sampling of two stations then the slope of the density field may change, especially near the current core where the baroclinicity of the density field is high. The resultant fractional error in the measured isopycnal slopes is equal to the ratio of the lateral velocity of the current path to the ship's velocity along the transect. Using repeat hydrographic sections, Pearce (1977) found that the Agulhas Current off Durban could shift laterally by up to 10km per day. At 31°S the path of the Agulhas Current is known to be considerably more stable, with a standard deviation about a mean position from the coast of 6km (Grundlingh, 1983). Estimating the maximum meander lateral velocity to be 6kmday$^{-1}$ on the ACE section and noting that stations 9 and 8, with a station spacing of 10km, were sampled 13 hours apart, then an error of 30% could potentially arise in the geostrophic velocity. This kind of error could account for the geostrophic departures found in the Agulhas Current.

Most of the patches of ageostrophic flow occur close to the surface and may simply be the result of the spatial averaging of LADCP profiles. In the upper waters Ekman shears can produce relatively small scale flow patterns making a spatial average doubtful in its representation of the flow between stations. Stations 6, 7 and 8 exhibit very different shears over the top 200m so that this is almost certainly a contributing factor.

# CHAPTER FIVE

# *VOLUME, HEAT AND SALT TRANSPORTS*

## 5.1 Volume transport of the Agulhas Current

Four estimates of Agulhas Current transport are made using the LADCP measurements. Firstly a straightforward integral of the LADCP velocities from station 11 to station 2 is taken in order to estimate a volume transport for the Agulhas Current from the LADCP data alone. Secondly a transport estimate is made using horizontal, linear extrapolation of the data to a zero velocity condition on the slope, thereby filling in bottom triangles. Thirdly the LADCP data is barotropically adjusted using near-surface shipboard ADCP measurements (no extrapolation). Finally, the LADCP results are used to reference the geostrophic velocities from the ACE hydrographic data and obtain a definitive geostrophic transport estimate (section 5.1.2).

### 5.1.1 Direct estimates of Agulhas Current transport

In order that the transport estimate from LADCP is comparable to TWs geostrophic estimate and to the geostrophic estimate made later in this chapter, it is first necessary to consider the respective areas of each integral. Since geostrophic velocity profiles appear between stations the volume transport is usually calculated by integrating the velocity over the area between a station pair. Over topography an area is lost close to the sea bed; these areas are called bottom triangles. Traditionally bottom triangles are filled in by integrating the deepest velocity from a station pair over half the distance between stations multiplied by the difference in the depth of the deepest measurement at each station (figure 5.1). A best estimate of geostrophic volume transport (as made in the next section) will include the transport through these bottom triangles.

In contrast LADCP velocity profiles are measured on station and here the volume transport is calculated by integrating the velocity over half the area to each neighbouring

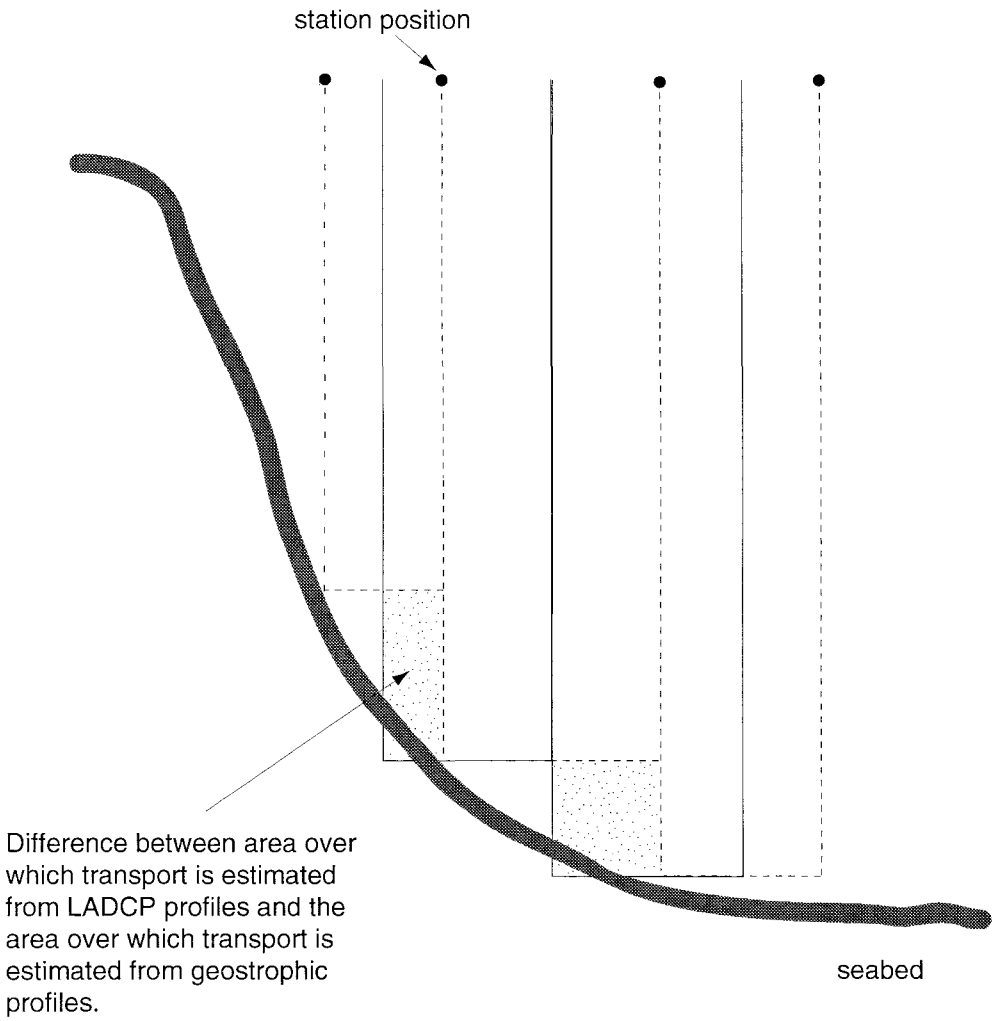


Figure 5.1 Diagram of the area over which transports are estimated. Dashed lines surround the area over which station-pair, geostrophic velocity profiles are integrated. Solid lines indicate the area over which on-station, LADCP velocity profiles are integrated. The difference between the two areas is shaded and is of equal area to the traditional bottom triangles which are used in the estimation of geostrophic volume transports.

station. At either end of the section, where there is only one neighbouring station, the velocity is integrated over half the distance to that one neighbouring station. Thus, bottom triangle transport is effectively accounted for in this integral (figure 5.1). In addition the LADCP data is vertically extrapolated to the sea surface with constants since no direct measurements are available over the upper 50m (due to a 30m blank-after-transmit). Therefore, the LADCP volume transport has been calculated over an equivalent area to that used for a geostrophic estimate (figure 5.1) and direct comparisons of the results from each technique can be made.

Calculated in this way the volume transport of the Agulhas Current from LADCP velocities alone is estimated as 75Sv (net) poleward. The distribution of transport across the section is shown in figures 5.2 and 5.3. The Undercurrent transport, taken as the accumulation of equatorward transport within 80km of the coast, is 5Sv. The total equatorward transport is 13Sv. Of the water masses in the Agulhas Current, as defined in figure 5.3a, only NADW has a net equatorward transport, which is 4Sv (figure 5.3b). The intermediate water masses contribute 19Sv to the poleward transport and the remainder is due to central and surface waters (figure 5.3b). The net flow of RSW is marginally equatorward at station 11, the station furthest onshore; across the remainder of the section RSW is transported to the south-west.

A more comprehensive cross-section of the Agulhas Current may be constructed by extrapolating the LADCP data to fill in data gaps and bottom triangles. Firstly, on-station gaps to the sea bed were vertically filled with constants. The data was then linearly interpolated onto a 1km by 20m grid and the remaining data gaps were linearly interpolated horizontally to zero velocity on the slope, as described in chapter 3 when Agulhas Undercurrent transport was estimated. The result is a much smoother cumulative transport across the current (figure 5.4). Figure 5.5 shows a contoured section of the extrapolated LADCP data. An extra 2Sv of poleward flux is gained using this technique and by far the largest contribution to the extra transport is from extrapolated near-surface velocities over the continental shelf, close to the coast. Equatorward transports are much the same as in the previous estimate, except at stations 11 and 10 where extrapolating strong bottom velocities in the Agulhas Undercurrent increases Undercurrent transport to 6Sv. Undercurrent transport may be underestimated, because its maximum velocity core may not have been sampled below 1600m depth and yet velocities are linearly decreased towards the slope from the last available data point. At the same time surface flux in the Agulhas Current may be overestimated, particularly

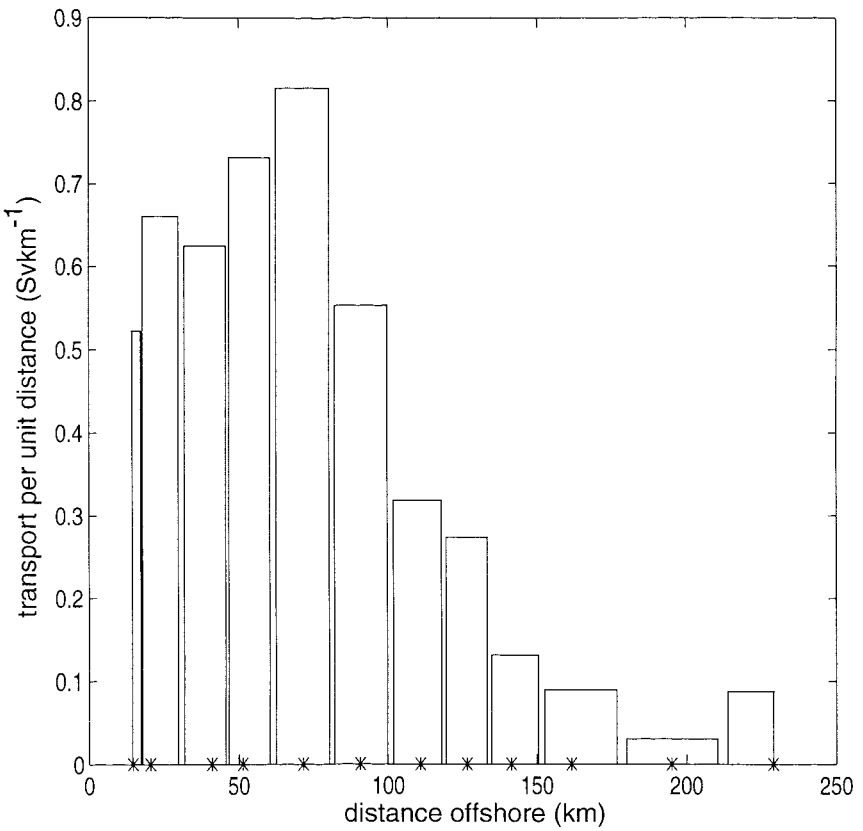


Figure 5.2 Distribution of transport across the Agulhas Current, estimated from direct LADCP measurements. Station positions are indicated by asterisks. The volume transport of the Agulhas Current using LADCP is 75Sv.

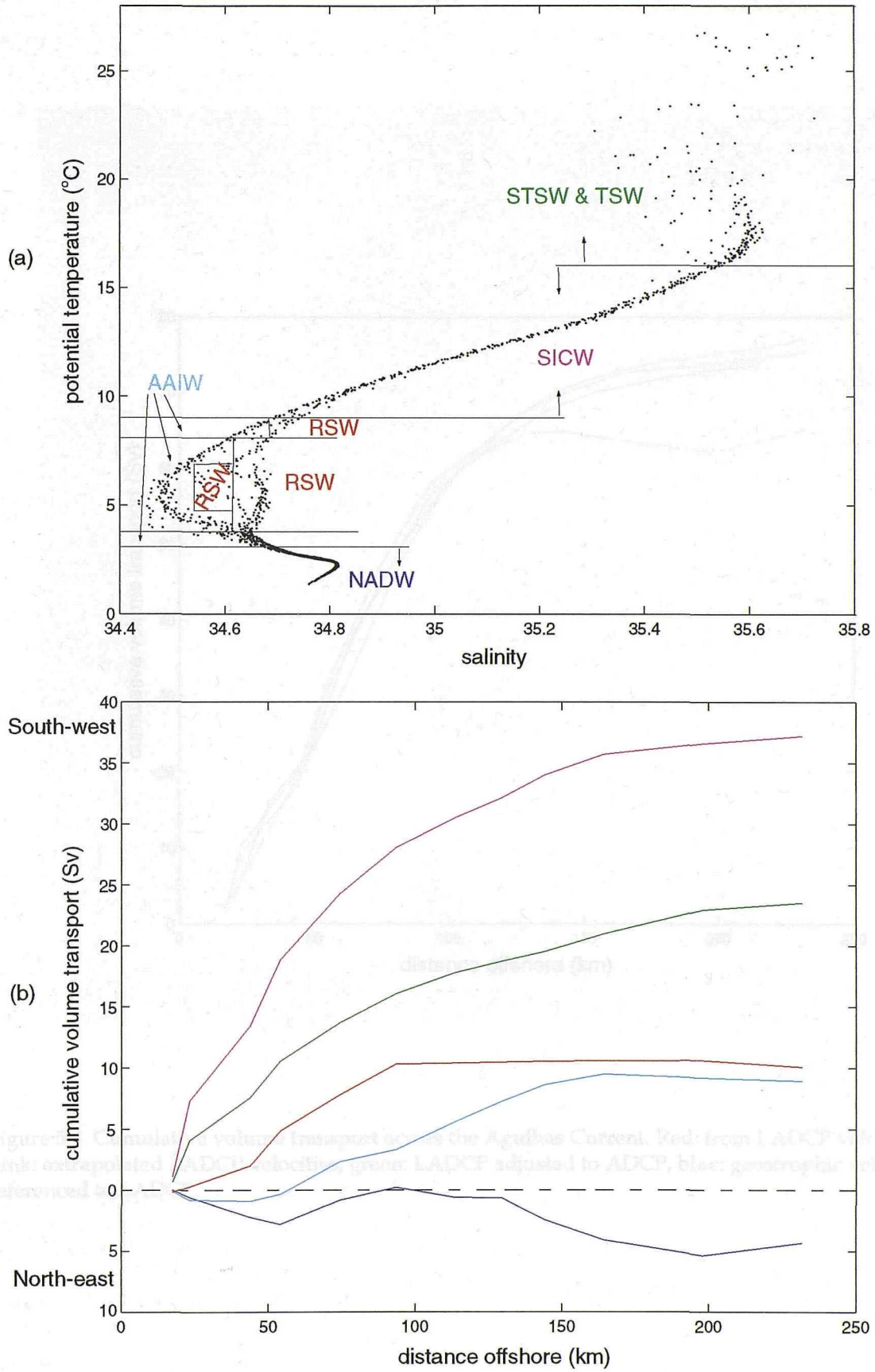


Figure 5.3 (a) Temperature - salinity relationship of water masses in the Agulhas Current. In order to compute fluxes each water mass is represented by temperature - salinity intervals as shown. The colours of the abbreviations correspond to the colours on the graph in (b). (b) Cumulative water mass transports across the Agulhas Current. Blue: North Atlantic deep water, cyan: Antarctic intermediate water, red: Red Sea water, green: tropical and sub-tropical surface waters, pink: South Indian central water.

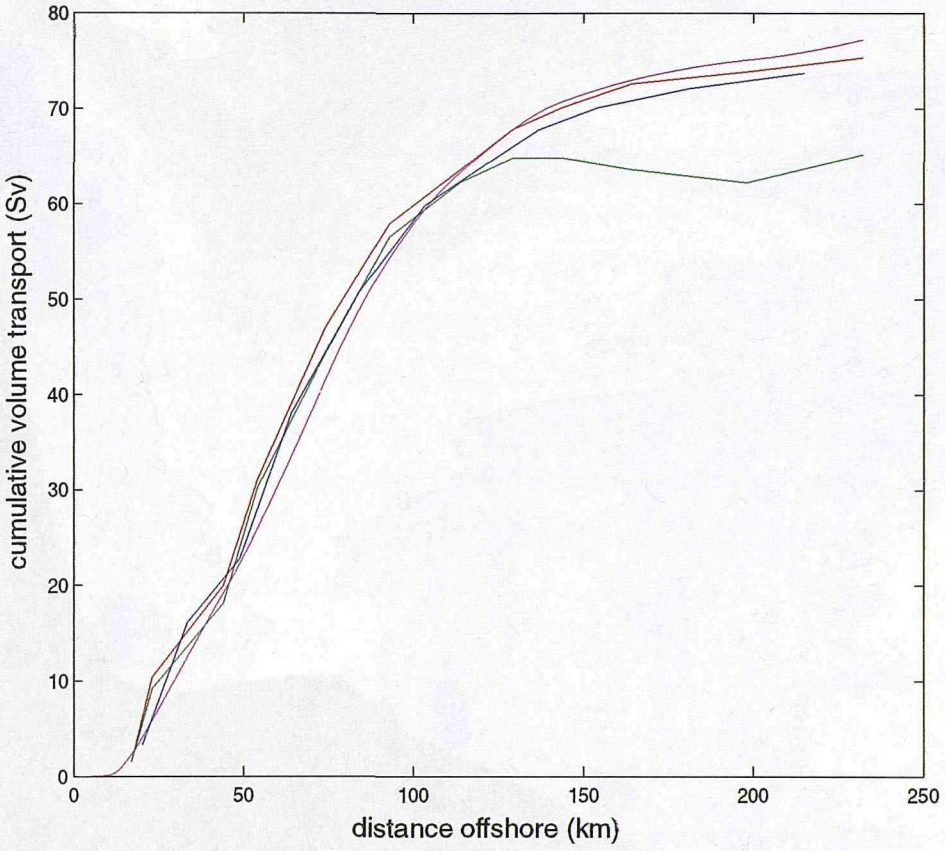


Figure 5.4 Cumulative volume transport across the Agulhas Current. Red: from LADCP velocities, pink: extrapolated LADCP velocities, green: LADCP adjusted to ADCP, blue: geostrophic velocities referenced to LADCP.

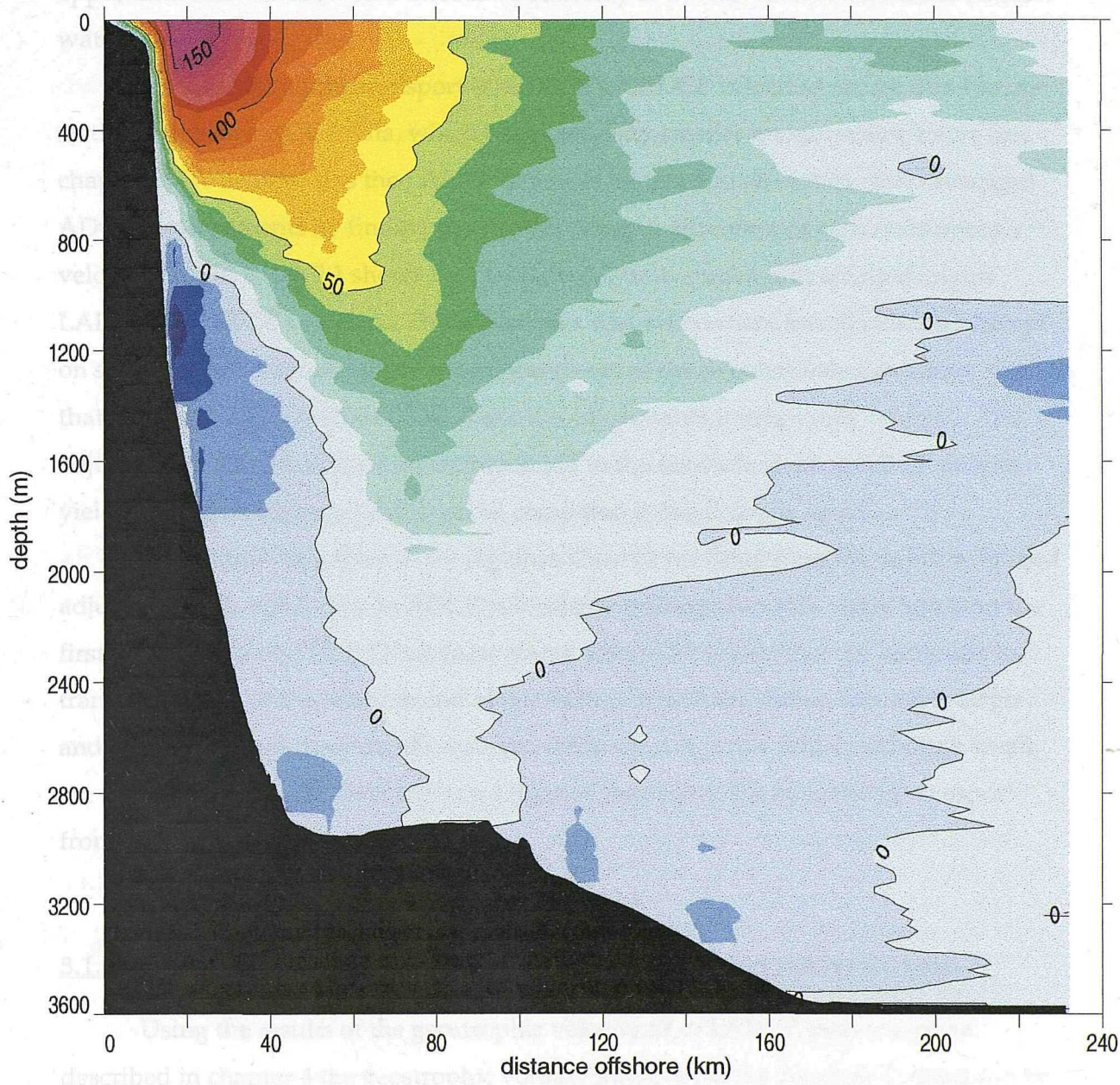


*Figure 5.5 Contoured section of extrapolated cross-track LADCP velocities. Velocities are positive to the south-west. Transitions in velocity are indicated by colour changes at intervals of 10cms$^{-1}$. (The LADCP data has been extrapolated vertically with constants to the sea surface and the sea bed then interpolated onto a 1km by 20m grid and subsequently linearly extrapolated horizontally onshore to zero velocity on the continental slope.) The volume transport through this section is 77Sv.*

over the continental shelf, where velocities may decrease more rapidly than a linear approximation will allow and there is a possibility of a weak counter-current in shallow waters.

For a third volume transport estimate, the LADCP velocities can be fitted to on-station shipboard ADCP data, which has potentially smaller measurement errors (see chapter 2). To achieve this the LADCP data was adjusted to on-station, time-averaged ADCP measurements by finding the depth-averaged difference of each instrument's velocity profile. Table 2.1 shows the resultant depth-averaged differences between LADCP and ADCP velocities. The adjustment was everywhere less than 4cms$^{-1}$, except on station 10 where it was 5.8cms$^{-1}$ and the shears of the two methods are similar enough that the standard deviations (SDs) about the adjustments average only 1.7cms$^{-1}$. The adjusted LADCP velocities were extrapolated to the sea surface using ADCP data to yield a transport estimate which can be compared to the first one above.

The volume transport of the Agulhas Current resulting from the depth-averaged adjustment of LADCP data to ADCP velocities is estimated as 65Sv, 10Sv less than the first, un-extrapolated LADCP estimate above. Figure 5.4 shows that the reduction in transport occurs at the offshore end of the section, where the station spacing is larger and where there are three depth-averaged-differences in a row which, although small, are all of the same sign. Over the first 120km of the section the cumulative transport from each method is similar.

### 5.1.2 Geostrophic volume transport referenced to direct measurements

Using the results of the geostrophic velocity fit to LADCP measurements described in chapter 4 the geostrophic volume transport of the Agulhas Current can be estimated with much greater accuracy than the original estimate made in chapter 3. Recall that in chapter 3 TW's water-mass-based reference level was used to produce a geostrophic transport estimate of 82Sv from the ACE hydrographic data. (This estimate did not include the transport from bottom triangles, but because bottom velocities were small due to the choice of reference level this contribution is also small.) Now, using a reference for the absolute geostrophic velocity as suggested from the direct LADCP measurements (*ie* V-shaped ZVS) the geostrophic volume transport of the Agulhas Current becomes 73Sv, including -2.3Sv of equatorward flux from bottom triangles. This is just 2Sv, or 3% smaller than the direct estimate given above using LADCP

measurements. The most recent estimate in the literature is given by TW who quote a transport of 85Sv which is 10Sv larger than our direct estimate and 12Sv larger than our geostrophic estimate. This discrepancy is almost entirely due to the difference between their chosen reference level and the one measured here using an LADCP.

It is clear from the literature that there have been many problems in the past attempting to reference geostrophic velocities with shipboard ADCP data (e.g. Saunders & King, 1995). Similar problems were faced here and, as a comparison to the success of using LADCP data to reference geostrophy, a brief description of the results follows.

The on-station time-averaged ADCP profiles were interpolated onto station pairs in the same manner as the LADCP profiles as described in the previous chapter. The geostrophic and ADCP velocity profiles at four station pairs are shown in figure 5.6. The shears of the two sets of velocities are not well matched over the limited depth range of the ADCP making it difficult to make a sensible barotropic fit for the absolute geostrophic velocity. A zero-mean fit over all depths results in an SD as high as $20cms^{-1}$ at station pairs 11-10 and 14-4. In chapter 4, LADCP shear was found to be most dissimilar to the geostrophic shear over the top 200m of the water column. As a result the top 200m were disregarded when finding the depth-averaged difference by which to offset the geostrophic velocity. In this case there is not enough data left below 200m to achieve a reliable fit. However an improvement is made by disregarding the top 100m of data, reducing the SD to a maximum of $6.2cms^{-1}$ on station pair 9-8 and to an overall average of $2.7cms^{-1}$ for all the station pairs.

When comparing LADCP velocities to ADCP velocities near the surface in the section above (and chapter 2) the shears were found to be consistent - unlike the comparison of both direct measurements with geostrophy near the surface. This suggests that the shears measured by the shipboard ADCP are real, and points towards a generally ageostrophic flow penetrating to at least 200m, much deeper than the expected Ekman layer depth. Indeed it was also concluded in chapter 4 that geostrophic departures are generally large over the top 200m. Therefore referencing geostrophic velocities using shipboard ADCP data, which generally penetrates to only 300m, would seem to be an inappropriate method. The volume transports estimated from ADCP-referenced geostrophic velocities would seem to support this. There is a difference of 9Sv between the transport estimated using a fit over all depths and the value estimated using the improved fit which omits the upper 100m. In contrast there was less than 1Sv difference between the LADCP full depth fit and the fit disregarding the top 200m.

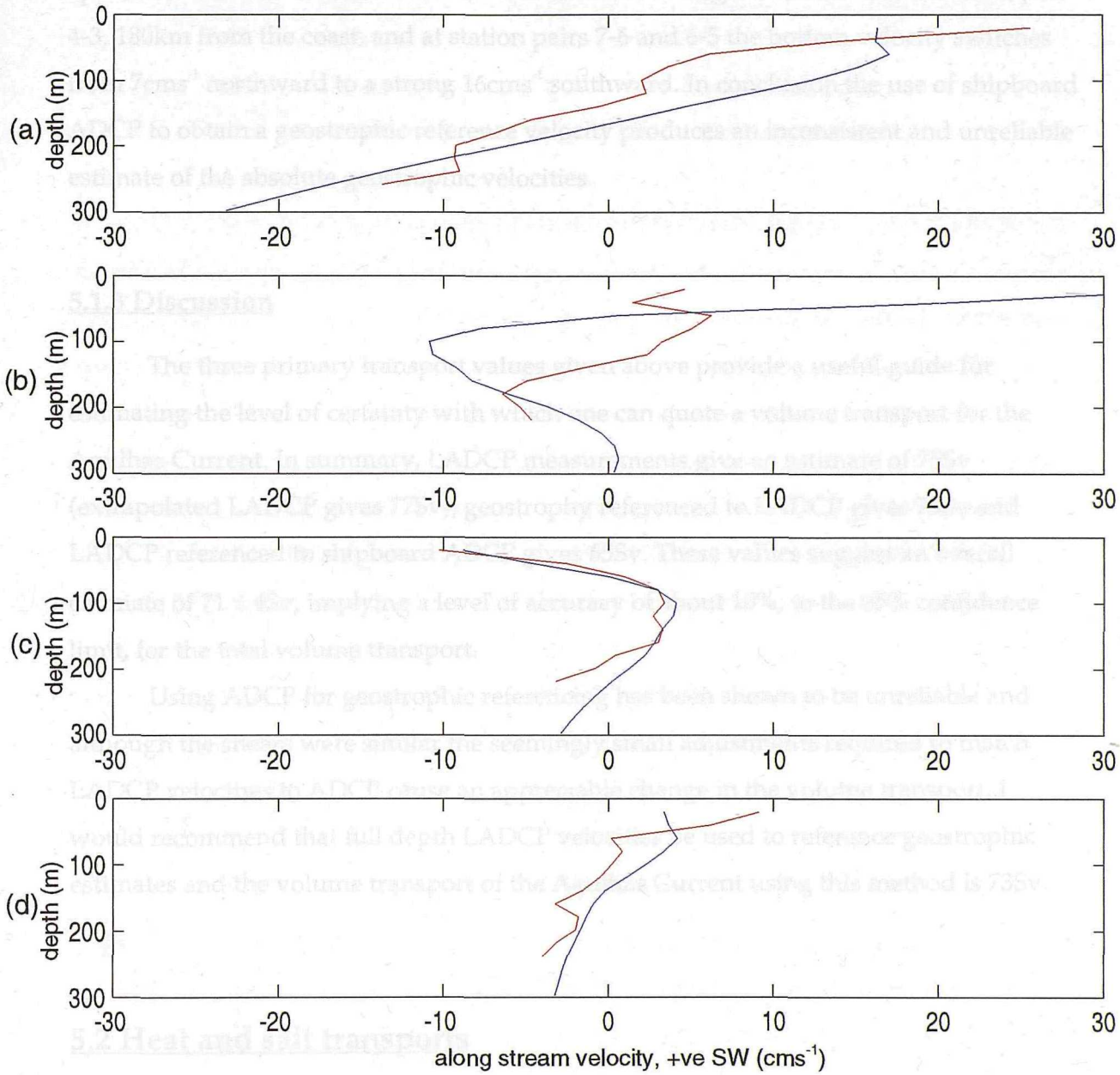


Figure 5.6 A comparison of ADCP and geostrophic velocity profiles on station pairs. Red: ADCP velocity, blue: geostrophic velocity. Both sets of velocities have been de-meaned over a depth interval from the surface to 300m. (a) station pair 10-9, (b) station pair 9-8, (c) station pair 8-7 and (d) station pair 6-5.

Moreover bottom velocities from both the ADCP methods not only vary widely but appear nonsensical. There are northward velocities as large as 14cms$^{-1}$ out at station pair 4-3, 180km from the coast, and at station pairs 7-6 and 6-5 the bottom velocity switches from 7cms$^{-1}$ northward to a strong 16cms$^{-1}$ southward. In conclusion the use of shipboard ADCP to obtain a geostrophic reference velocity produces an inconsistent and unreliable estimate of the absolute geostrophic velocities.

### 5.1.3 Discussion

The three primary transport values given above provide a useful guide for estimating the level of certainty with which one can quote a volume transport for the Agulhas Current. In summary, LADCP measurements give an estimate of 75Sv (extrapolated LADCP gives 77Sv), geostrophy referenced to LADCP gives 73Sv and LADCP referenced to shipboard ADCP gives 65Sv. These values suggest an overall estimate of 71 ± 4Sv, implying a level of accuracy of about 10%, to the 95% confidence limit, for the total volume transport.

Using ADCP for geostrophic referencing has been shown to be unreliable and although the shears were similar the seemingly small adjustments required to match LADCP velocities to ADCP cause an appreciable change in the volume transport. I would recommend that full depth LADCP velocities be used to reference geostrophic estimates and the volume transport of the Agulhas Current using this method is 73Sv.

## 5.2 Heat and salt transports

Heat and salt fluxes of the Agulhas Current are calculated using a combination of the ACE hydrographic and LADCP data and the transindian section made by TW in 1987, in order to make estimates for the heat and freshwater divergence of the Indian Ocean north of 32°S. These estimates will be based on the new estimate of Agulhas Current transport which is 15% less than TW's transport. Because the Agulhas Current transports relatively warm, salty waters poleward it is likely that a smaller Agulhas Current transport will affect the heat and freshwater divergences.

### 5.2.1 Heat flux convergence over the Indian Ocean north of 32°S

The heat flux due to ocean currents across any latitude can be expressed as:

$$T = \iint \rho C_p \theta V \, dz dx \qquad 5.1$$

where $C_p$ is the specific heat capacity of sea water at constant pressure, $\rho$ is the local density of seawater, $\theta$ is the potential temperature, $x$ is the longitudinal variable, $z$ is the depth variable and $V$ is velocity. The mass of the system must be conserved. This basin-wide transport can be split into three components (Hall & Bryden, 1982): the WBC contribution estimated using ACE data, the geostrophic ocean interior component estimated using hydrographic data from the transindian section of 1987, and the Ekman flux component estimated from the new Southampton Oceanography Centre (SOC) climatology compiled by Josey (Josey *et al*, 1996). The Indian Ocean is not closed to the north of 32°S so that to calculate the heat flux convergence of the ocean requires a fourth component, the Indonesian Through-Flow (ITF) which will be estimated using recent reports based on observations. The equation becomes,

$$T = -\iint_{WBC} \rho C_p \theta V_{WBC} \, dz dx + \iint_{IO} \rho C_p \theta V_{geos} \, dz dx + \iint_{IO} \rho C_p \theta V_{Ekman} \, dz dx + \iint_{ITF} \rho C_p \theta V_{ITF} \, dz dx \qquad 5.2$$

A positive flux implies transport into the Indian Ocean and a negative flux implies transport out of the Indian Ocean. Each of these integrals is referred to as a temperature flux, since individually they do not conserve mass. The value of $\rho C_p$ is taken to be a constant 4.09 J $°C^{-1}$ $cm^{-3}$ (Hall & Bryden, 1982) for each component.

The WBC component can be readily computed using the LADCP velocity field and potential temperature profiles from ACE. The transport-weighted potential temperature is calculated from the LADCP velocities (which have a volume flux of 75Sv) and the temperature flux is then computed for a volume transport of 71Sv, the 'best estimate' given above. The resulting temperature flux of the Agulhas Current is 4.016PW or 71.3Sv at a transport weighted temperature of 13.82°C. Next consider the third integral of equation 5.2. The Ekman volume flux can be estimated from the SOC climatology which is based on in situ ship reports over the period 1980-1993 and uses the drag coefficient given by Smith (1988) to estimate sea surface wind stress. The improved

drag coefficient reduces wind stress by over 30% when compared to previous estimates, for example Hellerman & Rosenstein's (1983) climatology. The thirteen-year-mean northward Ekman flux across latitude circles in the Indian Ocean is shown in figure 5.7. The 32°S section is in a region of small but rapidly changing Ekman volume transport. The transport is taken to be 0.5Sv and although a possible error of several hundred percent is accepted it is also noted that it will have little impact on the resultant heat convergence since the magnitude of the Ekman transport is small. For comparison, the seasonal mean Ekman transport from Hellerman & Rosenstein (1983) is 1.6Sv. To compute temperature transport the transindian section-averaged sea surface temperature, 19.4°C, is used and the Ekman temperature flux becomes 0.040PW.

Now consider the fourth integral. The volume transport of the ITF can be extremely variable both in the short term (Fieux *et al*, 1996a & b) and semi-annually due to the Australasian monsoon (Wijffels *et al*, 1996). Direct observations are scant in part because there are many passages through which the ITF may flow and additionally due to a lack of Indonesian cooperation in recent efforts. However, combining the time series observations of Murray & Arief (1988) in the Lombok Strait and those of Molcard *et al* (1994 & 1996) and Cresswell *et al* (1993) in the Timor Passage gives an estimate of 7±1.5Sv for the ITF. In addition Meyers *et al* (1994) has repeated an XBT line roughly every fortnight since 1983 across the Timor Sea west of the Lombok Strait, and Fieux *et al* (1996a) and Wijffels *et al* (1996) have each collected synoptic hydrographic data twice in different seasons. Although the geostrophic ITF transport has been calculated relative to and above different depths by Fieux *et al* (1996a) and Wijffels *et al* (1996), their combined mean transport of 3.8±11.7Sv westward agrees with the average of 3.9±3.5Sv from the long-term XBT data. Adding a mean Ekman transport from the SOC climatology to these estimates results in a total ITF transport of about 5.9±7.6Sv. Combining the direct (7.1Sv) and geostrophic (5.9Sv) estimates I shall assume an ITF of 6.4Sv (±100%) at an estimated temperature of 24.0°C (from Fieux *et al*, 1996b). Therefore the ITF has a temperature flux of 0.629 (±100%)PW.

Finally consider the geostrophic temperature flux across 32°S. The interior hydrographic section was constructed by joining ACE station 2 to TW station 15 in the eastern Natal Valley, thereafter all TW stations were used across to Australia. The ZVS was assumed to be 2000db everywhere, since this produced maximal exchange. In order to balance the mass in equation 5.2 a velocity of 0.0446cms$^{-1}$ was added barotropically and uniformly to the section to obtain a volume transport of 64.4Sv northward. The

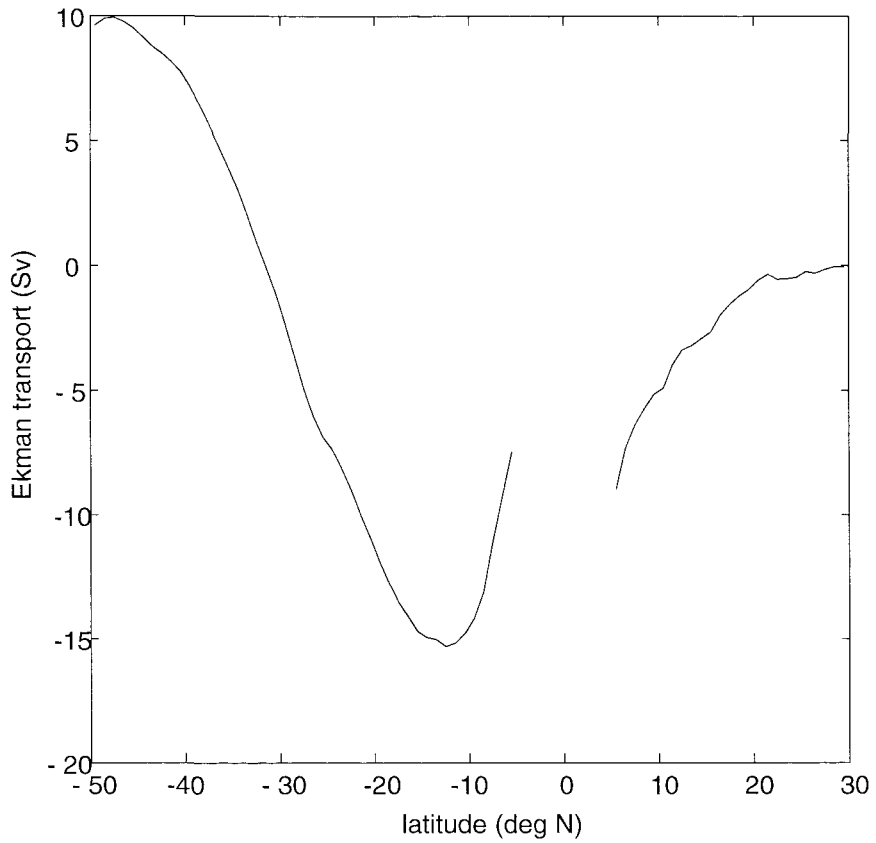


Figure 5.7 Meridional Ekman transport in the Indian Ocean from Josey et al (1996) wind stress climatology.

temperature flux consists of two components (Bryden *et al*, 1991), a flux due to the vertical meridional circulation of 2.459PW and an eddy (or horizontal) flux of -0.1044PW. Overall the 64.4Sv of northward interior flow has a transport weighted temperature of 8.9°C. The results are summarised in table 5.1 and in figure 5.8.

The resultant heat-flux divergence over the Indian Ocean north of 32°S is 0.993PW, implying that on average the Indian Ocean gains heat from the atmosphere. This is similar to the TW estimate of 0.98PW despite the smaller Agulhas Current transport, because TW used larger ITF and Ekman transports. It is larger than the Toole & Raymer (1985) estimate of 0.6PW for the case with no ITF, because their Agulhas Current transport is much smaller. The uncertainty in our estimate can be computed easily if we assume that it is well represented by the uncertainty of the ITF volume flux which is the single most significant error. A change in the ITF can be balanced by a volume flux across the interior at the flux-averaged temperature of 8.9°C, therefore the uncertainty in the heat gained by the Indian Ocean north of 32°S is approximately $\rho C_p \times$ $6.4Sv \times (24.0 - 8.9)°C$ or ±0.39PW for an ITF uncertainty of 6.4Sv.

| Component | Volume flux (Sv) | Temperature flux (PW) |
|---|---|---|
| Agulhas Current | 71.3 | -4.016 |
| Interior: Ekman | 0.5 | 0.040 |
| Interior: Geostrophic | 64.4 | 2.355 |
| Indonesian Throughflow | 6.4 | 0.629 |
| **Total convergence** | **0** | **-0.993** ±0.395 |

Table 5.1 Fluxes of heat into the Indian Ocean north of 32°S and the resultant heat flux convergence (negative indicates a divergence).

The deep transport below 2000db implied by this scheme is 16.8Sv northward, considerably less than the 27Sv found by TW, who chose reference levels across the interior which maximised deep northward transport to help balance their large Agulhas Current mass flux. The overturning of the Indian Ocean can be simplistically estimated by assuming that the deep water transported northward below 2000db is upwelled equally everywhere. Taking the area of the Indian Ocean at 2000m depth north of 30°S to be $3.89\times10^{7}km^{2}$ (TW) leads to an area-averaged upwelling rate of $4.3\times10^{-5}cms^{-1}$ or $13.6myr^{-1}$ across the 2000m surface. This is similar to an estimate by Warren (1981) who

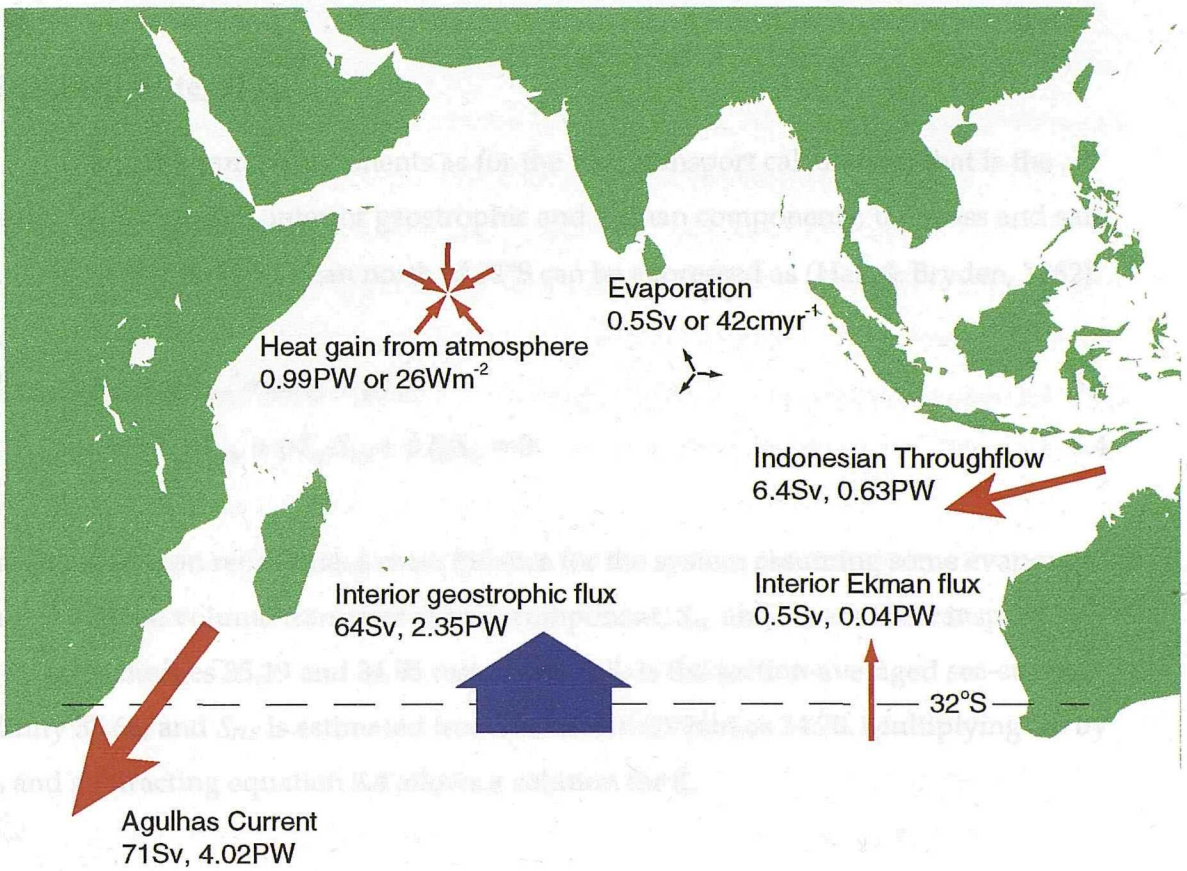


Figure 5.8 Cartoon of volume and heat fluxes of the Indian Ocean north of 32°S. Warm fluxes are shown in red, cold fluxes are shown in blue.

used a transindian hydrographic section at 18°S to estimate an upwelling rate of $4.0\times10^{-5}$ $cms^{-1}$ and to an estimate by Stuiver *et al* (1983) of $3.2\times10^{-5}$ $cms^{-1}$ from carbon-14 distribution. These results indicates that the upwelling rate in the Indian Ocean may be two or three times larger than that in the Pacific (TW). Based on their layer overturning TW estimated an upwelling rate of $6.9\times10^{-5}$ $cms^{-1}$, 60% larger than our estimate and implying an overturning four to five times larger than that in the deep Pacific.

### 5.2.2 Fresh water flux

Using the same components as for the heat transport calculation; that is the Agulhas Current, ITF, interior geostrophic and Ekman components, the mass and salt budgets for the Indian Ocean north of 32°S can be expressed as (Hall & Bryden, 1982):

$$\rho E = -\rho T_{AC} + \rho T_{ITF} + \rho T_{IO} + \rho T_E \qquad 5.3$$

$$-\rho T_{AC} S_{AC} + \rho T_{ITF} S_{ITF} + \rho T_{IO} S_{IO} + \rho T_E S_E = 0 \qquad 5.4$$

The first equation represents a mass balance for the system assuming some evaporative flux, $E$. $T$ is the volume transport of each component, $S_{AC}$ and $S_{IO}$ are the transport-averaged salinities 35.19 and 34.95 respectively, $S_E$ is the section-averaged sea-surface salinity 35.66, and $S_{ITF}$ is estimated from Fieux *et al* (1996b) as 34.70. Multiplying 5.3 by $S_{IO}$ and subtracting equation 5.4 allows a solution for $E$,

$$E = \frac{T_E (S_{IO} - S_E) + T_{ITF} (S_{IO} - S_{ITF}) - T_{AC} (S_{IO} - S_{AC})}{S_{IO}} \qquad 5.5$$

Density does not vary significantly and is omitted from the calculation. The freshwater flux is estimated as +0.52Sv, implying that evaporation exceeds precipitation and runoff in the Indian Ocean. For comparison TW estimate the freshwater convergence to be 0.469Sv and Baumgartner & Reichel (1975) estimate evaporation minus precipitation minus runoff for the Indian Ocean north of 30°S as 0.5Sv.

### 5.2.3 Discussion

It is surprising that the heat flux divergence estimated here, using an Agulhas Current transport 14Sv less than TWs, should be about the same as their estimate. However, the calculation made here is different to that made by TW in a number of ways. TW use reference levels for their mid-ocean section which maximise deep transport, particularly in DWBCs, in a bid to balance the large poleward fluxes of their Agulhas Current. There is no justification to use such a reference level here and thus a ZVS at 2000db has been adopted since this is close to the horizontal reference level which maximises exchange. In addition both the Ekman and the ITF components are different; TW use an Ekman volume flux of 1.5Sv (Hellerman & Rosenstein, 1983) and an ITF volume flux of 6.7Sv. Using these values in place of those described above for our estimate would reduce the overall heat flux divergence by about 10%. Further, the ACE data was collected in March, at the end of the southern-hemisphere summer, when the temperature of the Agulhas Current can be expected to be a maximum. Indeed transport weighted temperature from the ACE section is larger than that from the TW section and adds about 5% to the heat flux divergence.

For comparison, the heat flux divergence is re-computed using the exact same method described above, but with an Agulhas Current transport of 85Sv. In this case (assuming the added transport occurs at the ACE transport-weighted temperature) a barotropic velocity of $0.095 cms^{-1}$ is added everywhere to the geostrophic component across 32°S so that the northward volume flux is 78.1Sv. The resultant heat flux divergence is -1.275PW or 30% larger than the estimate above using an Agulhas Current transport of 71Sv. The basin average upwelling velocity increases by 40% to $6 \times 10^{-5} cms^{-1}$. In conclusion, the Agulhas Current is both warmer and saltier than the interior of the Indian Ocean and clearly contributes greatly to the overall heat and fresh water flux divergence. Furthermore the rate of thermohaline overturning in the Indian Ocean is sensitive to changes in the volume transport of the Agulhas Current which forms the only link between oceans at mid-latitudes and as such is an important part of the global conveyor belt.

It must be said that per Sverdrup the ITF has the greatest influence on the heat flux divergence over the Indian Ocean, because it has a transport-averaged temperature 10°C greater than the Agulhas Current. Therefore until the ITF and its volume transport are better understood the heat flux divergence over the Indian Ocean will remain uncertain.

# CHAPTER SIX

# *CONCLUSIONS AND FUTURE WORK*

## 6.1 Summary and conclusions

At 32°S the Agulhas Current, as measured by LADCP, flows south-westward at speeds exceeding 180cms$^{-1}$ in the Current core which is just 20km offshore. The Current is 90km wide between the 50cms$^{-1}$ isotachs and extends no more than 200km offshore. The Current core moves offshore with depth, so that at 900m depth it is situated 65km from the coast. Vertical shears are very strong at mid-depths in the cyclonic edge of the Current and as a result there is a flow reversal at about half the water depth between 15 and 40km offshore.

The deep velocity structure of the Agulhas Current as revealed by LADCP, is quite different to the structure suggested in the past from geostrophic estimates. Most previous investigations of the Agulhas Current assumed a near-horizontal level of no motion to estimate absolute geostrophic currents, in contrast LADCP results show a V-shaped level of no motion. At the continental slope the Agulhas jet separates from the sea bed at 800m depth and penetrates to full depth (3000m) about 80km offshore, then at the offshore end of the section (200km) its vertical extent once again reduces to the upper 1000m. At the continental slope, below 800m, LADCP velocities show an Undercurrent flowing north-east with maximum velocities of over 30cms$^{-1}$ at 1200m depth. Such an Undercurrent was not recognised during previous investigations.

Although the Agulhas Undercurrent had not been observed before, other evidence from surveys before and since ACE indicate that it is a persistent feature of the circulation at 32°S. TW found evidence for an Undercurrent in November 1987 when they used shipboard ADCP data to reference geostrophic velocities, before rejecting the technique through water mass considerations. The Undercurrent was directly measured again in April 1996, when LADCP velocities showed north-eastward flow of similar intensity and position to the ACE Undercurrent. Moreover, preliminary results from moored current meters show persistent north-eastward velocities averaging 10cms$^{-1}$ (over a year) at 2000m depth, a result consistent with LADCP findings.

The Agulhas Undercurrent carries North Atlantic Deep Water below 2000m depth, but at intermediate depth its waters are predominantly of Red Sea origin. Overall however, the net transport of Red Sea Water is poleward (directed away from its source) except on the station closest to the slope where there is a very small equatorward flux. The volume transport of the Agulhas Undercurrent is estimated to be 6±1Sv.

LADCP data are very useful for potential vorticity (PV) analysis, since velocity and density measurements are simultaneous and coincident. The pattern of PV across the Agulhas Current suggests the presence of a "mixing boundary" situated at intermediate depths and about 80km offshore. Beyond this boundary and along the section away from the coast, PV is essentially uniform along an isopycnal. Inshore of the boundary, between the 4°C and 14°C isotherms PV is large and negative with high horizontal gradients. Although the PV boundary appears to be coincident with the high vertical shears between the Agulhas jet and the Undercurrent, the planetary vorticity component also shows a region of high, negative PV, suggesting that the feature is primarily associated with a decrease in layer depth (increase in stratification) rather than an increase in velocity shear. On closer inspection the slope of the isopycnals doubles in the same region that the PV boundary occurs. There is some evidence that high, negative PV in the Agulhas Current may also act as a tracer of Red Sea Water (RSW), since the two are somewhat coincident.

LADCP results were compared with both shipboard ADCP and bottom tracked (BT) velocities. The shears from LADCP and on-station, time-averaged ADCP were well correlated over the upper 300m. The depth-averaged difference between LADCP and ADCP and then LADCP and BT were generally within the estimated measurement error of the LADCP (about $6cms^{-1}$ for a cast of 2500m depth) and as a result were found to be dissimilar in some cases.

A careful comparison of LADCP and geostrophic velocity profiles reveals that the baroclinic structure from the two methods is very similar. The largest geostrophic departures in the LADCP profiles occur over the upper 200 to 300m of the water column, below which the ageostrophic flow is everywhere less than estimated measurement errors. The geostrophic departures are not consistent with flow curvature, but are more likely a result of sampling biases due to the time lapse between stations. The spatial averaging of LADCP profiles onto station pairs results in additional inaccuracies, particularly in the Ekman layer where small scale shears make spatial averaging a doubtful representation of the flow. An equivalent comparison of shipboard ADCP and

geostrophic velocities over the upper 300m of the water column showed that the baroclinic structure from each method was different and any match unreliable. Since, on the other hand, the ADCP and LADCP shears are similar, it appears that the flow over the upper 200 to 300m is predominantly ageostrophic, even though this is two or three times deeper than Ekman layer depth.

The volume transport of the Agulhas Current has been estimated in several ways using LADCP, hydrographic and shipboard ADCP data. Directly from LADCP velocities the transport of the Agulhas Current is 75Sv. By referencing LADCP data with ADCP velocities (since one may expect ADCP data averaged over the period of the cast to be more accurate than a single LADCP cast) the volume transport of the Agulhas Current becomes 65Sv. Finally, since the geostrophy-LADCP comparisons were so convincing, a greatly improved geostrophic estimate is made by referencing geostrophic velocities to LADCP measurements. In this way the geostrophic transport of the Agulhas Current is 73Sv, only 2Sv less than the LADCP estimate above. In comparison, using a reference level based on water mass distribution after TW, the geostrophic transport estimated from the ACE data is 82Sv. The Agulhas Current transport is reduced as a direct result of the presence of the Undercurrent. Overall then, the transport of the Agulhas Current is estimated as 71±4Sv.

Since the Agulhas Current carries warm, salty waters out of the Indian Ocean a smaller transport will have an effect on the overall heat budget of the Indian Ocean. With an Indonesian Throughflow of 6.4Sv, an Ekman transport of 0.5Sv, and an Agulhas transport of 71.3Sv the resultant interior transport across 32°S is 64.4Sv northward and the heat flux divergence over the Indian Ocean is 0.99PW. This is about the same as the most recent estimate by TW despite their larger Agulhas Current, but they used larger Throughflow and Ekman transports. In fact, assuming their additional Agulhas transport occurred at the transport-weighted temperature from the ACE section and taking the same ITF and Ekman transports as above, their transport of 85Sv yields a heat flux divergence 30% larger than the value above.

For an Agulhas Current of 71Sv the resulting northward transport of cold waters below 2000dbars is 16.8Sv, implying a basin-averaged overturning rate of $4.3\times10^{-5}$ $cms^{-1}$. This is about half the rate of the most recent estimate (TW) and suggests that the thermohaline overturning in the Indian Ocean is only two or three times that in the Pacific, rather than the four or five times suggested by TW.

## 6.2 Future work

The observations presented in this investigation represent a synoptic survey of the Agulhas Current at 32°S in March-April 1995. But how representative is this one-time section of the Agulhas Current? This is an important question and one which has not been addressed in this thesis. The problem can be readily investigated, at least on a seasonal basis, by using the year-long current meter time series. Using this data may prove that sampling the Agulhas Current at the end of the summer gave higher than average volume and heat fluxes, although there is no evidence in the literature to support any annual cycle in the velocities of the WBC.

Of course there is always a case for more sea work in physical oceanography, and to make real advances in the understanding of the Agulhas Undercurrent it must be sampled again. Making LADCP/CTDO2 measurements upstream and downstream of 32°S would provide information about the development and course of the Agulhas Undercurrent. At approximately 33°S, 300km downstream in the Agulhas Current the continental slope is still steep and conditions for a fast WBC are similar to those at 32°S. At 30°S, about 300km upstream, the continental slope is much gentler and curves eastward away from the coast, leaving a wide shelf area. Here the dynamics of the WBC are potentially very different. Hydrographic and LADCP sections perpendicular to topography and extending about 400km offshore at 30°S and 300km offshore at 33°S would cross the Agulhas Current in each of these regions and help to answer questions about the origin and fate of the Undercurrent.

Of the ACE current meter moorings only a single instrument was recovered from the Undercurrent and although its data confirmed the presence of a persistent northward flow, it was positioned far from the Undercurrent core at a depth of 2000m. A monitoring array at 32°S consisting of three moorings, placed at depths of 1400m, 1800m and 2800m on the continental slope, could sample the Undercurrent effectively. On the first two moorings, which are placed at intermediate depths, temperature and salinity data should be collected in order to monitor the relative Antarctic intermediate water and Red Sea water content of the Undercurrent.

The combination of shipboard surveys and moored time series measurements described above would provide a comprehensive dataset of the Agulhas Undercurrent and allow more specific questions about its behaviour to be addressed. Is it a local recirculation feature or is it a continuous DWBC carrying waters equatorward into the

Indian Ocean? Does it grow in size or rise as it flows northward? Does its transport increase? How and where does Red Sea Water become entrained? Does it conserve potential vorticity along its path? And how similar is it to other DWBCs, such as the North Atlantic DWBC?

# APPENDIX 1

# *LADCP SETUP INFORMATION*

### *Overview*

Four different configurations were used for the LADCP during the Agulhas Current Experiment. The parameters which were varied most frequently are time per ensemble, number of depth cells and bottom tracking pings. A copy of the full setup file (bbsetup.rpt) for the first configuration is given below followed by each of the other configurations with only those parameters which were changed listed.

### *Configuration 1*

Used on station 2.

```
1. ADCP CONFIGURATION AND SETUP.

        System frequency              150 Hz
        Beam angle                     20 deg
        System power                 HIGH

        Water temperature              25 deg C
        Water salinity                 35 ppt
        Depth of transducer             0 m

        WT pings per ensemble           1
        Depth cell size              16.00 m
        Number of depth cells           14
        Blank after transmit         16.00 m
        WT profiling mode                1
        WT ambiguity velocity          400 cm/s

        BT pings per ensemble            0

        Time btwn ping groups         1.00 s
        Time per ensemble     00:00:02.00
        Deployment length            20.00 days
        Velocity collected             YES
        Coordinate system            EARTH
        Correlation collected          YES
        Intensity collected            YES
        Percent good collected         YES
        Status collected                NO
        Enable recorder                YES
        Enable serial output            NO
        Baud rate                    38400

2. PREDICTIONS.

        First depth cell             32.55 m
        Last depth cell             240.55 m
        WT max predicted range      244.12 m
        WT min ping time              0.69 s
```

```
WT vel std dev                2.32 cm/s

Bytes per ensemble             388
Min time per ensemble         0.83 s
Total space needed          335.23 MB
Energy required            7512.26 Wh
```

*Configuration 2*

Used on stations 3, 8 and 9.

```
1. ADCP CONFIGURATION AND SETUP.

        Number of depth cells          10
        Time per ensemble     00:00:01.00

2. PREDICTIONS.

        First depth cell            32.55 m
        Last depth cell            176.55 m
        WT max predicted range     244.22 m
        WT min ping time             0.51 s
        WT vel std dev               2.32 cm/s

        Bytes per ensemble            308
        Min time per ensemble        0.63 s
        Total space needed         532.22 MB
        Energy required          14588.00 Wh
```

*Configuration 3*

Used on stations 4, 5, 6 and 7

```
1. ADCP CONFIGURATION AND SETUP.

        Number of depth cells          20
        Time per ensemble     00:00:02.00


2. PREDICTIONS.

        First depth cell            32.44 m
        Last depth cell            336.44 m
        WT max predicted range     244.00 m
        WT min ping time             0.95 s
        WT vel std dev               2.32 cm/s

        Bytes per ensemble            508
        Min time per ensemble        1.13 s
        Total space needed         438.91 MB
        Energy required           7776.78 Wh
```

* On station 4 the ambiguity velocity was higher and pushed up the predicted velocity standard deviation:

```
        WT ambiguity velocity        480 cm/s
        WT vel std dev              2.55 cm/s
```

*Configuration 4*

Used on stations 10, 11, 14 and 15.

1. ADCP CONFIGURATION AND SETUP.

| | |
|---|---|
| Number of depth cells | 10 |
| BT pings per ensemble | 1 |
| BT ambiguity mode | 4 |
| Max tracking depth | 250.00 m |
| Time per ensemble | 00:00:02.00 |

2. PREDICTIONS.

| | |
|---|---|
| First depth cell | 32.55 m |
| Last depth cell | 176.55 m |
| WT max predicted range | 244.10 m |
| WT min ping time | 0.51 s |
| WT vel std dev | 2.32 cm/s |
| BT max predicted range | 399.93 m |
| BT min ping time | 1.00 s |
| BT vel std dev | 0.27 cm/s |
| Bytes per ensemble | 378 |
| Min time per ensemble | 1.65 s |
| Total space needed | 326.59 MB |
| Energy required | 37756.13 Wh |

# APPENDIX 2

# *LADCP DEPLOYMENT AND RECOVERY*

## OVERVIEW

Deploying the LADCP should take no more than 10 minutes, even if the instrument set up (e.g. bin length, time between ensembles...) is to be changed. Communication with the instrument is through RDI programs BBTALK and BBSC on the PC. The recovered data can be viewed using BBLIST. The data is written to a CODAS database with programs SCANBB and LOADBB.

## DEPLOYMENT

1. Connect up the instrument.

2. In the C:\BBADCP directory run BBTALK and press <END> to wake up the instrument. Note down the wake up time on the log sheet. A series of checks should now be made.

3. Enter TS? at the prompt and check the time against laboratory time. Adjust the LADCP time by entering the new time in the same format shown on the screen, otherwise press <ENTER> and the time will remain unchanged.

4. Enter PT2 and note VMVDC as the high voltage (HV) on the log sheet to check that the battery is not running down. HV should ramp up to 30.1 over a few tens of seconds after wake up. If the HV settles at less than 25V then the batteries should be replaced.

5. Enter R? and note the remaining memory on the log sheet. As a guide, a cast of 2000m depth requires 1MB of memory.

6. Finally, enter PT200 and check that the tests are passed. Sometimes there can be a transmit error, $C. This is usually cured by reloading a parameter file. Try the default parameters by entering CR0 and rerun the tests. Otherwise refer to the RDI manual.

(7. If you are not ready to deploy the instrument yet, CZ puts it to sleep.)

8. Press <ALT> X to exit BBTALK.

9. Next create a command file for the station. Do this by editing one of the old .CMD files found in this directory or by editing the previous station's .CMD file. Save the file as <CRUISE NUMBER> <CAST NUMBER>.CMD - e.g. D214001.CMD. Below is an example of a command file with a description of those parameters which are changed most often.

```
                    A001015.CMD
CR1
PS0
CY                  .....clear error status bits
EZ 0011101
EC 1500             .....nominal sound velocity
EX 11101
WD 111100000
WL 0,4
WP 00001
WN 020              .....number of bins
WS 1600             .....bin length in cm
WF 1600             .....blank beyond transmit in cm
WM 1                .....water tracking mode
WB 1
WV 400              .....mode 1 ambiguity velocity
WE 0150
WC 056
CP 255
CL 1
BP 000
TP 000100
TE 00000200         .....time between ensembles in hhmmss.ss
&R20
CF11101
&?
```

10. CD into directory DEPLOY, run BBSC and choose DEPLOYMENT on the menu.

11. Choose LOAD and enter in the .CMD file - e.g. ..\D214001.CMD, then chose DEPLOY. The set up scrolls down the screen and the instrument starts pinging. Note the time on the log sheet and exit the program. To exit BBSC use <ESCAPE> to get back to the top menu bar, then exit under FILE.

12. On deck place your ear close to the LADCP and listen for a ticking, just to be sure that the instrument is pinging. Disconnect the download wire and push on the blank.

RECOVERY

1. Connect up the LADCP again when the cast is completed.

2. In C:\BBADCP\DEPLOY run BBSC and choose RECORDER from the menu. Note the number of deployments on the log sheet. Go to RECOVER and use <TAB> to move around the options. Fill in the raw data filename - e.g. D214001.000 and write it on the log sheet, change the maximum file size to 100000 (a large number) and enter the deployment number (the last deployment on the LADCP recorder).

3. Press RECOVER and wait for the data to be downloaded. It seems difficult to predict how long this will take, since cast depths and instrument settings may change from station to station. A rough guide is 10 mins per 1000 m of cast.

4. Note the downloaded filename, size and the number of ensembles on the log sheet.

5. CD up a directory and run BBTALK. Enter PT2 and note the VMVDC on the log sheet as the high voltage HV. Enter CY? and write down the Error Status Word (ESW) on the log sheet. This word is updated whenever an error occurs, so if it has a value use the RDI manual (fax update) to interpret the problem.

6. Enter CZ to put the instrument to sleep, note the time on the log sheet and exit BBTALK.

(7. The data can be viewed at this point by running BBLIST in the C:\BBADCP directory. Find the downloaded file in the menu and choose DISPLAY. <+> and <-> scroll through ensembles and <J> jumps through them.)

8. Create a directory for the cast data - e.g. C:\D214\LADCP\D001 and move the downloaded file into it. Copy over (from an old station directory) LADY.DEF and the control file for creation of the CODAS database - e.g. D001.CNT.

9. Go to the new cast directory and run SCANBB by entering: ..\SCANBB followed by the raw data filename, e.g. D214001.000. Note the output details on the log sheet, making sure to copy down the start, down and end times accurately.

10. Edit the .CNT file, changing the database name, lat, lon, output file, input file, magnetic declination and the range of good ensembles using the details from the SCANBB output. Below is an example of a station control file - highlighted text shows what needs to be changed:

A015.CNT
DATABASE_NAME: **a015** /* each cast is a separate database */
DEFINITION_FILE: lady.def /* as is */
OUTPUT_FILE: load**015**.log
LATITUDE (DEG MIN N/S): **31 06.43 S** /* from log sheet */
LONGITUDE (DEG MIN E/W): **30 23.26 E** /* */
ORIG_MAG_DECL: 0 /* magnetic declination */ TRUE_MAG_DECL: **-22.3** /* " *
MAX_BLOCK_PROFILES: 400 /* leave this as is */
NEW_BLOCK_AT_FILE? no /* " */
OPTION_LIST:
skip_ensemble_range: 1 to **607** /* 1 to <scanbb xx-1> */

skip_ensemble_range: **3446** to 20000 /* <scanbb yyy+1> to big no.*/

/* first_date_time= 89/12/15 16:42:53 from Matlab td output */
/* ensemble_secs= 11.829579 " */

end
**a015.000** /* your raw input file */

11. Enter ..\LOADBB to create the CODAS database and the program will prompt you for the control filename.

12. Finally, copy LOAD<stn>.LOG, *.SCN, *.CNT and the *.BLK files onto disk (to sneaker-net to a SUN if necessary) as a back up.

...the LADCP data is downloaded and now it can be processed on a SUN using Firing's software.

# APPENDIX 3

# *LADCP PROCESSING*

OVERVIEW

The suite of programs to handle LADCP processing were created by Dr E Firing of the University of Hawaii. Most of the processing described below uses Firing's software, which is a mixture of perl and matlab scripts, but some parts e.g. the CTD and GPS data handling, use pstar programs or specially written software.

The processing is done in two passes: a first pass to look at the relative velocity data which is derived directly from the LADCP and a second pass in which CTD and GPS data are incoorporated to provide absolute velocities. When the final processing run is completed all the data can be converted to pstar using the simple shell script provided.

CREATING THE SUN DATABASE AND PLOTTING RELATIVE VELOCITIES

1. On the SUN, in the cruise directory, **../ladcp/ladcp/ladyproc/<cruise>** make a cast directory - e.g. **D001,** and two subdirectories, **merge** and **scdb.**

2. In **/scdb** copy **<stn>dir.blk**, **lady.def**, **<stn>.cnt** and the ***.blk** files from the PC station directory. The next program will change the data from PC to SUN format.

3. Copy **mkblkdir.cnt** from a previous **<cast>/scdb** directory and edit the file, changing the database name (keep the s for SUN) and the list of input files. See the example below:

```
                        mkblkdir.cnt
DB_NAME   d011s                 .....i.e Discovery, cast 11
PRD_NAME  lady.def              .....don't change
end
BLOCK_FILE d011001.blk          .....database files from PC
BLOCK_FILE d011002.blk                change these
BLOCK_FILE d011003.blk
BLOCK_FILE d011004.blk
BLOCK_FILE d011005.blk
BLOCK_FILE d011006.blk
BLOCK_FILE d011007.blk
```

4. Run **mkblkdir** (the path should be set up, if not the program is in **/ladcp/codas/codas3/bin/sun4**) and enter **mkblkdir.cnt** at the prompt. The program

creates a SUN version of the CODAS database, e.g. **d001s001.blk, d001s002.blk** ... The data in the CODAS database can be looked at by running **showdb** and entering the database name at the prompt - e.g. d001s. Press **<enter>** at the next prompt and a menu will appear. Type 16 for a list of the variables.

5. Go back up to the cast directory and copy in **domerge**, **merge__.cnt** and **proc.dat** from a previous cast. Edit domerge, changing the cruise, or database letter (ie 'd' for Discovery casts) and the profile list (and if necessary the program path) - see the example below:

```
                        domerge
#!/data3/packages/utilities/bin/perl -w

# This perl script runs "merge" on a whole set of LADCP profiles,
# using a single basic merge control file template, "merge__.cnt".
# It also requires a file with time ranges and bottom depths
# as explained below.
# The version of merge must be post-February 1993.

# add depth information to the latlon.asc file
# 08/31/92 Mei

# Label for a particular run, to be used in file names etc.
$out = "a";
# so far, 'a' is 10 % margin;
#       'b' is 1 % margin, all bins
#       'c' is 1 % margin, no first bin on upcast
#       'd' is 1 % margin, no first bin on up or down cast
#       'e' is 1 % margin, wake editing (hd_dif=20, ang=15, n_bins=1)
#       'f' is 1 % margin, wake editing (hd_dif=20, ang=15, n_bins=2)

# Components of directory and db names:
$cr     = "d";                          <--- change to match dbname
$prefix = "";
$suffix = "s";
# For example, profile 5:  t005s; $cr is "t", $prefix is "",
#                  $suffix is "s".
# Convention: one letter for the $cr (cruise name),
#  three digits for the profile number, no $prefix,
#  and a $suffix of "s" for the Sun database version.

# List of profiles:
@proflist = ('d011',);                  <--- change to cast number
# Alternative way to get the proflist:
#  for ($i = 251; $i <= 285; $i += 2)
#  {
#    push(@proflist, sprintf("$cr%03d", $i));
#  }
```

```
# The adaptation of this to any reasonable number
# sequence should be clear.



# Path to the subdirectories holding the profiles in a section:
$pa = "../";
#$pa = ".\\";

# File containing a profile data in groups of 4 lines:
#    1) profile name (e.g. t005)
#    2) down cast time range
#    3) up cast time range
#    4) bottom depth
# The time ranges are the usual:  yy/mm/dd hh/mm/ss to yy/mm/dd hh/mm/ss
# They should not overlap (to avoid trouble with the m-file routines).
# A blank line must follow each group of 4 lines to delimit it from
# the next profile.
$data_file = "./proc.dat";


# Subdirectory separator: "/" for Unix, "\\" for DOS:
#   (double backslash is needed because single \ is an escape.)
$s = "/";
#$s = "\\";

# path to the merge binary:   (include trailing separator)
$ladyprocbin = "/data4/ladcp/ladcp/ladyproc/bin/sun4/";
                                          <--- (may need to change path)
#  (This may be needed to avoid conflict with a unix command
#   of the same name.)

# How far off the bottom to cut the profile?  In meters.
$clip_margin = 30;

######## End of section that would typically be edited. ########
```

6. Edit **proc.dat** and change the cast name, insert the start and stop times of the down and up casts, input the bottom depth (data is clipped from 30m above bottom) and input the lat and lon. All these details should be on the log sheet. See the example below:

```
                    proc.dat
d015                                        .....change db name and cast

95/03/06 09:38:30 to 95/03/06 10:50:12   .....from scanbb output

95/03/06 10:50:14 to 95/03/06 12:27:00   .....from scanbb output
3560                                        .....bottom depth
```

32 06.9 S 31 52.286 E .....lat/lon of cast station

7. Run **domerge** by entering **>perl domerge** (perl is a shell like script interpreter). (If you need to change the data editing criteria in **merge_.cnt** see the *Editing* section at the end of this manual) Two matlab files and two ascii files are created (**a_dn** and **a_up**) in the merge directory, and a **latlon.asc** file is created in the cast directory.

8. Copy **do_abs.m** from a previous cast directory and change *plist*,and the *plot axis limits* (and some path names if necessary). Check that *have_sm = 0* for this first look at the data (sm points to the GPS nav file). See the example below:

```
% do_abs.m:
% script for running through a set of LADCP profile merge
%   output files, calculating absolute velocities,
%   plotting a standard set of curves for each profile,
%   and building up arrays with subsampled versions of
%   the main variables--that is, 2-D arrays with depth
%   down the row dimension and profile number along the
%   column dimension.  These are saved for use by other
%   scripts.
%
% This script can be used for a single profile at a time
%   simply be setting the cruise list "crlist" to one
%   profile rather than a whole range.  A simple naming
%   and numbering scheme for the profiles in a set is
%   needed.
% Be sure all the necessary m-files are in the MATLABPATH,
%   or in the same directory as this script.
% 12/06/93 Add flag_sm, flag_sm = 1, using sm.mat file from
% each station's merge directory, flag_sm = 0, using grand
% sm.mat file for all the stations.
%
clear
% path to the directory in which the profile subdirectories lie:
cr_root = '/working/hydrog/ladcp/ladcp/ladyproc/214_ace'
flag_sm = 0; %1, use individual sm.mat file, 0 use the grand one
                                          <--- relevant when have GPS file
%if flag_sm =0, specify the location of the big sm file:
sm_dir  = '/working/hydrog/ladcp/ladcp/ladyproc/214_ace/' <-- location
                                                    of GPS file
% Append to a log file:
global FID_LOG
FID_LOG = fopen('do_abs.log', 'a');
%fprintf(FID_LOG, '\n\ndo_abs,  %s\n', pctime);
fprintf(FID_LOG, '\n\ndo_abs');      % removed pctime rtt 03/02/95

% profile numbers
plist =  011;                          <--- change cast number
```

```
% merge output file root
run_name = 'a_';       % change for different settings in merge__.cnt etc

% plot axis limits                              <--- change as appropriate
umin = -140;
umax = 30;
dmax = 3600;

% flags
have_sm   = 0;                        <--- zero for first look at relative
pause_flag = 1;                          velocities. 1 when have GPS file
print_flag = 0;
plot_lat  = 1;   % 1 to use latitude, 0 to use longitude
plot_all  = 1;  % 1 for full set of plots, 0 for mn U,V only
int_up_dn  = 0;  % 0 to use mn shear prof; 1 to use up and down
                              % in uv_abs.m for calc of barotropic c
omp.

% depth value for different shear averaging schemes
avg_depth = 1200;

fprintf(FID_LOG, 'run_name: %s,  have_sm: %d,  int_up_dn: %d,  avg_depth: %4.0f\
n', ...
              run_name,     have_sm,     int_up_dn,     avg_depth  );


%%%%%% end of things that may need to be edited %%%%%%%
%% EXCEPT for cruise name items below, marked with "%%%"

old_uv0 = 0;  % for carrying through previous barotropic component
ncr = length(plist);

% The following file is output by domerge:
load latlon.asc
prof_xy = latlon(:,[1,3,2]);    % prof#  x  y
pxy = zeros(ncr,2);

% subsample: merge calculates on ((1:1100)-9)*5
% we subsample at 20-m intervals starting from zero:
i_samp = 9:4:1300; % changed from 1100, corresponding the change with NGRID, mei
n_samp = length(i_samp);
d_samp = 20 * ((1:n_samp)-1);

% arrays for the section: allocate space
su_up = zeros(n_samp, ncr);
sv_up = su_up;
su_dn = su_up;
sv_dn = su_up;
sw_up = su_up;
```

```
sw_dn = su_up;
su_mn = su_up;
sv_mn = su_up;
sw_mn = su_up;
% number of points in the depth bin
sn_dn = su_up;
sn_up = su_up;
sn_mn = su_up;
% shear variance
su_var_dn = su_up;
sv_var_dn = su_up;
sw_var_dn = su_up;
su_var_up = su_up;
sv_var_up = su_up;
sw_var_up = su_up;
su_var_mn = su_up;
sv_var_mn = su_up;
sw_var_mn = su_up;
% masks: good points
sm_dn = su_up;
sm_up = su_up;
sm_mn = su_up;

for iicr = 1:ncr,

  icr = plist(iicr);
  cr = sprintf('d%03.0f', icr);     %%%     <-- change database letter, d
  disp(cr)

 spos = pos_str(prof_xy, icr, plot_lat); % string: degrees N/S or E/W
  pxy(icr,:) = prof_xy(find(prof_xy(:,1) == icr), [2 3]); %position: [x y]
the_title = ['A.C.E. Feb/Mar 95, ' cr ', ' spos ', (' run_name ')'] %%%
                                <--- change the title for plots

  fprintf(FID_LOG, '%s\n', the_title);

  crdir = ([ cr_root '/' cr '/merge/']);
  if(flag_sm == 1)
    smdir = crdir;
                    ..... etc
```

9. Run **matlab** and enter **do_abs**. Two figures will appear showing plots of the relative u, v and w velocities (green: downcast, pink:upcast, blue:mean profile), the number of samples and the shear standard deviation against depth. Enter **pts** to get plots of the package heading and tilt variation during the cast. To print these figures to ps files enter: > **print -dpsc -f1 uv.ps** - where f1 is the figure window and uv.ps is the ps file name. Repeat for figures f2, f3 and f4 and put the plots in the log book.

ADDING CTD DATA

1. Make a directory called **ctd** at the same level as the LADCP cast directory. Find the directory containing the down/up CTD data, e.g. **ctd12787.du**. Using **mlist** create an ascii file ,-e.g **ctd/ctd001.asc**.containing time, press, temp and salin as columns 1, 2, 3 and 4 (data fields 1, 3, 4 and 15).

2. Change to the **ctd** directory and remove the first two lines (the header) of the ascii file. Run **matlab** and enter **>doctd(xxx)** - where xxx is the cast number, e.g. 001. This function creates a matlab file called **ctdxxx.mat.**

3. This step matches up the LADCP and CTD casts (in case of clock differences) by using the change in vertical velocity with time. Go to the cast directory and copy in set_xxx.m, where xxx is the profile number. Edit set_xxx.m as shown below:

```
                    set_001.m
% >>>>>>>>>>>>>>>>>>> Edit the following for each station >>>>>>>>>>>>
stanum = 011          %%% station number          <-- change cast no.
stalat = -31.1        % latitude for calculation of depth from pressure
                              <-- change latitude
ctdfile = '/working/hydrog/ladcp/ladcp/ladyproc/214_ace/ctd/ctd011.mat';  %%%
                                                        <-- (path to CTD data)
CTD input file - ASCII, matlab-loadable

t_adcp_lag0 = -20. ;%120;       % initial estimate in seconds:
              %   first adcp w time minus first ctd time

% mask index range in UNIFORMLY GRIDDED ADCP array
%first_index =  400
%last_index  =  10000
 first_index = 1
 last_index = 20000

%>>>>>>>>>>>>> Edit once for the cruise, ordinarily >>>>>>>>>>>>>>>>>
ppath = '/working/hydrog/ladcp/ladcp/ladyproc/214_ace/';
run_name = 'a';                    <-- should match file names in merge directory
cl = 'd';  % cruise letter used to form cast directory name
                                    <-- database letter
% output file
depthasc = sprintf('depth%03d.asc', stanum);

year_base = 95;
dt_a = 10;       %%%              <-- this must be 10 for 2s ensembles
dt_c = 1;     %%% sample time interval of CTD in sec, in this case, 1.0 sec
BB = 1;       % 1 for BroadBand data, 0 for NB data.
ladcp1
```

4. Run **matlab** and enter **set_xxx**; three plots will appear. Enter 2 at the prompt and follow the on-screen instructions. The LADCP data stream will be stretched to fit CTD. Repeat the stretching until the fit is satisfactory. There is no need to be too accurate because the fit will be optimized when you press enter. Note the lag_adcp value as a comment on the log sheet. If the fit is good, follow the instructions and enter **pp** followed by **ladcp2**. These programs plot the CTD and LADCP velocity time series and create a file of ensemble number, time, depth and sound speed, called **depthxxx.asc**.

5. The CTD information in **depthxxx.asc** is now added to the CODAS database. Change to the **scdb** directory and copy in **add_ctd.cnt** from a previous cast. Change the database name, ctd file and year as follows:

```
                    add_ctd.cnt
dbname:  d011s
ctd_file:  ../depth011.asc      /* output of Matlab ladcp2 run */
year_base= 1995
```

6. Run **add_ctdbb** and enter **add_ctd.cnt** at the prompt. The CTD data is added to the database as ANCILLARY_1 in the data list. Use **showdb** to check the data if required. To modify the data using the new CTD information **domerge** must be run again, but first the profiles can be checked and edited for bad data.

## EDITING

Most of the editing of the data is done automatically in **merge**, but Firing has written a number of matlab programs that make it easy to view the data in different forms and on different scales so that bad data can be flagged by hand. Any mistakes in editing are reversible. This editing is particularly useful for editing out bottom interference and data spikes.

1. Make an **edit** directory under the station directory and copy **setup.m** into it (there will be a copy in the **matlab4** directory). Edit **setup.m**, changing the database name and file path (to editing programs), and choosing the number of profiles to retreive and the editing criteria.

2. Start matlab and run **setup**. Type **getp(blk,prf)** to retrieve some data, where blk = starting block and prf = starting profile, ie type **getp(0,0)** for first profiles in cast. Use **r** to move forward in time and **l** to move backwards in time.

3. To visualise the data use:

**uvw1**: U, V, W, first beam of amplitude
**uvw2**: U, V, W, second beam of amplitude
**uvw3**: U, V, W, third beam of amplitude
**uvw4**: U, V, W, fourth beam of amplitude
**uvwp**: U, V, W, percent good
**uvwe**: U, V, W, error velocity

**ampall**: all four beams of amplitude

4. Use single plot screens when marking bad bins:
**amp1**, **amp2**, **amp3**, **amp4**: plot beams 1, 2 ,3 or 4 of amplitude
**u**, **v**, **w**, **e**, **p**: plot U, V, W, E or percent good

5. To change the key profile which is plotted as "+" (ie the profile to be edited), type **k(nprf)** to move on nprf number of profiles or type **k(blk,prf)** to move to a particular profile.

6. Use the following routines to mark bins as bad:
**bad(bin)**: marks 'bin' as bad in current key profile
**bad([2:5])**: marks a given range of bins, ie bins 2 to 5
**bad(bin,blk,prf)**: marks 'bin' as bad in given profile
**bad(bin, nprf):** marks 'bin' as bad in key profile and in the next nprf
**bad(bin, blk, prf, nprf):** marks 'bin' in specified profile and in next nprf profiles as bad
**markrg([blk,prf],nprf,[d1,d2]):** marks as bad all bins between depths d1 and d2, starting at the profile specified and continuing for the next nprf profiles

7. Bins can be marked using the mouse, only in the single plot screens, with the following routines:
**tmark**: marks range of bins in window; click mouse three times: first click - top of profile to mark, second click - top of bad bin range, third click - end of bad bin range.
**bmark**: same as tmark, but first click is on bottom of profile

8. If you make a mistake use these routines to unmark the bins:
**unmark**: use immediately following bmark or tmark
**restore( )**: use in exactly the same way as **bad( )**, but to unmark bins that had previously been shown as bad.

9. To view subsections of the data use **zoomin([blk1, prf1],[blk2, prf2])** or **zoomin** without any arguments to use the mouse. **zoomout** returns to viewing all profiles. To change the number or retrieved profiles type **resetup(nprf).**

10. After all editing is complete type **list** to print all bad bins to an ascii file, **badbin.asc**. This list is done automatically each time new profiles are retrieved, so that it need only be manually entered when exiting matlab. Finally run **badbin <database name> <badbin.asc>** to set flags in the ADCP database.

## MERGING

1. The editing criteria used automatically by **merge** appear in the control file **merge__.cnt**. All casts from one cruise would typically be processed using the same editing options. Below is an example of this file with a description of some of the editing

options with typical values. For a more detailed explanation see the *Merging* section in the LADCP Processing Document, **ladcp.doc**.

```
          MERGE__.CNT
 flag_mask:     ALL_BITS
   end
 stats:         all
 step_size=     1
 ensemble_secs= 0.0        used for corrections to LADCP clock
 w_bin0=        1          first bin for integrating vertical velocity
 w_bin1=        4          last bin for integrating vertical velocity
 u_bin0=        1          first bin for integrating horizontal velocity
 u_bin1=        4          last bin for integrating horizontal velocity
 u_pg_dif=      1
 u_pg_min=      40         minimum percent good to accept horizontal velocity
 w_pg_dif=      1
 w_pg_min=      40         minimum percent good to accept vertical velocity
 e_max=         0.1
 shear_dev_max= 3.5
 shear_sum_dev_max= 1.5
 first_z=        5         starting depth value for integration
 first_x=        0         starting x value for integration
 first_y=        0         starting y value for integration
 clip_z=         __clip_z__    max. depth of accepted data (set in domerge)

binned_shear_time_range:     __tr_dn__
 first_z=        5
 first_x=        0
 first_y=        0
time_range:     __tr_dn__

 output:        __out_up__
 step_size=     -1
 first_z=        5
 min_wake_w=     0.1       min. upward speed to consider for wake interference
 wake_hd_dif=   20         max. difference between wake and beam heading for
                           potential wake interference
 wake_ang_min= 15          min. angle of wake from vertical for potential wake
                           interference
 n_wake_bins=    2
binned_shear_time_range:     __tr_up__

 first_z=        5
 first_x=        0
 first_y=        0
time_range:     __tr_up__

end
```

2. This time all (or several) of the casts can be merged at once. Go to the cruise directory and edit the global **domerge**. Find *proflist* and type in the list of casts you want

to process. Next edit **proc.dat** (do not change directory) and copy in the information from all the individual cast proc.dat files. Run **domerge**. The **a_dn** and **a_up** files are created in the individual cast merge directories, but a global **latlon.asc** is created in the cruise directory.

3. To plot the corrected relative velocities change to the cast directory, run **matlab** and enter **do_abs**. Add a plot of the CTD corrected, relative u and v velocities to the log book for comparison with the first look velocities.

ADDING GPS SHIP DRIFT

1. Find the pstar continuous GPS file for the cruise (1s interval). Use **ptime** to change seconds to jday. Run **mlist** and create an ascii file called **sm.asc** in the cruise directory (same level as cast directory) with jday, lon, lat (in that order). Make sure jday is in "f7.4" format.

2. Remove the first two lines of the ascii file. Run matlab and enter the following:

```
>load sm.asc
>sm = sm(:,[2 3 4]);
>save sm sm
```

... this creates a matlab file called sm.mat which must be in the cruise directory.

3. Quit matlab and change to the cast directory. Edit **do_abs.m**, changing *have_sm* to 1 and making sure that *flag_sm* is zero, for a global GPS file - see the example of **do_abs.m** in step 8 of the first processing section above. Now run **matlab** and enter **do_abs** to calculate and plot the absolute velocities. Add a figure of absolute u and v velocities to the log book.

ROTATING VELOCITIES AND CONVERTING TO PSTAR

1. Rotating u and v is done by matlab script **rotate.m**, which must be run after **do_abs** and before quitting **matlab.** First edit **../ladcp/ladyproc/matlab4/rotate.m** (see below) and change the angle of rotation, theta_deg, which must be the angle of the ship's track (going clockwise) from true east . Also change the plot axes as appropriate.

rotate.m

```
% This program MUST run after do_abs.m.
% It calculates and plots the rotated U and V velocities;
% current and alongtrk.The angle of rotation is theta_rad
% degrees and can easily be changed below so that the current
% and alongtrk components are respectively normal and
% parallel to the oceanographic section.
%
% The results are written out to ascii file ladcp.asc, together
% with mean u,v,w and depth from do_abs, ready for conversion to
% pstar. A matlab file, ladcp.mat, is also created.
```

```
%
% Lisa M Beal   May 1995

theta_deg = 130;                          <--- change the angle of rotation
theta_rad = (theta_deg/360)*2*pi;

% Rotating the velocities:
alongtrk_dn = v_dn*cos(theta_rad) + u_dn*sin(theta_rad);
current_dn = u_dn*cos(theta_rad) - v_dn*sin(theta_rad);
alongtrk_up = v_up*cos(theta_rad) + u_up*sin(theta_rad);
current_up = u_up*cos(theta_rad) - v_up*sin(theta_rad);
alongtrk_mn = v_mn*cos(theta_rad) + u_mn*sin(theta_rad);
current_mn = u_mn*cos(theta_rad) - v_mn*sin(theta_rad);

hf4 = figure('Units', 'normal', 'Position', [0.1 0.1 0.5 0.8]);

% Plotting alongtrk component:
axes('position', [0.2 0.12 0.65 0.35], 'Box', 'on');
hold on
axis([-20 160 -1000 0]);              <--- adjust axes
hsht= plot(alongtrk_dn, d_dn, 'g:', alongtrk_up, d_up, 'm:', alongtrk_mn, d_mn,'c-');
grid on
ylabel('Depth (m)')
xlabel('alongtrk (cm/s)  [u,v rotated thru 130 deg]')
date_it
orient tall

% Plotting current component:
axes('position', [0.2 0.55 0.65 0.35], 'Box', 'on');
hold on
axis([-20 160 -1000 0]);              <--- adjust axes
hcur = plot(current_dn, d_dn, 'g:', current_up, d_up, 'm:', current_mn, d_mn, 'c-');
grid on
ylabel('Depth (m)')
xlabel('current (cm/s)  [u,v rotated thru 130 deg]')
title(the_title)

% Print out rotated velocity plots to ROT.jet file:
hf4, print -dpsc ROT;

d_mn = -d_mn;
pstar_out = [d_mn u_mn v_mn wg_mn current_mn alongtrk_mn];
save ladcp.asc pstar_out -ascii
save ladcp d_mn u_mn v_mn wg_mn current_mn alongtrk_mn
end
```

2. After running **matlab**, then **do_abs** in the cast directory enter **rotate**. A figure with current (cross track) and alongtrk velocity components will appear. The program also

creates a ps file called **ROT.ps** and two data files, **ladcp.asc** and **ladcp.mat** in the cast directory. The ascii file contains six columns of absolute data: depth, u, v, w, current, alongtrk - ready for converting to pstar format.

3. Quit matlab and print a copy of the rotated velocities, **ROT.ps** for the log book. The next step converts the data to pstar format, ready to grid and contour.

4. Find the pstar cruise directory and make a directory called **ladcp** below it. Copy **ladcp.asc** from the cast directory into the pstar ladcp directory as ldp<stn>.asc, e.g. **ldp001.asc**. When all the casts have been completed, copy **latlon.asc** (created by the global **domerge**) and **ladcpexec** from the cruise directory to the pstar ladcp directory.

5. Edit **latlon.asc**, changing stations 1 to 9 into 01 to 09 - so that the **ladcpexec** file will work. See the example below:

latlon.asc

| | | | | |
|---|---|---|---|---|
| 4 | -31.061167 | 30.370333 | 600 | ..change column 1 from 4 to 04 |
| 5 | -31.075167 | 30.380667 | 1000 | ..change column 1 from 5 to 05 |
| 6 | -31.631500 | 31.175833 | 2900 | " 6to 06 |
| 7 | -31.522333 | 31.014000 | 3044 | " and so on |
| 8 | -31.378833 | 30.885167 | 3000 | " |
| 9 | -31.098667 | 30.403333 | 1350 | " |
| 10 | -31.124333 | 30.445167 | 1720 | |
| 12 | -31.259833 | 30.569500 | 3000 | |
| 13 | -31.205500 | 30.454500 | 2600 | |
| 15 | -31.107167 | 30.387667 | 1320 | |
| 16 | -31.085500 | 30.371500 | 915 | |

6. Finally enter **ladcpexec** and the ascii files will be converted to pstar format.

# REFERENCES


**Africa Pilot** (1915) The southern and eastern coasts of Africa from Table Bay to Ras Hafun. *Hydrographic Dept., Admiralty,* London.

**Barlow E.W.** (1931) Currents in the western portion of the Indian Ocean. *Parts I, II, III, Maritime Observer*, **8**, 130-132, 193-194, 254-259.

**Baumgartner A. and E. Reichel** (1975) The world water balance. *Elsevier, New York*, 179pp.

**Bower A.S., H.T. Rossby and J.L. Lillibridge** (1985) The Gulf Stream - barrier or blender? *Journal of Physical Oceanography*, **15**, 24-32.

**Broecker W.S.** (1991) The great ocean conveyor belt. *Oceanography*, **4**, 79-89.

**Broecker W.S., T.-H. Peng, J. Jouzel, G. Russell** (1990) The magnitude of global fresh water transports of importance to ocean circulation. *Climate Dynamics* **4**, 73-79.

**Bryden H.L.** (1980) Geostrophic vorticity balance in midocean. *Journal of Geophysical Research*, **85** (C5), 2825-2828.

**Bryden H.L., D.H. Roemmich and J.A.Church** (1991) Ocean heat transport across 24°N in the Pacific. *Deep-Sea Research*, **38**, 297-324.

**Bryden H.L. et al** (1995) RRS *Discovery* cruise 214, 26 Feb-09 Mar 1995. Agulhas Current Experiment. *Institute of Oceanographic Sciences Deacon Laboratory, Cruise Report*, no.249, 85pp.

**Bunker A.F.** (1988) Surface energy fluxes of the South Atlantic Ocean. *Monthly Weather Review*, **116** (4), 809-823.

**Cheney R.E and P.L. Richardson (1976)** Observed decay of a cyclonic Gulf Stream ring. *Deep-Sea Research*, **23**, 143-155.

**Clowes A.J. and G.E.R. Deacon** (1935) The deep-water circulation of the Indian Ocean. *Nature*, December 14, 936-938.

**Cresswell G., A. Frische, J. Peterson and D. Quadfasel** (1993) Circulation of the Timor Sea. *Journal of Geophysical Research*, **98** (C8), 14379-14389.

**Darbyshire J.** (1964) A hydrological investigation of the Agulhas Current area. *Deep-Sea Research*, **11**, 781-815.

**Darbyshire J.** (1972) The effect of bottom topography on the Agulhas Current. *Pure and Applied Geophysics* **101**, 208-220.

**Defant A.** (1941) Die absolute topographie des physikalischen meeresniveaus und der druckflachen, sowie die wasserbewegungen im Atlantischen Ozean. Vol 6, *Deutsche Atlantische Expedition "Meteor"* 1925-1927, 191-260.

**Dickey F.R. and J.A. Edward** (1978) Velocity measurement using correlation sonar, *Proceedings of IEEE Conference on Position Location and Navigation, San Diego, USA.*

**Dietrich G.** (1935) Aufbau und Dynamik des sudlichen Agulhasstromgebietes. *Veroffentlichungen des Instituts fur Meereskunde*, **27**, Berlin, 79p.

**Duncan C.P.** (1970) The Agulhas Current. *PhD dissertation, University of Hawaii*, 76pp.

**Duncombe Rae C.M.** (1991) Agulhas Retroflection rings in the South Atlantic Ocean: an overview. *South-African Journal of Marine Science*, **11**, 327-344.

**Emery W.J. and J. Meincke** (1986) Global water masses: summary and review. *Oceanologica Acta*, **9** (4), 383-391.

**Fieux M., C. Andrie, E. Charriaud, A.G. Ilahude, N Metzl, R. Molcard and J.C. Swallow** (1996b) Hydrological and chlorofluoromethane measurements of the Indonesian throughflow entering the Indian Ocean. *Journal of Geophysical Research*, **101** (C5), 12433-12454.

**Fieux, M., R. Molcard and A.G. Ilahude** (1996a) Geostrophic transport of the Pacific-Indian Oceans throughflow. *Journal of Geophysical Research*, **101** (C5), 12421-12432.

**Firing E. and R. Gordon** (1990) Deep ocean acoustic Doppler current profiling. *Proceedings of the IEEE Fourth Working Conference on Current Measurements*. Clinton M.D., Current Measurement Technology Committee of the Oceanic Engineering Society, 192-201.

**Fischer J. and M. Visbeck** (1993) Deep velocity profiling with self contained ADCPs. *Journal of Atmospheric and Oceanic Technology,* **10**, 764-773.

**Gill A.E.** (1982) Atmosphere-Ocean Dynamics. *Academic Press Inc.*, 666pp.

**Gill A.E. and E.H. Schumann** (1979) Topographically induced changes in the structure of an inertial coastal jet: Application to the Agulhas Current. *Journal of Physical Oceanography*, **9**, 975-991.

**Gordon A.L.** (1986) Inter-ocean exchange of thermocline water. *Journal of Geophysical Research*, **91**(C4), 5037-5046.

**Gordon A.L. and W.F. Haxby** (1990) Agulhas eddies invade the South Atlantic - evidnce from GEOSAT altimeter and shipboard conductivity-temperature-depth survey. *Journal of Geophysical Research*, **95**(C3), 3117-3125.

**Gordon A.L., K. Horai and M. Donn** (1983) Southern hemisphere western boundary current variability revealed by GEOS 3 altimeter. *Journal of Geophysical Research*, **88** (C1), 755-762.

**Gordon A.L., J.R.E. Lutjeharms and M.L. Grundlingh** (1987) Stratification and circulation at the Agulhas Retroflection. *Deep-Sea Research*, **34**, 565-599.

**Gordon A.L., R.F. Weiss, W.M. Smethie and M.J. Warner** (1992) Thermocline and intermediate communication between the south Atlantic and Indian Oceans. *Journal of Geophysical Research,* **97**(C5), 7223-7240.

**Griffiths G.B., B. Dupee, G. Watson, P. Spain and T.Nguyen** (1995) Trials and evaluation of an RD Instruments Acoustic Correlation Current Profiler in the Agulhas Current on RRS Discovery Cruise 214. *Institute of Oceanographic Sciences Internal Document* 349, 61p.

**Grundlingh M.L.** (1985a) An intense cyclonic eddy east of the Mozambique Ridge. *Journal of Geophysical Research*, **90** (C4), 7163-7167.

**Grundlingh M.L.** (1985b) Occurrence of Red Sea Water in the southwestern Indian Ocean, 1981. *Journal of Physical Oceanography*, **15**, 207-212.

**Grundlingh M.L.** (1983) On the course of the Agulhas Current. *South African Geographical Journal*, **65**, 49-57.

**Grundlingh M.L.** (1980) On the volume transport of the Agulhas Current. *Deep-Sea Research*, **27**, 557-563.

**Grundlingh M.L.** (1979) Observation of a large meander in the Agulhas Current. *Journal of Geophysical Research*, **84**, 3776-3778.

**Grundlingh M.L.** (1978) Drift of a satellite tracked buoy in the southern Aghulhas Current and Agulhas Return Current. *Deep-Sea Research,* **25**, 1209-1224.

**Grundlingh M.L., R.A. Carter and R.C. Stanton** (1991) Circulation and water properties of the southwest Indian Ocean, Spring 1987. *Progress in Oceanography*, **28**, 305-342.

**Grundlingh M.L. and A.F. Pearce** (1984) Large vortices in the northern Agulhas Current. *Deep-Sea Research*, **31** (9), 1149-1156.

**Hall M.M and H.L. Bryden** (1985) Profiling the Gulf Stream with a current meter mooring. *Geophysical Research Letters*, **12** (4), 203-206.

**Hall M.M. and H.L. Bryden** (1982) Direct estimates and mechanisms of ocean heat transport. *Deep-Sea Research*, **29**, 339-359.

**Harris T.F.W.** (1972) Sources of the Agulhas Current in the spring of 1964. *Deep-Sea Research*, **19**, 633-650.

**Harris T.F.W. and D. van Foreest** (1978) The Agulhas Current in March 1969. *Deep-Sea Research*, **25**, 549-561.

**Hastenrath S. and R. Lamb** (1979) Climatic atlas of the Indian Ocean. Part 2: The oceanic heat budget. *University of Wisconsin Press*, 104pp.

**Hellerman S. and M. Rosenstein** (1983) Normal monthly wind stress over the world oceans with error estimates. *Journal of Physical Oceanography*, **32**, 1093- 1104.

**Jacobs S.S. and D.T. Georgi** (1977) Observations on the southwest Indian / Antarctic Ocean. In: *A Voyage of Discovery*, pp43-84. M. Angel, editor, Pergamon Press, Oxford.

**Johns E., D.R. Watts and H.T. Rossby** (1989) A test of geostrophy in the Gulf Stream. *Journal of Geophysical Research,* **94** (C3), 3211-3222.

**Johnson J.A.** (1989) On the generation of baroclinic Rossby waves in the presence of a semi-circular boundary. *Geophysical and Astrophysical Fluid Dynamics*, **48**, 107-121.

**Josey S.A., E.C. Kent and P.K. Taylor** (1996) A new global air-sea heat and momentum flux climatology. *International WOCE Newsletter*, **24**, 3-4.

**Joyce T.M.** (1977) A note on the lateral water mixing of water masses. *Journal of Physical Oceanography*, **7** (4), 626-629.

**King B.A., S.G. Alderson and D. Cromwell** (1996) Enhancement of shipboard ADCP data using DGPS position and GPS heading measurements. *Deep-Sea Research*, **43**, 937-947..

**King B.A. and E.B. Cooper** (1993) Comparison of ship's heading determined from an array of GPS antennas with heading from conventional gyrocompass measurements. *Deep-Sea Research,* **40**, 2207-2216.

**Leaman K.D., E. Johns and T. Rossby** (1989) The average distribution of volume transport and potential vorticity with temperature at three sections across the Gulf Stream. *Journal of Physical Oceanography*, **19**, 36-51.

**Liu M. and T. Rossby** (1993) Observations of the velocity and vorticity structure of Gulf Stream meanders. *Journal of Physical Oceanography*, **23**, 329-345.

**Lutjeharms J.R.E.** (1988) Remote sensing corroboration of the retroflection of the East Madgascar Current. *Deep-Sea Research*, **35** (12), 2045-2050.

**Lutjeharms J.R.E.** (1985) Location of frontal systems between South Africa and Antarctica: some preliminary results. *Deep-Sea Research*, **32** (12), 1499-1509.

**Lutjeharms J.R.E.** (1972) A quantitive assessment of the year to year variability in water movement in the southwest Indian Ocean. *Nature Physical Science*, **239** (91), 59-60.

**Lutjeharms J.R.E. and R.C. van Ballegooyen** (1988a) The retroflection of the Agulhas Current. *Journal of Physical Oceanography*, **18** (11), 1570-1583.

**Lutjeharms J.R.E. and R.C. van Ballegooyen** (1988b) Anomolous upstream retroflection in the Agulhas Current. *Science*, **240**, 1770-1772.

**Lutjeharms J.R.E and R.C. van Ballegooyen** (1984) Topographic control in the Agulhas Current system. *Deep-Sea Research*, **31** (11), 1321-1337.

**Lutjeharms J.R.E., N.D. Bang and C.P. Duncan** (1981) Characteristics of the current east and south of Madagascar. *Deep-Sea Research*, **28A**, (9), 879-899

**Lutjeharms J.R.E., R. Catzel and H.R. Valentine** (1989) Eddies and other boundary phenomena of the Agulhas Current. *Continental Shelf Research*, **9** (7), 597-616.

**Lutjeharms J.R.E. and H.R. Roberts** (1988) The Natal Pulse: An extreme transient on the Agulhas Current. *Journal of Geophysical Research*, **93** (C1), 631-645.

**Mamayev O.I.** (1975) Temperature - salinity analysis of world ocean waters. *Elsevier Scientific Publishing Co.*, Oxford.

**Mantyla A.W. and J.L. Reid** (1995) On the origins of deep and bottom waters of the Indian Ocean. *Journal of Geophysical Research*, **100** (C2), 2417-2439.

**McCartney M.S.** (1982) The subtropical recirculation of mode waters. *Journal of Marine Research*, **40**, 427-464.

**McDowell S., P. Rhines and T. Keefer** (1982) North Atlantic potential vorticity and its relation to the general circulation. *Journal of Physical Oceanography*, **12**, 1417-1436.

**Meyers, G., R.J. Bailey and A.P. Worby** (1994) Volume transport of Indonesian throughflow. *Deep-Sea Research*, **42**, 1163-1174.

**Molcard, R., M. Fieux and A.G. Ilahude** (1996) The Indo-Pacific throughflow in the Timor Passage. *Journal of Geophysical Research*, **101**(C5), 12411-12420.

**Molcard, R., M. Fieux, J.C. Swallow, A.G. Ilahude and J. Banjarnahor** (1994) Low frequency variability of the currents in Indonesian channels (Savu-Roti and Roti-Ashmore Reef). *Deep-Sea Research*, **41**, 1643-1661.

**Munk W.H.** (1950) On the wind-driven ocean circulation. *Journal of Meteorology*, **7**, 79-93.

**Murray, S.P. and D. Arief** (1988) Throughflow into the Indian Ocean through the Lombok Strait, January 1985-January 1986. *Nature*, **333**, 444-447.

**Pearce A.F.** (1980) Early observations and historical notes on the Agulhas Current circulation. *Transactions of the Royal Society of South Africa*, **44** (2), p205-212.

**Pearce A.F.** (1977) Some features of the upper 500m of the Agulhas Current. *Journal of Marine Research*, **35**, 731-753.

**Pearce A.F. and M.L. Grundlingh** (1982) Is there a seasonal variation in the Agulhas Current? *Journal of Marine Research*, **40** (1), 177-184.

**Pearce A.F., E.H. Schumann and G.S.H. Lundie** (1978) Features of the shelf circulation off the Natal coast. *S. African Journal of Science*, **74**, 328-331.

**Pedlosky J** (1986) Geophysical Fluid Dynamics - second edition. *Springer-Verlag*, 710pp.

**Pickart R.S. and R.X. Huang** (1995) Structure of an inertial deep western boundary current. *WHOI contribution number* 8681.

**Pickart R.S. and S.S. Lindstrom** (1993) A comparison of techniques for referencing geostrophic velocities. *Journal of Atmospheric and Oceanic Technology*, **11**, 814-824.

**Rennell J.** (1778) A chart of the bank of Lagullas and the southern coast of Africa. *Royal Geographical Society*.

**Reid J.L.** (1981) *On the mid-depth circulation of the world ocean*. in Evolution of Physical Oceanography. B.A. Warren and C. Wunsch ed. *The MIT Press*, 623pp.

**Rintoul S.R.** (1991) South Atlantic interbasin exchange. *Journal of Geophysical Research*, **96**(C2), 2675-2692.

**Rossby T., J. Fontaine and J. Hummon** (1991) Measuring mean velocities with POGO. *Journal of Oceanic and Atmospheric Technology*, **8**, 713-717.

**Saetre R. and A.Jorge da Silva** (1984) The circulation of the Mozambique Channel. *Deep-Sea Research*, **31** (5), 485-508.

**Sanford T.B.** (1975) Observations of the vertical structure of internal waves. *Journal of Geophysical Research*, **80**, 3861-3871.

**Saunders P.M. and B.A. King** (1995a) Bottom currents derived from a shipborne ADCP on WOCE cruise A11 in the South Atlantic. *Journal of Physical Oceanography*, **25**, 329-347.

**Saunders P.M. and B.A. King** (1995b) Oceanic fluxes on the WOCE A11 section. *Journal of Physical Oceanography*, **25** (9), 1942-1958.

**Schmitz W.J.** (1969) On the dynamics of the Florida Current. *Journal of Marine Research*, **27**(1), 121-150.

**Schumann E.H.** (1982) Inshore circulation of the Agulhas Current off Natal. *Journal of Marine Research*, **40** (1), 43-55.

**Schumann E.H.** (1981) Low frequency fluctuations off the Natal coast. *Journal of Geophysical Research*, **86**, 6499-6508.

**Smith S.D.** (1988) Coefficients for sea surface wind stress, heat flux and wind profiles as a function of wind speed and temperature. *Journal of Geophysical Research*, **93**, 15467-15474.

**Stommel H.M.** (1958) The abyssal circulation. *Deep-Sea Research*, **5**(1), 80-82.

**Stommel H.M.** (1948) The westward intensification of wind driven ocean currents. *Transactions, American Geophysical Union,* **29**(2), 202-206.

**Stuiver M., P.D. Quay and H.G. Ostlund** (1983) Abyssal water carbon-14 distribution and the age of the worlds oceans. *Science*, **219**, 849-851.

**Sverdrup H.U.** (1947) Wind-driven currents in a baroclinic ocean; with application to the equatorial currents of the eastern Pacific. *Proceedings of the National Academy of Sciences,* **33**, 318-326.

**Talley L.D. and M.S. McCartney** (1982) Distribution and circulation of Labrador Sea Water. *Journal of Physical Oceanography*, **12**, 1189-1205.

**Talley L.D. and M.E. Raymer** (1982) Eighteen degree water variability. *Journal of Marine Research*, **40**, 757-775.

**Toole J.M. and M.E. Raymer** (1985) Heat and fresh water budgets of the Indian Ocean - revisited. *Deep-Sea Research*, **32**, 917-928.

**Toole J.M. and B.A. Warren** (1993) A hydrographic section across the subtropical South Indian Ocean. *Deep-Sea Research I*, **40** (10), 1973-2019.

**Tripp R.T.** (1967) An atlas of coastal surface drifts Cape Town to Durban. *Univ. of Capetown, Dept. of Oceanography*, 10pp.

**Valentine H.R., J.R.E. Lutjeharms and G.B. Brundrit** (1993) The water masses and volumetry of the southern Agulhas Current region. *Deep-Sea Research I*, **40** (6), 1285-1305.

**Van Ballegooyen R.C., M.L. Grundlingh and J.R.E. Lutjeharms** (1994) Eddy fluxes of heat and salt from the southwest Indian Ocean into the southeast Atlantic Ocean: A case study. *Journal of Geophysical Research*, **99** (C7), 14053-14070.

**Veronis G.** (1973) Model of world ocean circulation: I Wind driven two layer. *Journal of Marine Research*, **31**, 228-288.

**Walker N.D.** (1990) Links between South African summer rainfall and temperature variability of the Agulhas and Benguela Current systems. *Journal of Geophysical Research*, **95** (C3), 3297-3319.

**Warren B.A.** (1981) Transindian hydrographic section at Lat. 18°S: Property distributions and circulation in the South Indian Ocean. *Deep-Sea Research*, **28**, 759-788.

**Warren B.A. and G.H. Volkmann** (1968) Measurement of the volume transport of the Gulf Stream south of New England. *Journal of Marine Research*, **26** (2), 110-126.

**Wijffels S.E., N. Bray, S. Hautala, G. Meyers and W.M.L. Morawitz** (1996) The WOCE Indonesian Throughflow repeat hydrography sections: I10 and IR6. *International WOCE Newsletter*, **24**, 25-28.

**Worthington L.V.** (1976) On the North Atlantic circulation. *The John Hopkins Oceanographic Studies,* **6**, 110pp.

**Wunsch C. and B. Grant** (1982). Towards the general circulation of the North Atlantic Ocean. *Progress in Oceanography*, Pergamon, 1-59.

**Wyrtki K.** (1973) Physical Oceanography of the Indian Ocean. In: *Ecological studies. Analysis and synthesis*, vol 3. B. Zeitzschel, editor, Springer-Verlag, Berlin, pp18-36.

**Wyrtki K.** (1971) Oceanographic Atlas of the International Indian Ocean Expedition. *National Science Foundation*, Washington, DC, 531pp.